Properties of Intergalactic Filaments at z = 2 and Implications for the Evolution of Galaxies

Nicolas Cornuault

UNIVERSITÉ PIERRE-ET-MARIE-CURIE

École Doctorale d'Astronomie et Astrophysique d'Île-de-France

THÈSE DE DOCTORAT

pour l'obtention du titre de
Docteur en astrophysique de l'Université Pierre-et-Marie-Curie

presentée par
NICOLAS CORNUAULT

Properties of Intergalactic Filaments at $z \approx 2$ and Implications for the Evolution of Galaxies

sous la direction de
MATTHEW LEHNERT ET FRANÇOIS BOULANGER,

préparée à
l'Institut d'Astrophysique de Paris, CNRS (UMR 7095),
Université Pierre-et-Marie-Curie (Paris VI),

et financée par
le programme DIM-ACAV de la région Île-de-France,

soutenue publiquement
le 25 septembre 2017,

devant un jury composé de

Rapporteurs:	GUILAINE LAGACHE	-	LAM, Marseille, France
	OLIVER HAHN	-	OCA, Nice, France
Directeurs:	MATTHEW LEHNERT	-	IAP, Paris, France
	FRANÇOIS BOULANGER	-	IAS, Orsay, France
Président:	BENOÎT SEMELIN	-	LERMA, OBSPM, Paris, France
Examinateurs:	ADRIANNE SLYZ	-	Dept. of Physics, Oxford, UK
	FRÉDÉRIC BOURNAUD	-	SAP, CEA, Saclay, France
	YUVAL BIRNBOIM	-	Racah Institute, HUJ, Jerusalem

Contents

Abstract

From numerical simulations, coupling the growth of large scale structure and of dark matter halos with gas physics, we now understand theoretically that galaxy evolution involves inflows of "cold" gas from the cosmic web. Galaxies in these "cold accretion" models have large amounts of baryons compared to observed galaxies. To overcome this issue, theorists focus on making star formation inefficient by blowing baryons out of star-forming disks through massive gaseous outflows. In my thesis, I explore a different road, investigating processes that may moderate gas accretion onto disks. My methodology is based on multiphase gas physics honed through studies of the interstellar medium (ISM) in our own and nearby galaxies over the past decades using analytical modelling and numerical simulations to follow the gas thermodynamics and structuration from cosmic web filaments to galaxy halos.

In Chapter 2, we present a phenomenological scenario where gas accretion flows – if it is shocked as it enters the halo as we assume – become biphasic and, as a result, turbulent. We consider a collimated stream of warm gas that flows into a halo from an over dense filament of the cosmic web. The post-shock streaming gas expands because it has a higher pressure than the ambient halo gas, and fragments as it cools. The fragmented stream forms a two phase medium: a warm cloudy phase embedded in hot post-shock gas. We argue that the hot phase sustains the accretion shock. During fragmentation, a fraction of the initial kinetic energy of the infalling gas is converted into turbulence among and within the warm clouds. The thermodynamic evolution of the post-shock gas is largely determined by the relative timescales of several processes. These competing timescales characterize the cooling, the expansion of the post-shock gas, the amount of turbulence in the clouds, and the dynamical time of the halo. We expect the gas to become multiphase when the gas cooling and dynamical times are of the same order-of-magnitude. In this framework, we show that this occurs in the important mass range of $M_{halo} \sim 10^{11} - 10^{13} M_{\odot}$, where the bulk of stars have formed in galaxies. Due to expansion and turbulence, gas accreting along cosmic web filaments may eventually lose coherence and mix with the ambient halo gas. Through both the phase separation and "disruption" of the stream, the accretion efficiency onto a galaxy in a halo dynamical time is lowered. De-collimating flows make the direct interaction between galaxy feedback and accretion streams more likely, thereby further reducing the overall accretion efficiency. As we discuss, moderating the gas accretion efficiency through these mechanisms may help to alleviate a number of significant challenges in theoretical galaxy formation.

To establish the likely initial conditions for accretion flows into halos, using the adaptive mesh-refinement code RAMSES, I performed a zoom-in simulation of a specific halo and extracted the results for a particular accreting intergalactic filament into a $\sim 310^{11} M_{\odot}$ at $z \sim 2$. This part of my work is presented in Chapter 3. After having presented the need for a simulation, I briefly describe the code RAMSES. I investigate the gas thermodynamics and structuration, along and across the filament, with respect to dark matter. I study several key quantities as they evolve along the filament and derive a refined paradigm to study filaments, as well as consequences regarding their fate after

entering a halo. I finally make use of these results to extrapolate gas processes that the simulation may not have captured accurately.

In Chapter 4, I offer some conclusions and perspectives on how to extend our phenomenological model presented in Chapter 2 and how the results of simulations from Chapter 3 relate to our phenomenological results generally. With this thesis I started exploring and understanding the importance of non-linear gas physics within the context of large scale structure and global halo-galaxy evolution. I introduced some of the physics of the multiphase gas, processes which are well known in the ISM, but not well-modeled within cosmic web filaments. I see my work as a first step towards dedicated numerical studies for understanding the impact of gas physics on galaxy evolution.

Résumé

Les simulations numériques, prenant en compte le couplage des structures d'échelle cosmique à la physique des gaz, nous ont appris que l'évolution des galaxies doit impliquer un apport de gaz « froid » provenant de la toile cosmique. Les modèles en tenant compte conduisent à des galaxies plus riches en baryons que celles observées. Pour surmonter ce problème, les théoriciens oisissent de rendre la formation stellaire inefficace grâce à une éjection massive de gaz par les disques en train de former leurs étoiles. Dans cette thèse, j'explore une autre voie, en étudiant les processus qui pourraient atténuer l'accrétion de gaz sur les disques. Ma méthode s'appuie sur la physique des gaz multiphases connue à travers les études du milieu interstellaire de notre galaxie et de ses proches voisines au cours des dernières décennies, à l'aide d'une modélisation analytique et de simulations numériques, pour suivre l'évolution thermodynamique et structurelle du gaz, des filaments cosmiques aux halos galactiques.

Le chapitre 2 expose un scénario phénoménologique dans lequel l'accrétion du gaz, s'il y a un choc viriel, devient biphasique et, en conséquence, turbulent. Nous commençons par considérer un courant collimaté de gaz tiède qui s'écoule dans un halo, à l'embouchure d'un filament cosmique. L'écoulement post-choc s'étend puisqu'il a une pression supérieure à celle du gaz environnant dans le halo et se fragmente au cours de son refroidissement. Le milieu comporte alors deux phases : un phase nuageuse et tiède baignant dans le gas resté chauffé par le choc. Nous expliquons en quoi cette phase chaude supporte le choc. Au cours de la fragmentation, une fraction de l'énergie cinétique est convertie en une turbulence parmi et au sein des nuages tièdes. L'évolution thermodynamique est alors en grande partie déterminée par les rapports d'échelles temporelles de différents processus, à savoir le refroidissement, l'expansion, la turbulence et la dynamique propre au halo. On s'attend à ce que le gaz devienne multiphase quand les temps de refroidissement et de la dynamique du halo sont comparables. Dans ce scénario, nous montrons que cela arrive dans la gamme de masses de halo $\mathrm{M_{halo}} \sim 10^{11} - 10^{13} \mathrm{M_\odot}$, pour lesquelles la majorité des étoiles est déjà formée dans les galaxies. L'expansion et la turbulence peut faire perdre à terme leur cohérence aux filaments et entraîner leur dissolution dans le gaz du halo. La séparation des phases et la « disruption » de l'écoulement conduit alors à amoindrir l'efficacité d'accrétion sur la galaxie en un temps ynamique du halo. La décollimation accroît de même la probabilité d'interaction entre le courant d'accrétion et les éjections galactiques, diminuant d'autant plus l'efficacité d'accrétion. Nous discutons enfin de l'effet de cette diminution en tant qu'elle permet de résoudre un certain nombre de problèmes théoriques concernant la formation des galaxies.

Afin d'établir les conditions initiales propres aux écoulements d'accrétion sur les halos et qui soient réalistes, nous avons utilisé le code à raffinement adaptatif de maillage Ramses pour simuler de façon ciblée un filament intergalactique accrétant sur un halo de masse $\sim 3\,10^{11}\,\mathrm{M_\odot}$ à $z \sim 2$. Cette partie de mon travail est exposée dans le chapitre 3. Après avoir établi la nécessité d'une simulation numérique, les propriétés du code lui-même sont présentées. J'ai ensuite étudié la thermodynamique et la structuration du gaz, le long et à travers le filament, corrélativement à la distribution de matière noire.

J'ai suivi l'évolution de quantités importantes le long du filament et ai dérivé un cadre plus judicieux pour l'étude des filaments, ainsi que les conséquences attendues sur leur destin après avoir pénétré dans le halo. J'ai enfin extrapolé, à partir de ces résultats, certains processus que la simulation pouvait n'avoir pas capturé avec précision.

Dans le chapitre 4, je propose des conclusions générales ainsi que les développements possibles de notre modèle phénoménologique présenté au chapitre 2, ainsi qu'une mise en rapport plus générale des résultats du modèle et de la simulation. Au cours de cette thèse, j'ai commencé à explorer et à circonscrire le rôle joué par la physique non-linéaire du gaz dans le contexte des structures cosmiques et de l'évolution globale des couples halo-galaxie. J'ai pu introduire une part de la physique des gaz multiphase, bien connue en ce qui concerne le milieu interstellaire, mais encore imparfaitement modélisée dans le cadre des filaments cosmiques. Ce travail constitue une premièr étape vers une série d'études numériques spécialement dédiées à la compréhension de l'impact de la physique des gaz sur l'évolution des galaxies.

Foreword

At the end of the writing of this thesis, I wondered: how is this work in particular related to science in general? Here is my view on science, and on how my particular experience relates to it, introducing the outline of this manuscript.

A lot has been written on science, but what results from it, is that there is no clear and simple formulation circumscribing all of what science is. Is it only a search for truth? Is it particular because of its usage of mathematics? Is it defined by a back and forth motion between experiment and theory? Has it emerged because of its relative ability to predict? Can it be reduced to the hypothetico-deductive model? All of these limiting assertions are way too simple and too naive.

I will propose here a very crude description of how science works.
Science is the product of social activities of finding correlations in nature, constrained by what the agents recorded from nature and by self-consistency, of finding explanations sufficiently convincing to improve the overall consistency, and of keeping a memory of itself.
I intentionally omitted any term like "aiming at" or "trying to".

It is a social activity. Science is made in a collective and organized way. Scientists have to think collectively, then share their findings and convince of the reliability thereof. Finding alone and keeping it to oneself is not doing science. Publishing is neither an end to a scientific process, but rather a step in its course. Convincing the community is fundamental. It makes science subject to individual and sociological internal conflicts of course. More, since scientists also live in a broader society, their interactions outside of their field matter, especially when metaphysical, ethical or technological questions arise therefrom. This is why science is essentially social. But rather than making it flawed, this essence makes it dynamic.

Its internal functioning is also formally, even if not always explicitly, constrained. The constraints come first from observed data, that is from nature. But these do not constitute an ultimate guide. One needs to know that no observation can be categorized as direct or indirect. It is always indirect, mediated by several physical transformations and observational biases. What are the measured

quantities? What do they trace? What is their accuracy? Previously established models are often needed to simply interpret what is seen in nature, setting up loops of trust that can be one day broken. Not only is the trust in measurements difficult to establish, but the way they are represented has much to do with their acceptation by a scientific community. To find correlations, certain combinations of observed quantities are to be tested and this choice may already be a source of distrust. Is the correlation robust? Is there enough data? What are the odds that it be coincidental?

After having recognized a new correlation as universal, or at least sufficiently general, scientists are eager to provide an explanation. This has nothing to do with a quest for causality. Explaining correlations consists in forging a symbolic structure. The most technical way of explaining involves modelling to some degree. Modelling is an abstract construction of reality which needs:

- to conceive, that is gathering a minimal set of relevant concepts and detailing relationships therebetween,
- to formalize, that is gathering a minimal set of symbolic forms and ordering them to translate the conceptual links.

Mathematics provide us with a considerably powerful symbolic formalism. And even if it leaves, in general, no room to doubt when used rigorously, it is rarely the essence of conviction. The choices lie rather mainly in the conceptualization, and both requirements of a minimal set and of its relevance are often the heart of the issue.

A given personal scientific work can also become a game[1]. So many observations were made through exploration, guided by a more or less sharp intuition, sometimes even luck! I can remember a past experimental work I was involved into, where by playing with the knobs of instruments I found new regimes of a physical instability. And this exploration is not limited to observation and experiment.

Exploring by means of models may be quite vertiginous and exciting. Given the existing models, one can extend their results to what has not yet been observed. We may refer to this as prediction. When scientists extrapolate from already accepted models, they address the invisible, the unknown. Instead of fabricating a magical belief related to a mystic world, they keep following the aforementioned constraints while stating a consistent hypothesis about unknown or unsure situations.

This is what we have done here. Few information from observational instruments indicate the existence of intergalactic filaments. Given the expected central role of filaments in shaping the evolution of galaxies, which we will set forth in

[1] I here mean a game with no competition and sometimes with strict rules, sometimes very free. In Roger Caillois' words, it would be more *alea* than *agôn*, more *ilinx* than *mimicry*, and oscillating between *ludus* and *paidia*.

Chapter 1, we chose to address what is not yet known, namely their descriptive and dynamical properties.

Current knowledge about gas physics at galactic and cosmological scales allowed to consistently envision what could happen to the gaseous filaments when approaching galaxies. We stated that, in common circumstances, microphysics alone would play such a role that accreting filamentary streams could lose their identity. The expected timescales of interaction with galaxies and their close environments are then reassessed. This work is presented in Chapter 2.

A combination of physical, fundamental models with conditions that are currently considered realistic allows for a mathematical estimation of plausible solutions. Given the complexity of the said conditions, a numerical computation was used to investigate the state of resulting intergalactic filaments. The analyses of the simulation revealed a possibly complex structuration of filamentary streams before their entry in a galactic halo, product of an interplay between dynamics ascribed by cosmic structures and physics specific to a condensing gas. We report our findings in Chapter 3.

Both consistently arose from current knowledge but figure new results, whose in turn are to be tested observationally. This is what would be enjoined by the empiricism. However, as said before, science can not be reduced to a simple cycle of hypothesis and falsification. We may later find that our results are not as general as we thought, or new developments may stem from them. Science is about acceptance of a finding by a community. I hope that this work will be a convincing, building brick to erect one new piece of the scientific edifice.

Chapter 1

The role of dark matter and gaseous filaments in galaxy evolution

Abstract

Over the last decade, it has been realized that galaxies may acquire much of their dark matter and baryonic mass through accretion along filamentary structures.These structures grow gravitationally from small fluctuations in the density field in the early Universe. Why are intergalactic filaments so important to the field of galaxy evolution? Such accretion flows shape many of the essential properties of galaxies, like their shape, their colors, their mass, their gaseous and stellar contents, and so on. We can only understand galaxy evolution as a balance or competition between gas accretion, through filamentary structures driven by the growth of large scale structure, star formation, and the outflows intense star formation or active galactic nuclei may produce. But the fuel for all this activity and galaxy growth are all connected to the way matter has fallen, and is falling, onto galaxies, in combination with the way they react to the condensation processes and outflows. Let us revise now the different theoretical elements needed to understand the role played by intergalactic filaments (IGFs) in galaxy evolution.

Contents

1.1 Cosmological framework

The most fundamental principles governing the characteristics of the Universe, its expansion rate, mix of baryonic to dark matter, dark energy, its initial primoridial fluctuation spectrum, are all of prime importance for understanding of processes that shaped the objects in the universe over the last ∼13 Gyrs, since the time of the Big Bang. The growth and evolution of galaxies is no exception. The cosmological conditions are the first building blocks of any pertinent theory aiming to explain the history of one given galaxy, and of course, that of the ensemble of observed galaxies. The most important of these are the rate and rate of change of the cosmic expansion and the dominance of dark matter over (ordinary) baryonic matter. These are most consistently explained through variants of the cold dark matter with a non-zero cosmological constant, the Λ-CDM, model.

1.1.1 Cosmic expansion

The further the luminous bodies, the longer it took the light to travel from the source to the observer. But that distance also correlates with a widening of the wavelengths, making visible light become redder—this is the *redshift*:

$$z = \frac{\lambda - \lambda_0}{\lambda_0} \tag{1.1}$$

that is, the light initially emitted at a wavelength λ_0 is observed at a wavelength λ and the redshift z measures, for any wavelength, the light travelling time.

The most satisfying and convincing explanation for redshift is the cosmic expansion. This led to the introduction of a new energy source term Λ in Einstein's field equation of general relativity, called the *cosmological constant*. The corresponding fraction of mass-energy density to the one needed to stop the inflation (i.e. to make the Universe flat) is Ω_Λ and is estimated from Planck measurements (Planck Collaboration et al., 2014, 2016) of the CMB to be about 0.69. The linear term in the rate of expansion of the Universe is the Hubble's constant, H, and its current value is estimated by the Planck collaboration to be $H_0 \approx 67.3\,\mathrm{km.s^{-1}.Mpc^{-1}}$. The density required for a flat Universe is called the *critical density* and is defined by:

$$\rho_{\mathrm{crit}} = \frac{3H^2}{8\pi G} \tag{1.2}$$

where G is the gravitational constant. This also means that a given redshift z also corresponds to a recessional velocity. The further the object, the faster it apparently recedes from the observer. This phenomenon impacts not only electromagnetic waves, but more generally all quantities whose dimension is proportional

to a length at some non-zero power. Three simple examples reveal the ubiquity of the notion, when writing physical models: densities, sizes and velocities.

1.1.2 Dark and baryonic matter

Several peculiarities arose from observations. Rotation curves of galaxies, if one only considered the distribution of luminous baryonic matter, show unexpected behaviour at large radii: they are almost flat. It was expected from Newtonian dynamics applied to the mass of detected stars and gas that the orbital speed should decrease inversely to the distance. More, general relativity allows for light rays to be bent by masses, resulting in the so-called lensing effect. From the deformation of a luminous background, we can derive the value of a mass lensing it. Surprisingly, lensing galaxy clusters appeared to have a much higher mass than that computed from its stellar content[1]. Finally, the study of the cosmic microwave background led to an oddity: its spatial power spectrum has peaks, signatures of primordial acoustic oscillations, but their amplitudes were incompatible with models that only considered luminous matter.

A solution to the three problems is now widely accepted: there exists in the Universe a massive matter that does not produce radiation, and its mass density exceeds that of light-emitting matter. The latter is referred to as *baryonic* matter[2], the former being *dark* matter (DM), and whose fundamental nature is still unclear.

Neglecting the density of mass-energy of radiation and assuming a flat Universe, the fraction owing to matter is $\Omega_\mathrm{m} \approx 0.31$ and, still from Planck measurements (Planck Collaboration et al., 2014, 2016), the fraction for baryons is $\Omega_\mathrm{b} \approx 0.05$, leaving a fraction of DM $\Omega_\mathrm{DM} \approx 0.26$. The ratio $f_\mathrm{b} = \Omega_\mathrm{b}/\Omega_\mathrm{m} \approx 0.16$ is called the *baryonic fraction* and this cosmic value is considered constant[3]. This enables us to write the redshift-dependent Hubble constant:

$$H(z)^2 = H_0^2 \left(\Omega_\mathrm{m}(1+z)^3 + (1-\Omega_\mathrm{m}-\Omega_\Lambda)(1+z)^2 + \Omega_\Lambda\right) \tag{1.3}$$

and, for a flat Universe, the middle term of the parenthesis vanishes.

Dark and baryonic matter are thought to follow the same initial distribution but with different amplitudes, in proportion of their cosmic fractions. This is referred to as *coupling* of DM and baryons. The dark matter particles must have had initial velocities negligible compared to the speed of light to let the models fit with observational data (see below about the large-scale structures) and this is

[1] We could also add the cases of bound galaxies in superclusters whose dynamics suggested a higher mass than that derived from total luminous mass in galaxies.

[2] The term is not the most accurate one: electrons are indeed not baryons, i.e. they are not sensitive to strong interaction. A more general term could be "fermionic" matter, since baryons are composed of quarks, which are fermions like the electrons.

[3] Neither DM or baryons are produced, destroyed, or converted one into the other.

why the currently leading theoretical ground on which astrophysics stands now is called Λ-CDM, for non-zero cosmological constant, Λ, *cold dark matter*.

1.1.3 Initial density fluctuations

Theory suggests that, in the young Universe, the distribution of matter was in a state of a slightly perturbed but generally homogeneous state. Such a smooth field with small fluctuations may be considered Gaussian in first approximation—its Fourier modes have independent imaginary and real parts, which simplified calculations of its evolution. The phases of these modes are however of prime importance in determining later growth of structure with the density field. Statistical properties of those fluctuations are derived from the knowledge gained in the last decades about the cosmic microwave background, notably the power spectrum. Research on non-Gaussianities is still currently at the frontier of what is known or knowable. Gravity then drives matter towards regions of highest densities. This amplification of density peaks has been studied theoretically by means of (early) linear and (more recent) non-linear analysis.

1.2 Gravity in action

1.2.1 Large scale structures

The consideration of a gravitational and small scale fluctuations within the cosmological density field in three dimensions led to the prediction that matter should grow an organized characterizable structure. Dark matter halos sitting at the nexus of elongated, overdense regions ("filaments"), themselves circumscribing slightly overdense patches ("sheets" or "walls"), themselves enclosing under-dense compartments ("voids"). We can see it as, at first, an amplification of distinct features of a bidimensional density field: low density "valleys" get deeper, intermediate density "crests" get sharper, and high density "summits" get higher.

Early views of halo formation

The modelling of the evolving density field has given a more solid ground to the idea that density peaks, or halos, grow by acquiring mass from their environment. After the setup of an ideal, isotropic formulation for a self-similar spherical collapse, the mathematical developments of tridimensional, anisotropic growth allowed for ellipsoidal (triaxial collapse), rather than perfectly spherical halos. This more realistic depiction would then support some fundamental explanations for the strong asymmetry of their observed central luminous components, namely the galaxies that lie within these dark matter halos. However, even very elongated

halos can not fit the profiles of observed filaments, nor can very oblate halos fit the observed sheets.

Detection

The easiest method to detect these particular spatial arrangements of dark matter was to look at the way galaxies and clusters were distributed in three dimensions (angular position and redshift). Zeldovich et al. (1982) observed alignments and aggregation in clusters of galaxies, leaving giant voids in between. de Lapparent et al. (1986); Geller & Huchra (1989) reported a distribution in sheets bounding "bubbles", now called "voids". Klypin & Shandarin (1983) modelled the structures numerically and found a two-point correlation function in relatively good agreement with observations. Blumenthal et al. (1984); Davis et al. (1985) studied the structures to find that the Λ-CDM paradigm was particularly adapted to numerically reproducing observations, a work that opened the way to many others.

Fig. 1.1 shows a galaxy distribution slice of a plane in the sky computed from the galaxies the Sloan Digital Sky Survey (SDSS). In this slice following the northern equatorial plane, filamentary distributions of galaxies (here plotted in each galaxy's g-r color) are visible. Fig. 1.2 is a snapshot of the Millennium Simulation (Springel et al., 2005). Represented is the dark matter distribution, also organized in large-scale structures. Even visually, it is evident that galaxies and dark matter are both distributed in halos, filaments, walls, and voids.

Often described as a honeycomb or form architecture, the pieces of that cosmic skeleton approximately draws a tessellation of the space, and they were entitled *large-scale structures*. In *voids*, matter flows as if expanding in all directions, as a negative pressure, until encounters a comparable flow from neighbouring voids, building panels, or *sheets*. In turn, matter from the sheets flows as if expanding on a surface, reaching other sheet-like flows and forming *filaments*. Finally, matter expands in two directions along each filaments, pulled to the regions where filaments meet, namely the *halos*. This scenario for matter condensation is reminiscent of the chemical process of reticulation. From massive halos hosting galaxy clusters down to low-mass, dwarf galactic halos, the larger-scale structures should embed smaller-scale, similar ones. The model is hierarchical.

Dynamics

The formation and the flows associated with the growth of large-scale structure can be understood with a simple metaphor: rain, which occupies a tridimensional volume, falls on a sloping roof and forms a mostly bidimensional sheet, that in turn runs down to a gutter, giving rise to a thicker but mostly one-dimensional flow, and the water finally gets trapped into the sink that connects the gutters.

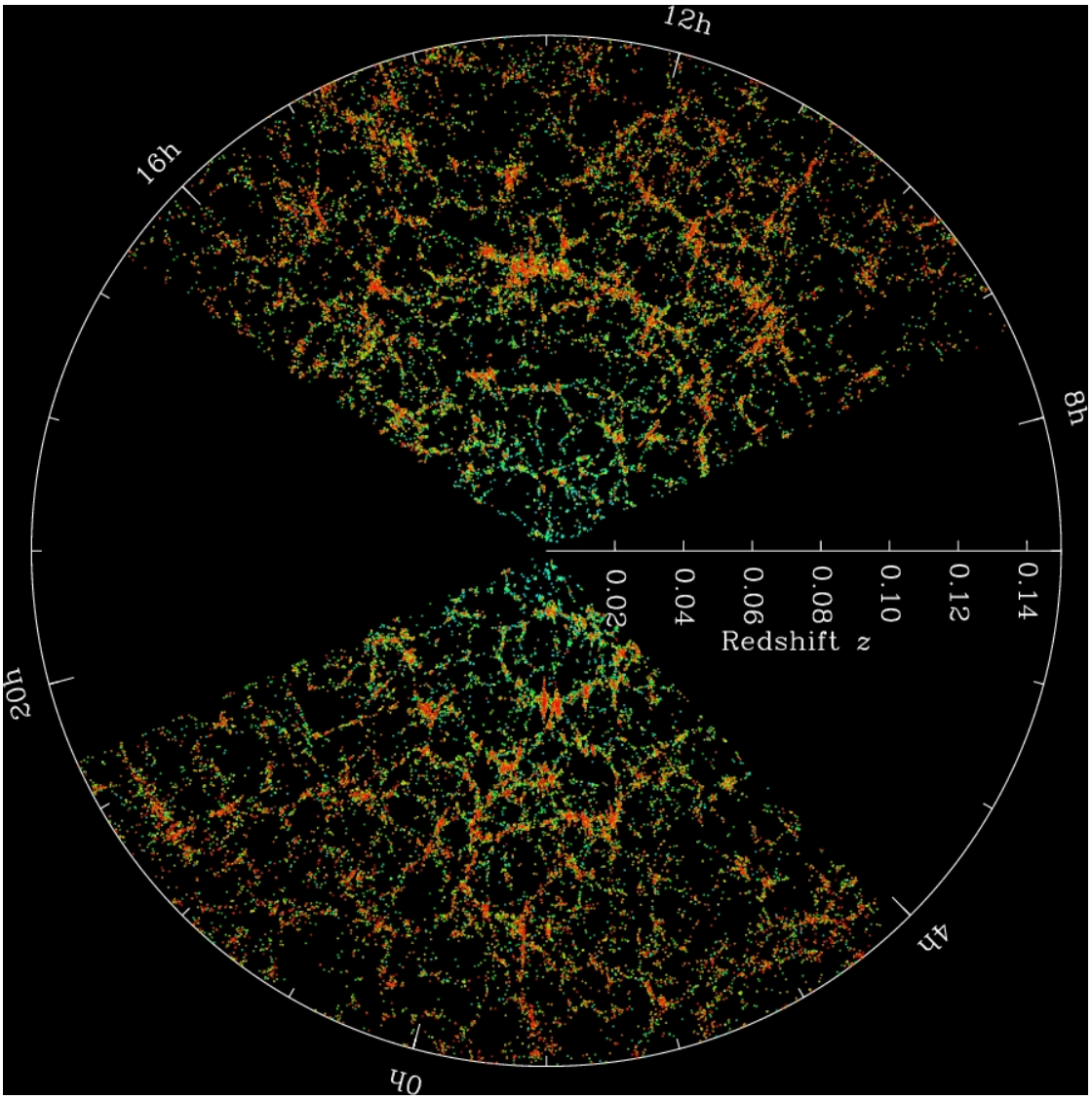

Figure 1.1: SDSS Galaxy map. Galaxies are arranged in large-scale structures. Image Credit: M. Blanton and SDSS. License: Standard SDSS image license.

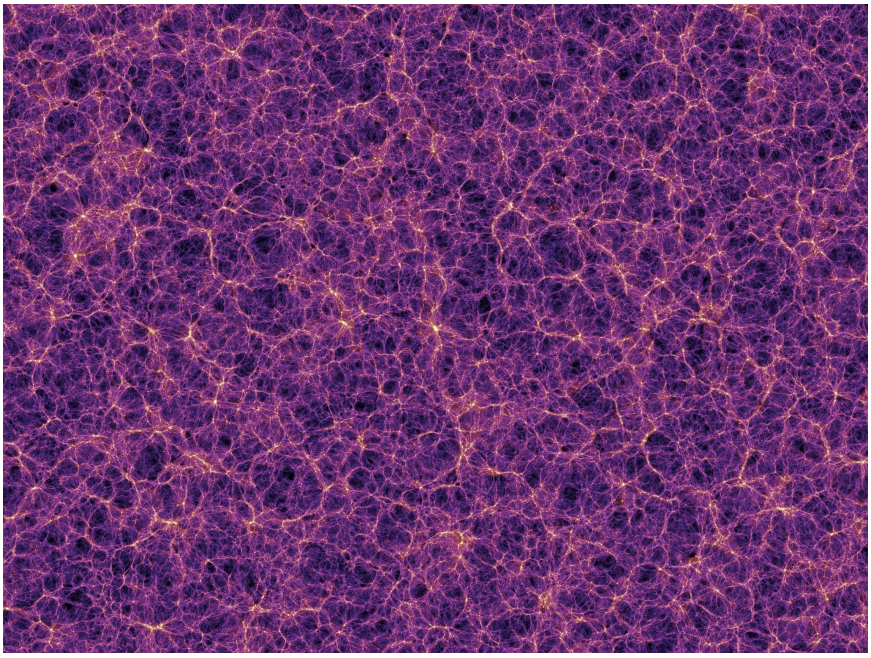

Figure 1.2: Snapshot of the Millennium simulation; dark matter distribution. From Springel et al. (2005).

Although useful, this picture proves inadequate, when describing the motion of the large-scale structures, and the associated deformation of the network. Indeed, dense structures not only give rise to a gravitational field, but they also are subject to it. Individual structures, as they grow from the surrounding density field, will eventually merge with any neighboring halos as they become gravitationally attracted. It is through this growth pattern where from the concept of hierarchical growth comes – smaller halos grow and merge to form larger and larger halos. Halos growth from the small to larger scales, from numerous small low mass halos, into larger and larger halos.

In that way, halos, albeit pulling matter down their filaments, are likely to "ascend" in the direction of their shortest feeding filament, pulled by the closest halo, at the other end. Depending on the mechanical conditions, gravitationally bound halos (for example, subhalos within a larger more massive one) may orbit each other. In the same way, filaments can exhibit a woven pattern, with their axes transiently intertwined. Halos may undergo a merger, followed by some of their filaments and finally some of their sheets.

Notwithstanding the cosmic expansion, these dynamics of the large-scale structure have a measurable impact: the two-point correlation functions should give different results depending on the redshift.

1.2.2 Halo growth

Merger mode

From the dynamics of large-scale structures, we have seen that the densest neighboring ones are attracted by each other. Because they travel until they merge with an similarly moving neighbor, and so on, halos follow a tree-like, or *hierarchical* storyline for their mass growth. The Press-Schechter formalism (Press & Schechter, 1974) is the earliest attempt to analytically predict the results. In a way, this paradigm for matter condensation is reminiscent of the process of coagulation and coalescence.

Accretion modes

As a corollary to the geometry of the large-scale structures and the associated flows, halos collect matter from filaments, but also sheets in the corner of which they sit, and from voids in the vertices of which they sit. Similarly, filaments accrete from sheets at the intersection of which they lie, but also from voids, Finally, sheets only receive mass flows from the voids they separate.

Smooth accretion, or (quasi-)spherical accretion corresponds to that coming from voids. It crosses a typical sphere around the halo with the widest angular sector but is also characterized by the lowest densities. Then comes the anisotropic accretion: from sheets (walls, or pancakes, representing the extremely oblate halos from the triaxial theory), and from filaments. The *filamentary accretion* represents the densest flows (in both gas and dark matter) and cover the least angular sector on the spheres they cross.

Describing a halo

Halos, no matter how dark and baryonic matter constitute them, are commonly described by geometrical (a radius) and kinematic (a speed) parameters, that in turn are related to its mass $M_{\rm H}$ and the redshift z. From a model of an initially isothermal gas exhibiting an isolated spherical over-density, Jeans derived a criterion to characterize the scales at which the system would be unstable to a gravitational collapse. Under the assumption that the system is initially virialized, we can derive the average over-density, compared to the critical density at that redshift. Overdense structures are gravitationally bound and will collapse. With the cosmology know cosmological parameters, yields an overdensity of $\Delta = \overline{\rho_{\rm H}}/\rho_{\rm crit} \approx 100$ (Bryan & Norman, 1998). But in this paradigm the Universe was thought to be matter-dominated, the same calculation gave $\Delta = 18\pi^2 \approx 177.7$ and most researchers continue to use this value of 200. Nevertheless, the idealized models being far

from the reality, it is really only an arbitrary choice, chosen simply to make it easier to compare different and especially, older, studies.

Considering the sphere centered around the density peak of a halo and which, on average, has a density Δ times the critical one, its radius is then set and denoted r_Δ. Its relation to the halo mass is simply:

$$M_{\rm H} = \frac{4}{3}\pi\Delta r_\Delta^3 \rho_{\rm crit} \tag{1.4}$$

and conversely, if the mass had been given first:

$$r_\Delta = \left(\frac{3M_{\rm H}}{4\pi\Delta\rho_{\rm crit}}\right)^{1/3} \tag{1.5}$$

Using the definition of the critical density,

$$r_\Delta = \left(\frac{2GM_{\rm H}}{\pi\Delta H(z)^2}\right)^{1/3} \tag{1.6}$$

Note that if the Universe was matter-dominated, we would get

$$r_\Delta \propto M_{\rm H}^{1/3}(1+z)^{-1} \tag{1.7}$$

This means that, the halo mass being constant, the virial radius grows with time (i.e. with decreasing redshift). This effect may sometimes produce the illusion of growth ("pseudo-growth"), although the cosmic expansion is the sole responsible. A typical order of magnitude for $r_{\Delta=200}$ is 100 kpc.

Having defined a radius and assuming a spherically symmetric distribution, it is possible to compute the speed at which a mass point would orbit precisely at that radius. It is called the *virial velocity* (for it may be derived in the simplest way from the virial theorem) and is defined by

$$v_{\rm vir} = \left(\frac{GM_{\rm H}}{r_\Delta}\right)^{1/2} = \left(\sqrt{\frac{\pi\Delta}{2}}H(z)GM_{\rm H}\right)^{1/3} \tag{1.8}$$

Note that if the Universe was matter-dominated, we would get

$$v_{\rm vir} \propto M_{\rm H}^{1/3}(1+z)^{1/2} \tag{1.9}$$

A typical order of magnitude for $v_{\rm vir}$ is 200 km.s^{-1}.

Setting arbitrarily $\Delta = 200$, and calling r_{200} the *virial radius*, we can describe any halo in a minimal way. Additionally, we may define a typical time called the *dynamical time* of the halo:

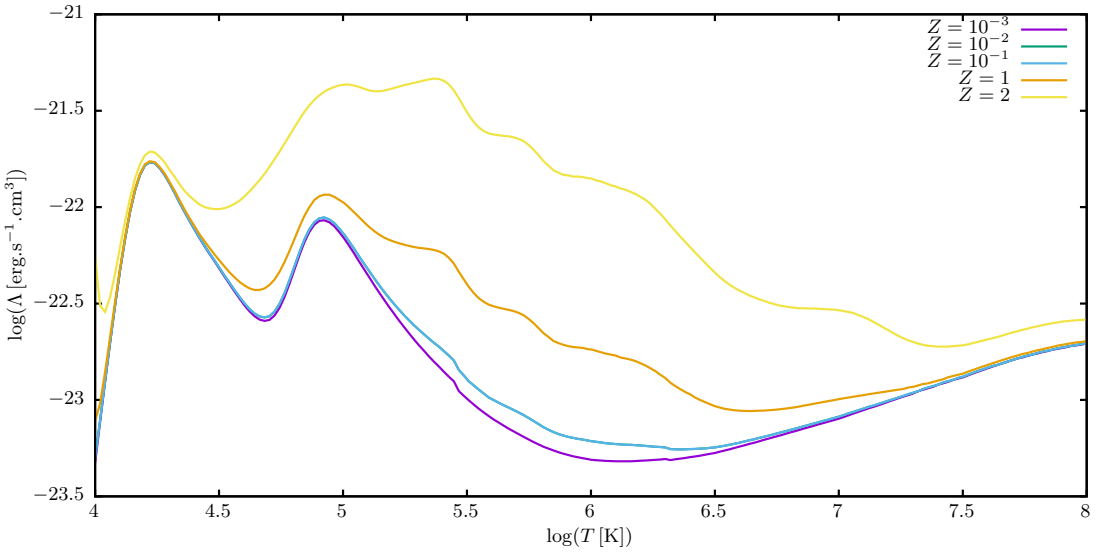

Figure 1.3: Cooling functions from Gnat & Sternberg (2007), in collisional ionization equilibrium, for five different metallicities (relative to solar).

$$t_{\mathrm{dyn}} = \frac{r_{\mathrm{vir}}}{v_{\mathrm{vir}}} \tag{1.10}$$

which is close to a free-fall time from the virial radius to the center of the halo, if its mass was concentrated in its center, or alternatively an orbital time. It is remarkable that this time does not depend on the halo mass, and in a matter-dominated Universe, it would be simply proportional to $(1+z)^{-3/2}$.

1.3 The importance of gas physics

Between gas and dark matter, a decoupling may occur at some stage of the condensation process, due to (baryonic) gas physics emerging from microphysical interactions (e.g., collisions) and the transitions between and losses of different energy types (e.g., thermal, micro-kinetic, to electronic excitation through collisions leading to radiative cooling as the atoms recombine or change electronic states). The gas may either resist gravitational forces due to its own internal pressure, or endure a "secondary" condensation phase resulting from its cooling in pressurized environment and self-gravitation.

1.3.1 Radiative cooling

The interaction between the particles of gas may convert its internal energy into radiation. If the gas is largely transparent to this radiation, radiative losses represents a net cooling. The temperatures of interest in this work concern largely the circum-galactic and intergalactic media, and thus range from 10^4 to 10^8 (but only for the most extremely massive halos at low redshifts).

More precisely, for temperatures between 1 and 3 10^4 K, atoms of hydrogen get ionized, while helium atoms are collisionally excited. When ions recombine with an electron, they emit a photon. When atoms spontaneously decay (or de-excite), they also emit a photon. Around 10^5 K, helium is ionized. At temperature higher than 10^6 K, another phenomenon occurs: the plasma is almost fully ionized and the electrical interactions make fast electrons to deviate from their linear trajectories. This braking is, again associated with radiation: this is the bremsstrahlung, which gets more intense with faster particles, so its intensity increases with increasing temperature. Immediately below 10^4 K, a gas of composition close to the primeval one displays a very inefficient radiative cooling; this explains our temperature floor that we will assume subsequently in our phenomenological modeling. It also justifies in many simulations why the cooling is truncated at 10,000 K.

Pristine gas being composed only of hydrogen and helium (with number density ratio $n_{\rm He}/n_{\rm H} \approx 1/12$), Fig. 1.3 gives an example of the cooling power per unit of number density of such a very low metallicity ($10^{-3}\,Z_\odot$). These curves have been computed under the assumption that the gas is at all times in a collisional ionized equilibrium. Other higher metallicities are also represented and we can see the strong impact of metals on the cooling rate.

Given such tabulated values for the cooling efficiency $\Lambda(T, Z)$, it is possible to evaluate the temperature loss:

$$\frac{{\rm d}T}{{\rm d}t} = -\frac{n_{\rm e} n_{\rm H} \Lambda(T, Z)}{(3/2 + s)(n_{\rm e} + n_{\rm H}) k_{\rm B}} \tag{1.11}$$

with $n_{\rm e}$ and $n_{\rm H}$ the number densities of electrons and hydrogen respectively, s is either 0 or 1 if the cooling is assumed to be isochoric or isobaric, respectively. Although the effect of pressure may prevent the gas from following precisely the gravitational field generated by the dark matter distribution as the dark matter grows into ever denser structures, the radiative cooling is often crucial for relieving that pressure and allowing gravity and external work from a still hot environment to compress the gas to an even larger extent than the dark matter would have allowed on its own in the absence of radiative cooling.

1.3.2 Shock due to condensation

When do compression effects occur to gas as it is gravitationally driven by dark matter? Let us reason with a theoretical, idealized formalism. When dark matter converges toward a dense structure, DM particles cross the system, because matter is "transparent" to them. After one crossing, and while the structure gains mass, they turn around, thus describing an orbital curve around the barycentric locus—a plane for sheets, an axis for filaments and a point for halos. Once a distribution of mass is settled, with a density decreasing with the distance to that locus, newly accreted shells (planar, cylindrical or spherical) will cross the distribution. The surfaces of shell-crossing are called caustics and their mathematical study is still ongoing (see for example Hidding et al., 2014). At this point, the accompanying gas shells collide with the previously condensed ones.

The shell crossing of dark matter is hence a source of the decoupling between dark and baryonic matter. The gaseous shell collision translates into an increase in pressure, that propagates to further shells. As can be seen from the scalings given above (Eqns. 1.2,1.9), densities are proportional to $(1+z)^3$ and speeds to $(1+z)^{1/2}$, meaning that the higher the redshift, the stronger the collision. It is then expected that a so-called accretion shock should occur in the external regions of dense structures.

At high redshift, this efficient conversion of kinetic energy density (scaling like $(1+z)^4$) to thermodynamic and the associated entropy production must shape not only the spatial discrepancy between dark and baryonic density gradients, but also the history of the gas condensation. This motivated Birnboim & Dekel (2003) and later Birnboim et al. (2016) in determining the stability of such shocks against the pressure loss due to the ensuing radiative cooling.

1.3.3 From warm gas to stellar light

From halo growth to galaxy growth

The first global theory for the formation of a dense, gaseous region at the center of dark matter halos, presumably then into forming realistic galaxies, came with Rees & Ostriker (1977); White & Rees (1978a); Fall & Efstathiou (1980a). They stated that while matter settles in isotropically converging flows forming halos, gas is prevented from condensing because of its collisional nature. The high pressure supports it, its temperature increases as the halo grows in mass, scaling as if the speed of sound was close to an orbital speed in the halo. More precisely, we call this temperature the virial one and define it as:

$$T_{\rm vir} = \frac{\mu m_{\rm p}}{3k_{\rm B}} v_{\rm vir}^2 \tag{1.12}$$

where $\mu m_{\rm p}$ is the average particle mass ($m_{\rm p}$ being the mass of a proton), and $k_{\rm B}$ is the Boltzmann constant. Its typical values are around $3\,10^5 - 10^6$ K.

The densest, innermost gas would then cool radiatively, up to a radius where the cooling time (density-dependent, so radius-dependent, as soon as a density profile is specified[4]) is equal to the dynamical time of the halo. This radius where the two time scales are equal is called the cooling radius.

At the cooling radius, the gas loses its pressure, the central region further collapses and the larger shells of gas lack the necessary pressure support, collapsing as well, until a new pressure equilibrium is reached. This may never happen for very low-mass halos since neither the virial temperature is high nor the equilibrium can be reach quickly, leading to a rapid gas condensation. On the other hand, high-mass halos (say, $M_{\rm H} > 5\,10^{11}\,{\rm M}_\odot$) exhibit a virial velocity higher than the speed of sound in the incoming gas ($T_0 \approx 10^4$ K), thus possibly producing a spherical shock. The post-shock gas may then keep its pressure support for more than one dynamical time, and the rate of gas condensing in the center of the potential is strongly decreased.

During its cooling and compression, the gas, in this model, conserves its angular momentum which leads to a faster rotation. This has been one explanation for the formation of planar dense gaseous regions, precursor of (spiral) galaxies. We only talked about the migration and the condensation of accreted gas through the halo, but what happens next? The central, oblate region reaches high densities and undergoes further gravitational instabilities that fragments it into much smaller but much denser disks and eventually forming stars. Populated with stars in a gaseous bath, the central regions of halos are now galaxies, within the context of this simple cooling picture.

Gaseous filamentary accretion onto galaxies

Since the works of Birnboim & Dekel (2003); Kereš et al. (2005); Dekel & Birnboim (2006); Dekel et al. (2009), a new paradigm has emerged. Kereš et al. (2005) showed that a substantial fraction of the mass of gas accreted by a galaxy came from thin, dense, almost unidimensional channels, with the peculiarity of being warm ($\sim 10^4$ K) even when the halo gas was much hotter. This filamentary accretion was found to be dominant over other modes, even mergers, above a redshift of about 1. While Birnboim & Dekel (2003) had provided a new explanation for the change of regime in smooth accretion, by reducing the "virial" shock stability to a simpler criterion based on an effective adibatic index, Dekel & Birnboim (2006) extended this study to the filamentary accretion. The involved densities being separated by orders of magnitude, the stability criterion was met so that even in

[4]The simplest case is that of an isothermal sphere at pressure equilibrium. An alternative would make use of an NFW density profile.

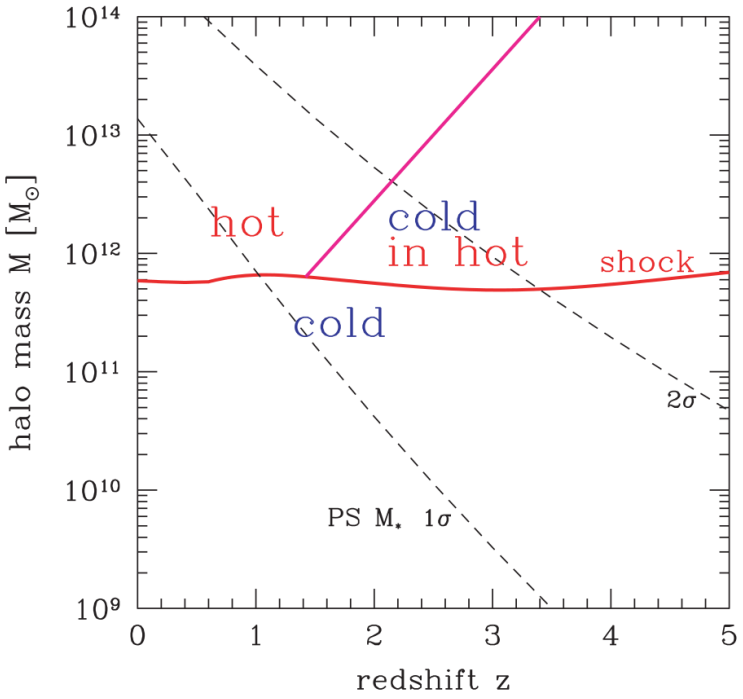

Figure 1.4: An important and influential figure from Dekel & Birnboim (2006). Below $\sim 5\,10^{11}\,M_\odot$, the smooth accretion cools faster than it is compressed and stimulates galactic star formation; above that limit, a stable shock prevents any efficient cooling. The "cold-in-hot" zone represents the masses and redshifts for which filaments are most likely to undergo no stable shock, thus feeding the galaxy with warm gas. Dashed lines show the Press-Schechter 1- and 2-σ typical halo masses as functions of the redshift, to guide the eye through the process of halo growth. However, such a picture leads to galaxies "drowning" in baryons. To alleviate this, models then require very efficient outflows to moderate the gas content of galaxies and to keep their growth inefficient. We concern ourselves in this thesis with this supply of gas. Can micro-physical processes prevent or at least lengthen the time it takes for gas to accrete onto galaxies? Lowering the accretion efficiency alleviates a number of significant astrophysical challenges as we discuss in Chapter 2.

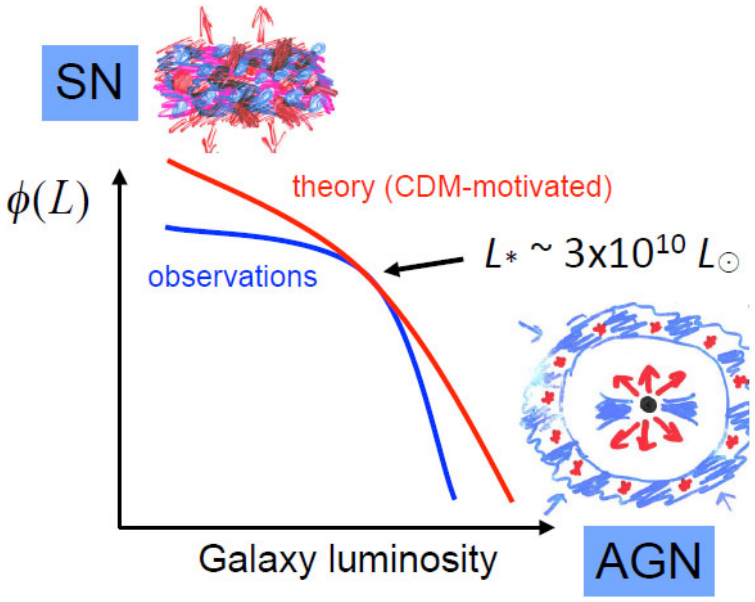

Figure 1.5: Illustrative figure from Silk & Mamon (2012) A sketch of the observed (blue) and theoretical (red) distributions of galaxies, according to their luminosity, a proxy to their stellar mass. showing the challenges of contemporary galaxy evolution studies. Galaxies are simply not following the development of dark matter and its distribution in halos. Various processes must have made galaxy formation "inefficient". As can be seen in this figure, the authors concern themselves with the loss term, outflows, where active galactic nuclei eject mass from the high mass halos, while supernovae (SN) remove the gas from low mass halos. In this thesis, we concern ourselves with the supply side, how does the gas form into structures and accrete into individual dark matter halos.

the case when the spherical accretion is shocked, filaments may endure no such shock and penetrate the halo, feeding the galaxy with "fresh" fuel to support the growth of the stellar populations within galaxies. As seen in Fig. 1.4, this "cold mode" accretion was found to occur at redshifts higher than 2 and for halo masses lower than a value which increases with redshift.

The work presented here is precisely an attempt to better understand the nature and the dynamics of this accretion mode. The next section explains why it is important to investigate this mode of accretion in more detail.

1.4 Challenges of galaxy evolution

Several pieces of observational information are intriguing. First of all, the overall average star formation rate (SFR) reaches a clear maximum up to a redshift of about 1.5 and then abruptly declines (e.g. Madau et al., 1996; Madau & Dickinson, 2014). Why would galaxies form more and more stars and then decline so precipitously? Moreover, as highlighted by Fig. 1.5, if one naïvely states that the stellar mass of galaxies should be proportional to their host halo mass, Λ-CDM would provide strong overestimates for low-mass and high-mass galaxies. So, what prevented low-mass and high-mass halos to grow a galaxy with a stellar component consistent with that of "average" $L_\star$ galaxies? This apparent lack of stars is connected to the broader question of the so-called missing baryon problem (less than 50% of the expected baryons are observed), the other side of the same coin being the over-cooling problem (numerical simulations tend to heavily overestimate the gas condensation by cooling). Why is galaxy formation so inefficient? Two families of explanations were provided, and neither totally excludes the other.

1.4.1 Extrinsic explanations for inefficient galaxy formation

The first explanation may come by investigating processes for limiting the accretion of gas. As we said before, if a stable shock propagates outwards in the halo gas, baryons may remain at constant radius, supported by the hydrostatic pressure of the halo gas, for a time larger than one dynamical time, if for example, the circumgalactic medium is very dilute. This may be the case for the highest scale structures like inter-cluster filaments or cluster halos. Hard X-ray emission is the signature of hot gas with a long cooling time. Within this context, "missing baryons" would lie in multi-phase gas retained in the halo as warm-hot intergalactic gas. It's emission would be extremely weak due to its rarity (low density).

Then, a new question arises: if strong mass inflows of warm gas is allowed via a "cold-mode" accretion at high redshift, would not this mode stimulate the formation of baryon-rich, luminous galaxies? Without ruining the judicious reasoning that accounted for early massive galaxies, we need to investigate the precise fate of intergalactic filaments close to the point where their role in supplying galaxies with gas shifts from leading to negligible. There may well be mechanisms to reduce their galaxy-feeding efficiency earlier, at higher redshifts and in lower mass halos, than currently expected from theory.

1.4.2 Intrinsic explanations for inefficient galaxy formation

The second possible type of explanation as to why galaxy formation is so inefficient is illustrated in Fig. 1.5. These intrinsic explanations involve processes that are a

result of the formation history of the galaxy itself. A galaxy is basically composed gaseous and a stellar components, and it exchanges mass and energy with its immediate environment, the circum-galactic medium, possibly the local inter-galactic medium. Internal evolution, correlated with mass growth and the evolution of its stellar populations or the growth of a supermassive black hole through gas accretion, could lie at the heart of galaxies evolving from a rapid accretion and vigorous outflows mode of growth and evolution to a more quiescent growth of gas and stars with only limited outflow rates.

On the low-mass end ($\sim 10^8\,M_\odot$) of the galaxy and dark matter mass distribution, the gravitational well of the dark matter halo is neither sufficient to overcome the gas pressure up to a point where the cooling becomes efficient, nor, on the other hand, can it retain the gas expelled due to the combined energy output supernovae (if such energy is effectively thermalized). On the high-mass end ($\sim 10^{13}\,M_\odot$), mass accretion is accompanied by growth of a central (super)massive black hole. The more massive it gets, the more energy it extracts from the gas at constant accretion rate, which increases its bolometric luminosity and mechanical energy output in the form of intense radiation and powerful outflows. This ejection, even if it is collimated and as long as it couples effectively to the ambient gas, disrupts and heats the interstellar medium. Since internal processes give rise to the shutdown of star formation, nominally by removing the gas, but also perhaps through the strong generation of turbulence, such processes are collectively called *negative feedback*.

1.4.3 Accretion–feedback interaction?

Feedback processes generally involve energy, mass, and momentum ejection from the galaxy. The thermal, turbulent, and kinetic energies, as well as the momentum must be deposited in the surrounding medium, that is the circum-galactic medium (CGM), possibly in to the IGM well beyond the virial radius. But these are also the very regions crossed by accreting material, themselves carriers of energy and momentum.

We expect the two families of flows to interact in some extent[5] . The result of such an interaction is difficult to predict: there exist many sets of conditions, allowing or preventing from condensing again and "raining" on the galaxy (see e.g. Voit et al., 2015b). In other words, the interaction between accreting and outflowing gas could turn into either a positive or negative feedback loop. In fact, in reality, it is probably both. That's not the real question. The really poignant

[5]The "efficiency" of such an interaction depends on several factors, fro example the geometry of the flows: if an AGN produces a jet perpendicular to the galactic plane while a warm filament reaches the ISM parallel to that plane, they would not directly interact.

question is does feedback increase or decrease the gas accretion efficient overall. With the current state of the art simulations, it appears that this interaction moderates the inflow rates but it is not exactly clear how. In this context, it is essential to study the stability of the accreting IGFs, as a possible disruption would not only alter the accretion efficiency, but also the way they interact with galactic feedback outflows.

Chapter 2

Modeling the entry in the halo

Abstract

Simulations of cosmological filamentary accretion reveal flows ("streams") of warm gas, T$\sim 10^4$K, which are efficient in bringing gas into galaxies. We present a phenomenological scenario where gas in such flows – if it is shocked as it enters the halo as we assume – become biphasic and, as a result, turbulent. We consider a collimated stream of warm gas that flows into a halo from an over dense filament of the cosmic web. The post-shock streaming gas adjusts its pressure with the ambient halo gas, and fragments as it cools. The fragmented stream forms a two phase medium: a warm cloudy phase embedded in hot post-shock gas. We argue that the hot phase sustains the accretion shock. During fragmentation, a fraction of the initial kinetic energy of the infalling gas is converted into turbulence among and within the warm clouds. The thermodynamic evolution of the post-shock gas is largely determined by the relative, competing timescales of several processes: the cooling, the expansion of the post-shock gas, the amount of turbulence in the clouds, and the dynamical time of the halo. We expect the gas to become multiphase when the gas cooling and dynamical times are of the same order-of-magnitude. In this framework, we show that this occurs in the important mass range of $M_{\rm halo} \sim 10^{11} - 10^{13}\,M_\odot$, where the bulk of stars have formed in galaxies. Due to expansion and turbulence, gas accreting along cosmic web filaments may eventually loose coherence and mix with the ambient halo gas. Through both the phase separation and "disruption" of the stream, the accretion efficiency onto a galaxy in a halo dynamical time is lowered. De-collimating flows make the direct interaction between galaxy feedback and accretion streams more likely, thereby further reducing the overall accretion efficiency. As we discuss, moderating the gas accretion efficiency through these mechanisms may help to alleviate a number of significant challenges in theoretical galaxy formation.

Contents

2.1 Motivations

The physical state of the gas accreting onto a galactic halo is thought to largely determine the star formation history of the galaxy itself. When most of the accreting matter is still coming from intergalactic filaments (IGFs), studying theoretically the physical conditions of the gas they carry into the halo is therefore of prime importance in understanding how galaxies grow and evolve. Two families of scenarii have been envisioned theoretically. The first one, the gas is warm[1], $\sim 10^4\,\mathrm{K}$, as falls into the potential of the halo ultimately feeding the galaxy with fresh gas and supporting its star formation. In the other scenario the gas is hot, $\gtrsim 5\,10^5\,\mathrm{K}$, and due to mixing generally leads to feeding the halo with hot gas. Unless the cooling time of the gas penetrating the halo is short relative to the dynamical time of the halo, it will simply feed the halo with gas, generally not the galaxy itself except perhaps over a very long timescale.

The filamentary accretion obviously shares common features with the "spherical"[2] accretion because the gas it involves is considered of the same general nature, but with a higher density and an expected lower temperature, and because its dynamics is also strongly driven by the potential well of the dark matter halo. Nevertheless, the geometry of a filament, as opposed to spherical diffuse accretion, has a stronger influence on how the galaxy evolves. First, due to its collimated nature as its travel through the halo, its cross section is small enough that it may not encounter outflows from the galaxy. The cross section of a stream is roughly two orders of magnitude less than the surface of a sphere encompassing the galaxy itself. More particularly, by conservation of angular momentum, infall trajectory of streams tends to align with the galactic plane, avoiding then possible powerful outflows from an AGN or intense star formation occurring within the halo's central galaxy. Secondly, its possibly high overdensity compared to most of the halo gas provides it with enough inertia to penetrate deeply into the circum-galactic medium (CGM) of the galaxy. Because of their possible high efficiency in reaching the galaxy proper, IGFs are expected to be major drivers of the gas supply within galaxies and hence support their star formation, when suitable conditions are met.

As with spherical accretion, the two scenarios rely on the existence of a shock propagating upwards into the cooler core of an IGF. When it exists, its stability,

[1] This situation is often refered to as "cold mode accretion". However, we will use the term "warm", since this is the common nomenclature in studies of the interstellar medium for ionized and neutral gas at a few 1000 to 10^4 K such as the warm ionized or the warm neutral medium (WIM/WNM). The term "cold" is reserved for gas below these temperatures – the cold neutral and the cold molecular media.

[2] "Spherical", or "isotropic" accretion are named this way because of idealized spherical halos. It is of course rather unrealistic, as dark matter halos are expected to be ellipsoidal and irregular. Some authors use the word "smooth" to refer to this kind of accretion.

its strength and the propensity to cool all determine whether the mode of accretion is hot or warm. If it is unstable, as predicted by Dekel & Birnboim (2006) at low redshifts ($z \lesssim 2-3$) and for high halo masses, the shock collapses down and no heating occurs. Its stability may be inferred from the radiative nature of the shock, as well as the compression due to the converging flowlines and the pressure increase in the halo when falling in. If it is not strong enough (Mach numer $\mathcal{M} \lesssim 5$), the gas is heated up to only $\sim 10^5$ K and the density is increased by a factor > 3.5. In such a case, the radiative cooling is efficient on a timescale shorter than the infall timescale (here the relevant dynamical time) and the stream ends up warm.

2.2 Rationale

Numerical simulations may be of great help to understand the fate of the gas driven along filaments, especially their dynamics. Chapter 3 shows that a great deal of information about the physical conditions are revealed in zoom-in simulation. However, there are limitations that are inherent to numerical computations, such as the finite resolution or the finite number of processes modeled. A number of phenomena that stem from excluded (or of which scale is unreachable) microphysical processes, such as many hydro- and thermodynamic instabilities, may not develop in simulations of relatively low resolution. In particular, the turbulence–because of the extended range of scales needed to cover the turbulent cascade(s)–, and the thermal fragmentation–because of the small-scale fluctuations needed to seed the first fragments– would not be computed. For example, observations of the ISM in the MW suggest that turbulence is dissipated on scales well below a pc (e.g., Miville-Deschênes et al. 2017).

We already noted the importance of the weak interactions between the halo gas and the galactic outflows on the one hand, and the IGF material on the other hand, when accreting in "warm mode". Allowing for the possibility to have both hot and warm gas leads to the possibly increased efficiency of such interactions. As far as this model allows it, we will then address at least the question of the effective cross-section of the filament when it penetrates into the virial sphere.

The redshift 2 will be the one we exemplify in specific illustrative calculations, but the model does not restrict to that value. There are two reasons for this. First, this is the epoch when, statistically, the co-moving density of star formation of the ensemble of galaxies is at a turning point. The star-formation rate (SFR) density evolution bends from increasing to decreasing around $z \approx 2$. The prediction from Dekel & Birnboim (2006) that warm filaments would stop feeding galaxies efficiently in massive halos matches this value. Thus, learning more about the gas physics of filamentary accretion will help refining models that explain this evolution in the star-formation rate density with cosmic time.

Secondly, the redshift at which the dominant contribution to the growth of galactic halos shifts from the filamentary accretion to the halo mergers is estimated to be around $z \sim 1.5$. Below this redshift, the study of IGF accretion may be somewhat less relevant within the context of galaxy growth, even if it would still be interesting to understand peculiarities of halo gas and CGM close to galaxies at all redshifts.

But as said, our model is more general and is aimed at determining the conditions under which a filamentary flow becomes turbulent and multiphase, and in what amount.

2.3 The beginnings of a phenomenological model for a turbulent and multiphase post-shock medium

In this section, we discuss our initial analysis of the formation of bi-phasic turbulent post-shock medium of the streams. We discuss the initial conditions of the stream and halo gas the stream is flowing into. In this early analysis, our basic assumption was that the post-shock gas was in thermodynamic equilibrium. Thus, if the post-shock gas met the criterion for becoming thermally unstable (Field, 1965), then it would become bi-phasic. Turbulence would also be generated from the transformation of the bulk kinetic energy into random motions of the warm clouds and in turbulence within the clouds. However, subsequently, we realized that the assumption of thermodynamic equilibrium was not necessary, and perhaps even difficult to justify within the context of a phenomenological model. We developed a more general case where the stream develops inhomogeneities due to, for example, the shock being oblique, having a range of velocities due to shock curvature, and/or having an initially inhomogeneous stream (where the inhomogeneities are amplified in the post-shock gas). This section captures the development of our initial ideas and initial conditions and assumptions for a more fully developed model of gas accretion into galaxy halos.

2.3.1 Overview

The phenomenological and somewhat idealized models all considered an initially cylindrical flow of confined, warm gas and the possible shock was stationary, with *a priori* laminar, homogeneous post-shock flow, surrounded by a medium at hydrostatic equilibrium. We considered the case where:

- there is a stable, stationary shock;
- the IGM is at very low metallicity ($Z < 10^{-3} Z_{\odot}$);

- turbulence is produced[3] by the shock;
- the post-shock medium, being in thermodynamic equilibrium, heterogeneously cools to develop a multiphase medium leading to two phases: the *warm* one and the *hot* one;
- the relative motion of warm clouds has captured all of the turbulent motions.

2.3.2 Fixed parameters

Our model applies to any given halo mass $M_{\rm H}$ at any given redshift z. Thus, the critical density of the Universe $\rho_{\rm crit}$, the virial radius $r_{\rm vir}$ and the virial velocity $v_{\rm vir}$ are considered known. A floor temperature is fixed at $T_0 = 10^4\,{\rm K}$, below which the gas can not cool. This is a consequence of the abrupt fall of the cooling efficiency at low metallicities. The initial temperature of the filament, defined as 'warm', is set to T_0.

2.3.3 Free parameters

A few parameters are kept free. The over-density of the filament compared to the surrounding IGM is denoted f and is considered free because simulations show that it may widely vary from one filament to another, and from one halo to another. The final volume-averaged turbulent pressure over the initial ram pressure is labelled η and is free because it is extremely difficult to reliably quantify the energy conversion to random turbulent motions. We would indeed need, first, a robust model for shock instabilities, and for compressive, non-isothermal, turbulence in radiating medium. Even with those, we would need to expand the number of assumptions and postulate realistic values for supplemental parameters. The volume filling factors of the warm and hot components are $\phi_{\rm v,w}$ and $\phi_{\rm v,h} = 1 - \phi_{\rm v,w}$. The use of $\phi_{\rm v,w}$ as an input parameter is complementary to the use of $\phi_{\rm m,w}$, the mass fraction of the gas falling into warm temperatures. It is a free parameter because only few may be known about the phase separation without the knowledge of power-spectra of thermodynamic quantities and other information related to microphysics. This, again, prevents us from making the model too intricate and too dubious due to an oversized set of assumptions. We note that ultimately, some of these parameters are not truly "free" but that microphysics within the gas must regulate the amount of energy, for example, it transformed into cloud-cloud motions.

[3] We can either consider that turbulence is *produced* or that the turbulent velocity dispersion in the pre-shock medium was negligible compared to the total pressure but strongly amplified by the shock.

2.3.4 Foundational definitions

Definition 1 – The properties of the halo gas useful to our scenario are its density at the virial radius, $\rho_{\rm H}$, its temperature, $T_{\rm H}$, and the law for ideal gases let us also directly derive its pressure $P_{\rm H}$. The density of IGM/halo gas close to the virial radius, is the fundamental density of the model: $\rho_0 = \rho_{\rm H}$.
Definition 2 – The filament is cylindrical (perfectly collimated), homogeneous, its initial density is:

$$\rho_1 = f\rho_0 \tag{2.1}$$

Definition 3 – Its initial pressure is then:

$$p_1 = (k_{\rm B}/\mu m_{\rm p})\,\rho_1 T_0 \tag{2.2}$$

Definition 4 – The density of the warm and hot components are respectively designated as $\rho_{\rm w}$ and $\rho_{\rm h}$.
Definition 5 – The volume-averaged densities of the warm and hot components, of the overall medium are:

$$\widetilde{\rho_{\rm w}} = \phi_{\rm v,w}\rho_{\rm w},\ \widetilde{\rho}_{\rm h} = \phi_{\rm v,h}\rho_{\rm h} \tag{2.3}$$

which allows us to define the overall average density as:

$$\rho_2 = \widetilde{\rho_{\rm w}} + \widetilde{\rho}_{\rm h} \tag{2.4}$$

Definition 6 – The mass fractions of each component are easily defined:

$$\phi_{\rm m,w} = \widetilde{\rho_{\rm w}}/\rho_2,\ \phi_{\rm m,h} = \widetilde{\rho}_{\rm h}/\rho_2 \tag{2.5}$$

Definition 7 – The initial speed of sound in the filament is (squared):

$$c_{\rm s}^2 = \gamma\,(k_{\rm B}/\mu m_{\rm p})\,T_0 \tag{2.6}$$

so that the initial Mach number is:

$$\mathcal{M}_1 = v_1/c_{\rm s} \tag{2.7}$$

Definition 8 – The final post-expansion or contraction cross section of the flow is increased by a factor S. Note that it may take any real, positive value, meaning that $S < 1$ implies an actual contraction.

2.3.5 Hypotheses and their formal expressions

To allow for a sufficiently simple modelling, we posited a number of hypotheses that were plausible from what was known about cold streams, virial shocks, and gas physics in this kind of environment. We here present them, with their formal translations into mathematics, using the previous definitions.

Hypothesis 1 – The filament comes in at the virial velocity:

$$v_1 = v_{\rm vir} \tag{2.8}$$

This is equivalent to the case where gas is falling from infinity toward an isolated halo. It is compatible with the findings of Goerdt & Ceverino (2015a).

Hypothesis 2 – The whole system (including the shock) is stationary.

The Rankine-Hugoniot jump relations apply easily to a stationary shock and that is why it is often easier to choose the reference frame of the discontinuity front. Would the shock propagate in the frame of the halo? Birnboim & Dekel (2003) numerically found that an accretion spherical shock would settle close to the virial radius along the cosmic expansion and the halo growth. Our intuition that the possible existence of a shock in the penetrating filament would occur at the virial radius and thus correspond to a virial shock led us to postulate that this shock would also be stationary. Assuming its existence also means that we assume that the conditions for its stability are met, implying that its post-shock medium would support it, even if dissipative processes occur afterward. To ensure this, the simplest hypothesis consists in the stationarity of the whole system.

Hypothesis 3 – Halo is in hydrostatic equilibrium with an NFW profile. Halo is set to be at the virial temperature:

$$T_{\rm H} = T_{\rm vir} = \frac{\gamma - 1}{2} \left(\mu m_{\rm p} / k_{\rm B}\right) v_{\rm vir}^2 \tag{2.9}$$

The isothermal sphere is a common assumption that fits to observations of cluster halos. Our goal being to model cases where the halos are massive, this is acceptable. The hydrostatic equilibrium is an idealized situation, as it is specifically applicable to isotropic and homogeneous gaseous halos. Using the virial temperature also means that the halo gas has itself been shocked, or at least compressed, without being able to radiate away its heat.

The density in the halo follows an NFW profile:

$$\rho_0 = f_{\rm b} \rho_{\rm NFW} \left(r_{\rm vir}\right) \approx 37.0 \times f_{\rm b} \rho_{\rm crit} \tag{2.10}$$

The profile derived in Navarro et al. (1997) is known to fit the observed density profiles of halos. It is then appropriate to estimate the values of our initial conditions. However, the NFW profile applies to dark matter. By multiplying it with

the cosmic baryonic fraction, we simply express the fact that before the entry in the halo, gas and dark matter are still coupled. This of course is an extreme assumption, but recent observational results seem to suggest that perhaps the CGM of galaxies has a significant reservoir of gas (e.g., Werk et al. 2014).

The pressure close to the virial radius is then:

$$p_{\rm H} = (k_{\rm B}/\mu m_{\rm p})\,\rho_0 T_H = \frac{\gamma-1}{2}\rho_0 v_{\rm vir}^2 \tag{2.11}$$

This directly results from the two previous choices. As we may see later, this assumption is of great importance, as it sets the thermodynamic boundary condition of the flow.

Hypothesis 4 – The system is impermeable, i.e. mass is conserved along the flow:

$$S\rho_2 v_2 = \rho_1 v_1 \tag{2.12}$$

and there is no (immediate) mixing with the surrounding gas and such mixing only takes place when the hot stream gas has expanded and reached pressure equilibrium with the ambient halo gas.

If the gas originally coming from the IGF mixed at some point with the halo gas, the imaginary boundary of our system would be permeable and we could not rely anymore on the mass conservation relation. The mixing may occur wherever the surface separating the two fluids is the site of a sheared flow. Giving rise to hydrodynamical instabilities such as that of Kelvin-Helmholtz (KHI), the growth rate thereof is to be evaluated. It appears to be, for the choices of densities we will make, of the order of the transverse sound-crossing time, which is in some cases shorter than other times typical of the evolution of our system. However, the rate may only be evaluated at the onset of the instability, where it is maximal, decreasing when entering the nonlinear regime. If the KHI develops, the resulting mixing layer would be restricted in width at its saturation and it would still be correct to apply then our model to a narrower system that does not undergo any rapid mixing.

Hypothesis 5 – The flow system entirely reaches pressure equilibrium with the halo:

$$\rho_{\rm w} T_{\rm w} = \rho_{\rm h} T_{\rm h} = \rho_{\rm H} T_{\rm H} \tag{2.13}$$

This assumption will be tested. The propagation of rarefaction waves from the interface with the halo gas to the innermost region of our flow should occur in a few times the transverse sound-crossing time. Computing this time and comparing it to other dynamical times has proved fundamental to our approach, as will be discussed subsequently.

Hypothesis 6 – The system is adiabatically bounded (no heat exchange) and there is no momentum exchange, momentum is conserved:

$$S\left(\rho_2 v_2^2 + \eta\rho_1 v_1^2 + p_{\rm H}\right) = \rho_1 v_1^2 + p_1 \tag{2.14}$$

which, in virtue of Hypothesis 3, can be written as:

$$S\rho_2 v_2^2 = \left[1 - S\left(\frac{1}{3f} + \eta\right)\right]\rho_1 v_1^2 + p_1 \tag{2.15}$$

For a monatomic gas, the Prandtl number is $\mathrm{Pr} = 2/3$. It relates the viscous term to the heat diffusion term of the energetic equation, so that if viscosity is neglected at the interface with the halo gas, thermal diffusion would also be. Like for the KHI, this layer may be omitted if needed, but viscous effects are very likely to be weak on the scales considered in our model: the Reynolds number is lower than a few hundreds, still close to a laminar regime.

Hypothesis 7 – The warm component has radiated away its heat and ends at the floor temperature:

$$T_{\rm w} = T_0 \tag{2.16}$$

The floor temperature is set by the cooling efficiency of a metal-poor gas, which is very low below 10^4 K and also by possible heating sources of gas at this temperature such as the meta-galactic flux. The ability for the gas to cool down to that temperature is measured by the cooling time, defined later. Like the sound-crossing time, it is essential to compare its value relative to other times in order for our model to be valid.

Hypothesis 8 – The flow first endures a normal shock and the Rankine-Hugoniot equations apply at this stage:

$$\begin{aligned} \rho_{\rm ps} &= \frac{\frac{\gamma+1}{2}\mathcal{M}_1^2}{\frac{\gamma-1}{2}\mathcal{M}_1^2 + 1}\rho_1 && \approx \frac{\gamma+1}{\gamma-1}\rho_1 \\ p_{\rm ps} &= \frac{\gamma-1}{\gamma+1}\left(\frac{2\gamma}{\gamma-1}\mathcal{M}_1^2 - 1\right)p_1 && \approx \frac{2\gamma}{\gamma+1}\mathcal{M}_1^2 p_1 \end{aligned} \tag{2.17}$$

where the subscript $_{\rm ps}$ stands for 'post-shock', and the rightmost members of each line correspond to the asymptotic case of a Mach number much greater than 1.

In fact, this is the strongest assumption we make. The post-shock conditions are indeed derived from it, and hence all the subsequent calculations. The existence of a shock inside the filament is debated. Numerical simulations may have found that it propagates up to a few virial radii but can not accurately resolve the discontinuity. Analytical arguments are not easy to develop either. In the next chapter we will hypothesize about possible ways of forming such a shock. The

planarity and the orthogonality to the flow are chosen for the sake of simplicity. Nevertheless, oblique shocks would not result in very different numbers and curved shocks imply many more parameters to be correctly defined. But ultimately, we will argue that oblique and curved shocks may be central to understanding how post-shock gas may fragment.

Hypothesis 9 – If the phase separation occurred after having expanded, both component have the same bulk motion:

$$v_{\rm w} = v_{\rm h} = v_2 \tag{2.18}$$

and if the phase separation occurred before the expansion, then:

$$v_{\rm w} = v_{\rm ps},\ v_{\rm h} = v_2 \tag{2.19}$$

In other terms, the mass of gas that will end up being warm must keep the velocity it has when the cooling begins, since both its mass and its momentum are constant, provided that warm clouds fly freely into the hot component. In one asymptotic case, the warm component forms rapidly just after the shock, it keeps the post-shock velocity. In the other asymptotic case, it starts cooling after the pressure has adjusted to the halo and thus after the bulk velocity has evolved accordingly to the cross-section of the flow. This relation is needed to close the system of equations. But it depends on the ratio of the cooling to the sound-crossing time. As we will see, even if the intermediate situation is the most likely one, the two extreme cases (a ratio much greater or much lower than one) are of great help in understanding the evolution of the flow.

Hypothesis 10 – The hot component has only adiabatically and reversibly, i.e., no heat transfer and no entropy increase, expanded since the post-shock stage:

$$\rho_{\rm h}^{\gamma} p_{\rm ps} = \rho_{\rm ps}^{\gamma} p_{\rm H} \tag{2.20}$$

which is strictly equivalent to:

$$\rho_{\rm h}^{\gamma-1} T_{\rm ps} = \rho_{\rm ps}^{\gamma-1} T_{\rm h} \tag{2.21}$$

This directly derives from Hypothesis 6 and from the assumption that the loss of pressure due to the cooling of a fraction of the gas will not significantly affect the remaining hot fraction.

Hypothesis 11 – Turbulence is only carried by the warm phase in the form of relative random motions:

$$\eta \rho_1 v_1^2 = \widetilde{\rho_{\rm w}} \sigma^2 = x_{\rm w} \rho_{\rm w} \sigma^2 = y_{\rm w} \rho_2 \sigma^2 \tag{2.22}$$

where σ is the velocity dispersion associated with turbulence, more precisely the final warm cloud velocity dispersion. Written this way, this term has the dimension

of a pressure and precisely corresponds to the Reynolds-averaged stress tensor, when inserted into the Reynolds-averaged Navier-Stokes equation (RANS).

2.4 From our initial phenomenological analysis to a more general model

The model that we have just outlined, with its set of hypotheses, enabled us to successfully derive various relations that are useful for a more general and perhaps more appropriate model for streams passing through an accretion shock. The fact that several quantities are free parameters also allowed us to explore a wide range of parameter space. Some surfaces in the $(f, \eta, \phi_{\rm v,w})$ space bound with the subspace where the solutions to the equations exist. This is also one of the reasons why we performed a numerical experiment as described in the next chapter, as a means to constrain parameters and to better understand the initial conditions for the stream before it penetrates the halo.

After a year and a half of exploration, we developed a more complete phenomenological model for streams penetrating halos. The development just described in the previous section was useful for setting the stage for the evolution of the post-shock streaming gas. Now however, to understand the impact of allowing for expansion and fragmentation of the post-shock accreting gas within the context of galaxy evolution, we have to consider various timescales that are relevant for galaxies. The salient time scales that necessary to understand the evolution of the the post-shock gas are: the time necessary for the gas to cool – the post-shock cooling time scale; the hot post-shock gas will expand into the ambient halo gas. We estimate this expansion timescale as a relative rate of change in the pressure, assuming the expansion is adiabatic. The leads to the concept of the "post-expansion" cooling time; to understand how the stream may evolve, we compare these timescales with the dynamical time of the halo. There are other relevant timescales of course, as we describe, but it is the relationships between these characteristic timescales, that are essential for establishing the regimes in which the post-shock gas might become bi-phasic and turbulent. Doing a parameter space search phenomenologically by comparing various timescales for different post-shock temperature (halo masses) and stream over-densities, always us to investigate which regimes where the gas will not develop a bi-phasic structure. For example, in what regime the post-shock gas will remain hot or cool quickly reforming a warm stream of gas. To make such an analysis, we rely now on the assumption that through a variety of mechanisms, like obliqueness of the shock or inhomogeneities in the accreting stream, the post-shock gas is inhomogeneous. With these more general developments and timescale comparisons, we can now

investigate: When and how do post-shock gas in streams become multi-phased and turbulent?

2.5 Are cosmological gas accretion streams multi-phase and turbulent?

We here reproduce *in extenso* the article submitted to Astronomy and Astrophysics and whose initial version had been published on ArXiv as Cornuault et al. (2016). We added two subsections developping and extending the model for a time-evolving distribution which we used in the paper.

2.5.1 Introduction

The realization that we live in a dark matter dominated universe led to the development of the first comprehensive theory of galaxy formation (e.g. White & Rees, 1978b; Fall & Efstathiou, 1980b). These analytic models embedded simple gas physics into the hierarchical growth of structure whereby smaller halos merged over time forming successively more massive halos (White & Rees, 1978b). Despite the successes of this model in understanding the scale of observed galaxy masses, it was soon realized that there were a number of problems. The most significant is that modeled galaxies form with a higher fraction of baryons than is observed (e.g., Ferrara et al., 2005; Bouché et al., 2006; Anderson & Bregman, 2010; Werk et al., 2014). This failure was dubbed the "over-cooling problem" (Benson et al., 2003).

As numerical simulations allowed for galaxy growth to be coupled to the development of large scale structure, they showed that much of the accreting mass may penetrate into the halo as filaments of gas and dark matter (Kereš et al., 2005; Ocvirk et al., 2008a). Whether or not these streams pass through a stable accretion shock as they penetrate the halo depends on the mass and redshift of the halo (Birnboim & Dekel, 2003; Dekel & Birnboim, 2006, hereafter BD03 and DB06 respectively). If the shock is not stable, the accretion flow is "cold". This "cold mode" accretion in simulations occurs as streams of warm (10^4 K) gas entering the halo, smooth at kpc-scale and weakly coupled to the infalling dark matter filaments (Danovich et al., 2015; Wetzel & Nagai, 2015). Cold mode accretion is efficient in reaching down to a few tenths of a virial radius (Dekel & Birnboim, 2006; Behroozi et al., 2013). The high efficiency of gas accretion in some simulations leads to model galaxies with unrealistically high baryon fractions emphasizing the over-cooling problem. To alleviate the problem of excess baryons in simulated galaxies, efficient outflows and feedback were introduced (e.g., Hopkins et al., 2012,

2016). Feedback both heats the gas in the halo, preventing it from cooling, and also ejects gas from both the galaxy and halo lowering their total gas content.

The circum-galactic media of galaxies are certainly not devoid of gas, perhaps containing up to approximately half of the total baryon content of the halo (e.g., Werk et al., 2014; Peek et al., 2015). This gas is known empirically to be multiphase. The multiphase nature of halo gas is most evident in local high mass halos, those with masses on the scales of cluster or groups. In clusters, for example, even at constant pressure, a very wide range of gas phases are observed, from hot X-ray emitting gas to cold, dense molecular gas (e.g., Jaffe et al., 2005; Edge et al., 2010; Salomé et al., 2011; Tremblay et al., 2012; Hamer et al., 2016; Emonts et al., 2016). In galaxy halos, the detection of multiphase gas is mostly through the absorption lines from warm neutral and ionized gas ($\lesssim 10^4$ to $\sim 10^6$ K) and dust via the reddening of background galaxies and quasars (Ménard et al., 2010; Peek et al., 2015, but see Pinto et al. 2014 for the detection of hot gas in X-ray emission lines). Outflows from galaxies are also multiphase (e.g., Beirão et al., 2015; Heckman & Thompson, 2017) and are likely crucial for creating and maintaining the multiphase gas in halos (e.g., Gaspari et al., 2012; Sharma et al., 2012a; Borthakur et al., 2013; Voit et al., 2015b; Hayes et al., 2016).

There is only circumstantial evidence for smooth, collimated accretion streams penetrating into galaxy halos (e.g., Martin et al., 2015; Bouché et al., 2016; Vernet et al., 2017a, and references therein). In analogy with analyses of gas in halos and outflows, a phenomenological approach may provide additional insights into the nature of flows and halos that galaxy simulations are perhaps not yet achieving (e.g., Sharma et al., 2010, 2012a,b; Singh & Sharma, 2015; Voit et al., 2015b,a; Thompson et al., 2016). The notion that over-cooling remains a problem in simulations, that there is scant observational evidence for the streams of the type currently simulated, and because high speed collisions of gas can lead to multiphase turbulent media (Guillard et al., 2009, 2010; Ogle et al., 2010; Peterson et al., 2012; Appleton et al., 2013; Alatalo et al., 2015), all motivated us to analyze gas accretion flows phenomenologically.

Just as with the explanation for the lack of cooling flows in clusters (e.g., Peterson et al., 2003; Rafferty et al., 2008), our current understanding of accretion flows in galaxy halos may also suffer from an overly simplistic view of gas thermodynamics. In clusters, it is now understood that heating and cooling are in approximate global balance, preventing the gas from cooling catastrophically (e.g., Rafferty et al., 2008; Sharma et al., 2012a,b; McCourt et al., 2012; Zhuravleva et al., 2014; Voit et al., 2015a). In analogy with gas in cool core clusters, and in contrast to what a number of cosmological simulations currently show, the gas in streams may not cool globally. Instead, if the gas in streams is inhomogeneous and subject to thermal and hydrodynamic instabilities (e.g., Sharma et al., 2010), the

differences in cooling times between the gas phases will lead to fragmentation of the gas. If streams are unstable, their gas will not remain monophasic or laminar. Thus, our goal in this paper is to investigate the question posed in the title: "Are Cosmological Gas Accretion Streams Multiphase and Turbulent?". If yes, the gas energetics may regulate the gas accretion efficiency. Dekel et al. (2013) estimated the penetration efficiency over large halo scales at z$\sim$2 of $\sim$50% but this estimate only considered macroscopic processes that may influence the accretion efficiency. Because heating and cooling are controlled by the mass, energy and momentum exchanges between the gas phases, a careful investigation of the gas physics on microscopic scales is required to investigate whether those microphysical processes may further reduce the efficiency of gas accretion onto galaxies.

To investigate the question posed in the title, we begin by presenting a qualitative sketch of our scenario, make a quantitative investigation of the impact of expansion in the post-shock gas on an accretion flow, and then discuss the case where the post-shock gas has small fluctuations in density and temperature, developing a criterion for when the gas will fragment (§ 2.5.2). In § 2.5.3, we discuss the consequences of the formation of a multiphase flow on the thermodynamic evolution of the stream after it penetrates the halo. To gauge the astrophysical pertinence of our model, we analyze the evolution of an idealized gas accretion stream into a halo of $10^{13}\,M_{\odot}$ at z=2 (§ 2.5.4). In Section 2.5.5, we discuss why simulations may be missing some ingredients necessary for modeling accretion shocks robustly and outline a few simple consequences of our proposed scenario.

2.5.2 Our framework for multi-phased streams

The idea that gas in halos is multiphase has been suggested for decades (e.g., Binney, 1977; Maller & Bullock, 2004). More recent studies of halo gas attribute the development of multiphase gas to the growth of local thermal instabilities (e.g., Sharma et al., 2010) or galaxy outflows (e.g., Thompson et al., 2016; Hayes et al., 2016). Thermal instability is only relevant when the cooling time of the unstable gas is of the same order-of- magnitude or smaller than the dynamical time of the halo (e.g., Sharma et al., 2012a; McCourt et al., 2012). In ambient halo gas and outflows from galaxies, the gas must often meet this requirement given that they are observed to be multiphase. However, in an accreting stream of gas, it is difficult to understand how the gas might achieve such a balance in heating and cooling. We may have to consider other processes to determine if it is possible for streams themselves to become multiphased as they flow into the halo. In the following sections, we examine the physics of gas flowing into halos from cosmic web filaments.

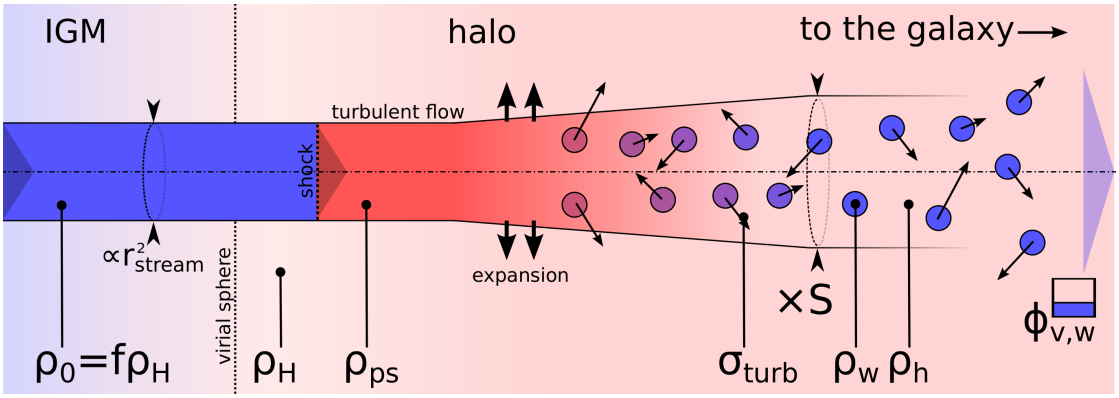

Figure 2.1: Sketch of our phenomenological picture of flows of gas passing through a virial shock. The initial inflowing gas (in blue) is over-dense relative to the halo gas at the boundary by a factor f ($=\rho_0/\rho_{\rm H}$ or the stream density divided by the density of the ambient halo gas at the virial radius), shocks at the boundary between the inter-galactic medium (labeled as "IGM") and the hot halo gas (labeled as "halo"). The persistent virial shock and the higher pressure of the post-shock gas compared to the ambient halo gas, allows the flow to expand after being shocked (labeled as "expansion"). The post-shock gas may become unstable, fragmenting to form a biphasic medium. The fragmentation enables a fraction of the initial momentum and energy of the stream to be captured as turbulent clouds of warm gas with a dispersion, $\sigma_{\rm turb}$, and a volume-filling factor, $\phi_{\rm v,w}$. The clouds may move beyond the initial radius of the stream, de-collimating the flow. Eventually, the hot post-shock gas mixes with the ambient halo gas which prevents it from cooling further. See text and the Appendix for definitions of the variables.

Qualitative sketch of our specific framework

We briefly qualitatively outline our scenario of gas accretion through streams, sketched in Fig. 2.1, introducing the concepts developed later in the paper. We consider a collimated stream of warm gas with a temperature of 10^4 K that penetrates into a dark matter halo filled with hot gas at the halo virial temperature. The smooth density distribution of the hot gas follows the density distribution of the underlying dark matter halo. The ambient halo gas has a long cooling time and has constant density and temperature during the flow. The speed of the flow is set to the virial velocity of the halo and is highly supersonic relative to the sound speed of the gas within the stream. In the following we introduce the three basic physical ingredients of our modeling of streams.

As the stream penetrates at the virial radius, we assume it is shock-heated whenever the hot halo gas provides the necessary pressure support for sustaining the shock (§ 2.5.2). The post-shock gas is over-pressurized relative to the ambient halo gas and expands, invalidating the classical one-dimensional analysis of streams (DB06, Mo et al., 2010). The hot post-shock gas mixes with the ambient halo gas, which prevents much of the gas initially in the stream from cooling completely to form a monophasic post-shock stream. We further posit that the post-shock gas will develop inhomogeneities due to, for example, non-planarity or obliqueness of the shock-front or through inhomogeneities in velocity and/or density of the stream before it is shocked. The fragmentation of the gas into hot and warm cloudy phases is central to our scenario. If certain physical conditions are met, the expanding inhomogeneous gas will cool and fragment, forming a two phase medium – a hot phase with an embedded warm cloudy phase (§ 2.5.2). Density and velocity inhomogeneities in the post-shock gas may be amplified through gas cooling, leading to the formation of a multiphased flow (see § 2.5.2).

We expect that part of the kinetic energy of the infalling gas will be converted to turbulence within the warm clouds and random cloud-cloud motions (e.g., Hennebelle & Pérault, 1999; Kritsuk & Norman, 2002a; Heigl et al., 2017). If the level of turbulence is high or if the clouds are formed while the gas is expanding, the warm clouds may spread beyond the initial boundary of the collimated inflowing stream (Fig. 2.1 and see § 2.5.3). If these conditions are met, the stream will decollimate. The thermodynamic evolution of the post-shock gas in the stream is largely determined by the timescales of several relevant processes – gas cooling, expansion of the hot phase, dynamical time of the halo, and the stream disruption due to turbulent motions – which we quantify in the remainder of this and the next section.

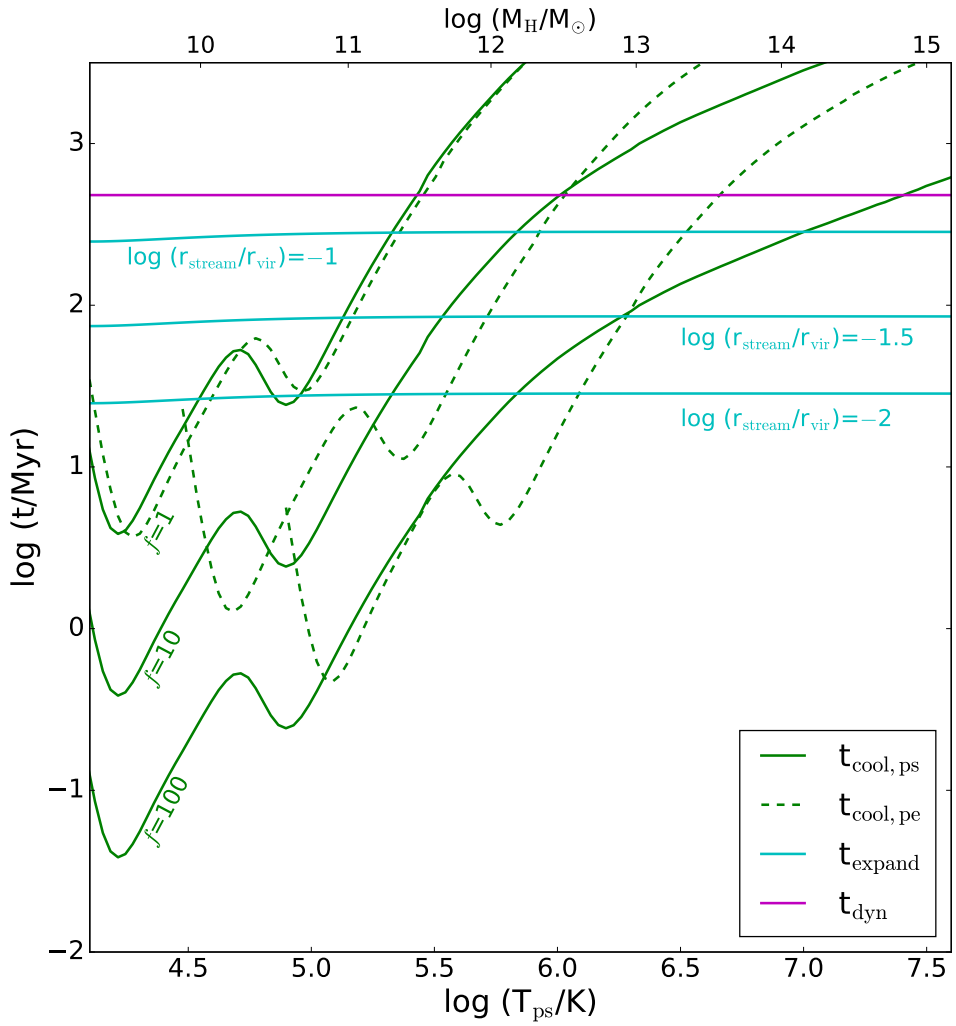

Figure 2.2: Timescale comparison of the competing relevant processes of cooling, expansion, and halo dynamics, for different post-shock temperatures (i.e., different halo masses), at redshift $z = 2$. Cooling times (green) are times of isobaric cooling from a given temperature-density couple. The solid green curves indicate the instantaneous post-shock cooling time, $t_{\rm cool,ps}$, and the green dashed curves indicate the post-expansion cooling time, $t_{\rm cool,pe}$ – the cooling time of the post-shock after it has expanded sufficiently to reach pressure equilibrium with the ambient halo gas. The cooling time curves for the post-expansion gas are truncated at the minimum temperature spanned by the curves, 10^4 K. The cooling time curves were computed for three values of the initial over-density f, as indicated by green labels on the left side of the panel. Expansion times (solid cyan lines) are shown for three different relative filament radii, $\log_{10}$ $\rm r_{stream}/r_{vir}$=−1, −1.5, and −2. The dynamical time, $t_{\rm dyn,halo}$, which is independent of halo mass, is indicated by the horizontal magenta line.

The Impact of Expansion on the Phenomenology of Accretion Flows

Since the pioneering work of White & Rees (1978b) decades ago, the accretion of gas onto galaxies or into halos has been analyzed in one, radial dimension, assuming homogeneity of the flow (see Mo et al., 2010). The one-dimensional approximation is also used for streams, where it is valid only if one can ignore lateral expansion. To know if this approximation is valid, one has to compare the expansion to cooling time of the gas within the flow. Historically, even the analysis of the stability of the accretion shock neglected the possibility that the post-shock gas may expand into the ambient halo gas gas (DB06; Mo et al., 2010). In our study, we reconsider the sustainability of the accretion shock that occurs as the infalling filament collides with the ambient halo gas. To conduct this analysis, we compare the cooling time of the post-shock gas to various other measures of its dynamical evolution. For simplicity, we only compare the cooling time to the expansion time of the post-shock gas into the surrounding ambient halo gas and the dynamical time of the halo. Intuitively, one can understand that if the cooling time is significantly shorter than either the expansion or dynamical times, the stream after the shock will quickly cool down and maintain much of its integrity. Such a shock can be unstable and this is essentially the textbook situation that has been considered already (Mo et al., 2010). If the cooling time of the post-shock gas is significantly longer than either the expansion or dynamical times, then the post-shock gas will mix the ambient halo gas further supplying it with hot gas and entropy. This is another textbook example that has been analyzed one-dimensionally (DB06; Mo et al., 2010). However, if the cooling time is of the same order-of-magnitude of the expansion and halo dynamical times, a wider range of outcomes of the post-shock gas are possible (e.g., Sharma et al., 2010, 2012b). This is the point of this paper – to describe phenomenologically this more complex regime.

We now consider the impact of expansion on the properties of the post-shock gas. To estimate the cooling, expansion, and dynamical timescales, we introduce two parameters specific to the flow, its over-density relative to that of mean density of gas at the virial radius, f, and the radius of the stream, $r_{\rm stream}$. All variables used in this and subsequent sections are summarized in Tables 2.1 and 2.2 of the Appendix. As we now show, the gas in the stream immediately after being heated to a high post-shock temperature, $T_{\rm ps}$, has a pressure, $P_{\rm ps}$, higher than the ambient halo gas, $P_{\rm H}$, and thus expands into the surrounding ambient halo gas of density, $\rho_{\rm H}$. All of the post-shock quantities are given by the normal Rankine-Hugoniot shock relations (see Appendix for appropriate formulae). The halo pressure at the virial radius is,

$$P_{\rm H} = \left(\frac{k_{\rm B}}{\mu m_{\rm p}}\right)\rho_{\rm H} T_{\rm H} = \frac{(\gamma-1)}{2}\rho_{\rm H} v_{\rm vir}^2 = \frac{\gamma \mathcal{M}_1^2}{3f} P_0 \tag{2.23}$$

where $T_{\rm H}$ is the temperature of the ambient halo gas, which we have assumed to the be virial temperature. The pressure ratio just after the shock is,

$$\frac{P_{\rm ps}}{P_{\rm H}} = \frac{2f}{\gamma\,(\gamma+1)\cdot g\,(\mathcal{M}_1)} \tag{2.24}$$

where $g : M_1 \mapsto (2\gamma/(\gamma-1) - M_1^{-2})^{-1}$. For $\gamma = 5/3$ and within the domain $[1,+\infty]$, this function rapidly decreases from 1/4 to 1/5. Hence the pressure ratio, $P_{\rm ps}/P_{\rm H}$ is between 9/5 and 9/4 times the initial stream over-density, f. Since $f \gtrsim 1$, the pressure of the post-shock gas is higher than the pressure of the ambient halo. Thus, since the pressure ratio is always greater than one, the flow will expand into the ambient halo gas.

To define the expansion time of the flow, we approximate this as the inverse of the relative rate of change of pressure in the post-shock gas as it expands. Quantitatively, this is,

$$t_{\rm expand} = P_{\rm ps}/\dot{P}_{\rm ps} = -2\gamma r_{\rm stream}/\dot{r}_{\rm stream} \sim 2\gamma r_{\rm stream}/c_{\rm ps} \tag{2.25}$$

where $r_{\rm stream}$ is the initial radius of the stream before it expands and $c_{\rm ps}$ is the sound speed of the gas immediately after passing through the shock front. As a first order approximation, in the case of a homogeneous post-shock medium, one can easily compare the cooling and expansion times. Our definition of the expansion time means it is a differential measure of the expansion and so the most appropriate comparison is with the instantaneous cooling time of the gas immediately after the shock. The isobaric cooling time is defined as,

$$t_{\rm cool}(T) = T\left|\frac{dT}{dt}\right|_P^{-1} = \frac{5k_{\rm B}\rho T}{2\mu n_e n_{\rm H}\Lambda(T)} \approx 4.3 \times \frac{5k_{\rm B}\mu m_{\rm p} T}{2\rho\Lambda(T)} \tag{2.26}$$

where $k_{\rm B}$ is the Boltzmann constant, $\Lambda\,(T)$ is the electronic cooling efficiency as a function of temperature, T (Sutherland & Dopita, 1993; Gnat & Sternberg, 2007), μ is the mean molecular weight[4], $m_{\rm p}$ is the mass of the proton, ρ is the mass density of the cooling gas, n_e is the electronic density and $n_{\rm H}$ the Hydrogen particle density[5]. Hereafter, the cooling time of the post-shock is denoted by, $t_{\rm cool,ps}$. We also refer to the cooling time after expansion, noted $t_{\rm cool,pe}$.

The other timescale with which to compare the cooling time is the dynamical time of the halo. It is simple to estimate the dynamical time. We estimate the

[4] $\mu = 0.6\,m_{\rm p}$ for a fully ionized gas.

[5] The factor 4.3 in Eq. 2.26 comes from $n_e = 1.2 n_{\rm H}$ and $n_{\rm H} \approx \rho/(1.4\,m_{\rm p})$.

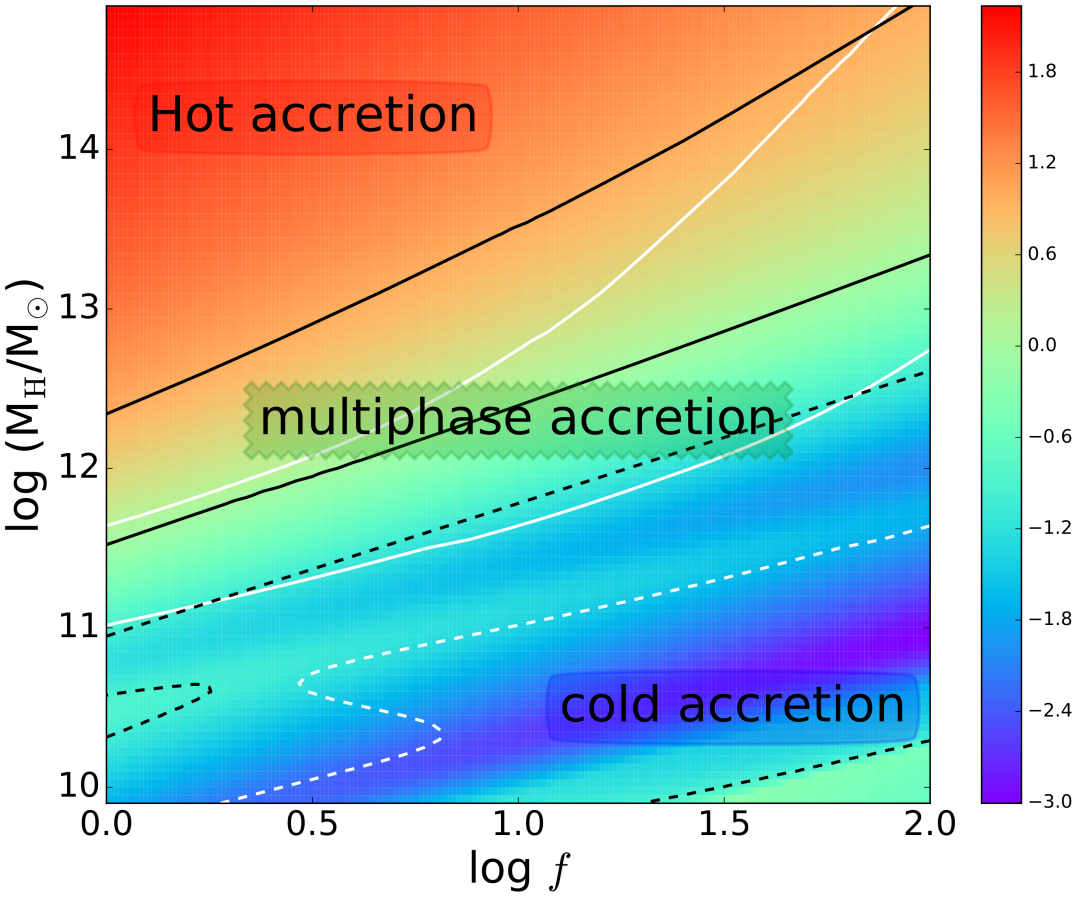

Figure 2.3: Ratio of the post-expansion cooling and halo dynamical timescales as a function of halo mass, $M_{\rm H}$, and stream over-density, f, at redshift, z=2. The colors represent the $\log(t_{\rm cool,pe}/t_{\rm dyn,halo})$ (Eqs. 2.26 and 2.27) whose corresponding values are indicated by the color bar. The solid black lines indicate $\log(t_{\rm cool,pe}/t_{\rm dyn,halo})$ of increasing values of 0 and 1 from the middle to the top of the diagram. Dashed black lines indicate $\log(t_{\rm cool,pe}/t_{\rm dyn,halo})$=−1. The white contours indicate values of $\log(t_{\rm cool,ps}/t_{\rm expand})$ (Eqs. 2.25 and 2.26) equal to 0 and 1 (solid), and −1 (dashed). For this analysis, we have assumed $\log({\rm r_{stream}/r_{vir}})$=−1.5. We highlight regions where the cooling times are significantly longer than the halo dynamical times as "hot accretion", regions where the cooling time is significantly shorter than the dynamical times as "cold accretion", and regions where the cooling times are of the same order-of-magnitude as the dynamical times as "multiphase accretion" (see text for details). These labels are illustrative and are not intended to precisely delineate a clean separation in the timescales.

dynamical time for matter falling from the virial radius with a radial velocity of v_2 (the post-shock velocity) directed at the center of the potential as,

$$t_{\rm ff} = \alpha \frac{r_{\rm vir}}{v_2} \approx t_{\rm dyn,halo} \tag{2.27}$$

For this estimate, we assume a NFW dark matter potential (Navarro et al., 1997) and α, is a factor of-order unity to account for the integrated gravitational acceleration during the fall. Assuming that the characteristic velocity and radius are the virial values, $v_{\rm vir}$ and $r_{\rm vir}$, the dynamical time is independent of halo mass (Mo et al., 2010).

Fig. 2.2 illustrates how these time scales depend on the post-shock temperature, directly related to the halo mass (top x-axis) and for a range of relative stream over-densities, f, and relative stream radii, $r_{\rm stream}/r_{\rm vir}$ at z=2. The initial stream penetrating the halo gas and the warm post-shock clouds are assumed to have a temperature of 10^4 K, which is maintained through external heating processes, such as the ionization by the meta-galactic flux or ionizing photons from the galaxy in the halo. Since the post-shock temperatures are proportional to velocity, the post-shock temperature translates into dark matter halo mass. From this analysis, we see that the expansion times are almost constant above $M_{\rm H} \gtrsim$ few$10^{10}\,{\rm M}_\odot$ since the virial shock is sufficiently strong such that $t_{\rm expand} \propto t_{\rm dyn,halo}$. As f increases, the cooling times decrease systematically, which means for low temperatures (low mass halos at z=2), the cooling time is always less than the expansion time. For very high mass halos, even for wide streams with relatively high densities, the cooling time is much longer than the expansion time and can be longer than the halo dynamical time for low to moderately over-dense filaments. A wide range of values in f and $r_{\rm stream}/r_{\rm vir}$ lead to cooling times that are less than the halo dynamical time and within an order-of-magnitude of the expansion time. Whenever the expansion time is comparable to the cooling time, the gas flow will globally cool neither purely adiabatically or isobarically.

We can understand the competition between these time scales, $t_{\rm cool,ps}$, $t_{\rm cool,pe}$, $t_{\rm dyn,halo}$, and $t_{\rm expand}$, more clearly by considering them as a function of the stream over-density, f, and post-shock temperature or halo mass (Fig. 2.3). For the case where $t_{\rm cool,ps} >> t_{\rm expd}$ and $t_{\rm cool,pe} > t_{\rm dyn,halo}$, the post-shock gas will expand rapidly remaining hot over at least a dynamical time of the halo. In this regime the hot post-shock gas will likely mix with the ambient halo gas preventing significant cooling. This is akin the "hot mode accretion" discussed by Dekel and collaborators (e.g., DB06). In Fig. 2.3, we have labeled this regime, "hot accretion". At the other extreme in Fig. 2.3, when $t_{\rm cool,ps} << t_{\rm expand}$ and $t_{\rm cool,ps} << t_{\rm dyn,halo}$, the gas cools before significant expansion and before the stream has penetrated deeply into the halo. Accretion in this regime corresponds to their "cold mode accretion" and have labeled it as such in Fig. 2.3. In between these two regimes, $t_{\rm cool,pe}$, $t_{\rm cool,ps}$,

$t_{\rm dyn,halo}$, and $t_{\rm expand}$ are all about the same order-of-magnitude. In this regime, there is not a simple dichotomy between the types of accretion streams – they can be both hot and warm if the post-shock gas has a range of temperature and/or densities and the thermodynamic evolution of the post-shock gas will be more complicated. We labeled this regime "multiphase accretion" in Fig. 2.3.

Inhomogeneous infalling streams and post-shock gas: differential cooling

We now discuss the physical mechanisms behind the development of multiphasic accretion streams. Although our previous discussion of the relevant timescales considered homogeneous streams, density and velocity inhomogeneities may arise through the dynamics of the shock itself (Kornreich & Scalo, 2000; Sutherland et al., 2003). Simulations show that stream are not accreted homogeneously but have substructure in both density and velocity (Nelson et al., 2016). Inhomogeneities may arise due to a range of curvature in accretion shock-fronts, translating into a range of Mach numbers and post-shock temperatures and densities. Density fluctuations at constant shock velocity will also lead to inhomogeneities in the post-shock gas in both temperature and density resulting in a range of cooling times (Guillard et al., 2009). As we now discuss, once such "differential cooling" sets in, it acts like the thermal instability, leading to phase separation in the flow (Sharma et al., 2012a), but over a finite range of time in the absence of a heating process balancing cooling of the hot phase.

To understand how the inhomogeneous post-shock gas evolves, we investigate how small fluctuations in the density and/or temperature are amplified. Neglecting the influence of any heating process, the radiative cooling is not balanced and there are no fixed equilibrium points. Following closely the development in Sharma et al. (2012a), we begin with a parcel of gas that is over-dense relative to an ambient medium. The magnitude of the over-density is, $\delta \equiv |\delta\rho/\rho| \sim |\delta\,\mathrm{T}/\mathrm{T}|$ for isobaric conditions. The inverse of the effective cooling time of the over-dense gas parcel relative to the ambient medium is then

$$\frac{1}{t_{\rm cool,eff}} = -\frac{1}{t_{\rm cool,parcel}} + \frac{1}{t_{\rm cool,ambient}} \ . \tag{2.28}$$

As already shown by Sharma et al. (2012a), for small over-densities, $\delta \leq 1$, the inverse of the effective cooling time under isobaric conditions is

$$\frac{1}{t_{\rm cool,eff}} \sim -\delta \frac{\partial}{\partial \ln \mathrm{T}} \left(\frac{1}{t_{\rm cool}}\right)_{\rm P} = \frac{\delta}{t_{\rm cool}} \left[2 - \frac{\mathrm{d}\ln\Lambda(T)}{\mathrm{d}\ln T}\right] \ . \tag{2.29}$$

Marginally denser gas cools faster than the gas in which it is embedded and the cooling becomes a runaway process for temperatures below a few $10^5\,\mathrm{K}$. We

refer to this process as *"differential cooling"*. As soon as heterogeneities form in approximate pressure equilibrium with their surroundings, denser cooler regions of the gas will cool rapidly, forming clouds, leaving a hotter, rarer, high volume-filling inter-cloud medium. Thus, differential cooling leads to multiphasic post-shock accretion flows. This is akin to what occurs for thermally unstable gas (Field, 1965) but the phase separation is transient in the absence of a heating process of the hot gas balancing cooling.

Of course, a natural consequence of differential cooling is that even for halo masses where the post-shock gas has on average a long cooling time, gas with fluctuations in temperature or density may locally cool sufficiently rapidly to form a multiphased stream.

Analytically, inhomogeneities can be accounted for as is done in phenomenological analyses of the formation of stars through the use of probability distribution functions (PDFs) in gas density and/or temperature (e.g., Hennebelle & Chabrier, 2009). We follow the thermodynamical evolution of the temperature and density PDFs using the energy equation, namely,

$$\dot{e} = -\rho \frac{\Lambda(T)}{4.3 \mu m_p} + P \frac{\dot{\rho}}{\rho^2} \ , \tag{2.30}$$

where e is the specific internal energy. We illustrate the isobaric evolution of inhomogeneities in a flow using such an approach in Fig. 2.4. In this illustration, we consider a log-normal PDF in temperature with a dispersion of $\sigma_T = 0.3$ (1σ dispersion of $\log \frac{\rho}{\rho_0} = \log \frac{T}{T_0}$, where ρ_0 and T_0 are the initial mean values of the density and temperature, with corresponding cooling time $t^0_{\rm cool}$). We have chosen a gas pressure and mean temperature appropriate for the post-shock gas of a flow into a massive, 10^{13} $M_\odot$, halo at z=2 (see § 2.5.4). For this illustration, the gas pressure is $P/k = 5.8 \times 10^4$ K cm^{-3}, and the initial mean temperature T_0=2.7 $\times$ 10^6 K. We find that a substantial fraction of the accreting gas cools to 10^4 K in a fraction of $t^0_{\rm cool}$, while the peak of the hot gas temperature PDF does not shift with time (see Fig. 2.4).

We show in Fig. 2.5 both the mass fraction and volume-filling factor of the gas that cools to 10^4 K as a function of time. Note that since the results shown on Figs. 2.4 and 2.3 are plotted as a function of the initial cooling time $t^0_{\rm cool}$, to a first approximation they are not much dependent on the specific values of ρ_0 and T_0. Those results also apply to the gas cooling after expansion when $t_{\rm expand} << t^0_{\rm cool}$. Figure 2.3 shows that the warm gas becomes the dominant mass phase, within about half of the post-shock cooling time, and that the warm gas only fills a small fraction of the volume. For a larger value of the temperature dispersion $\sigma_{\rm T}$, $\Phi_{\rm m,w}$ increases over a broader range of fractional times distributed around the same mean value.

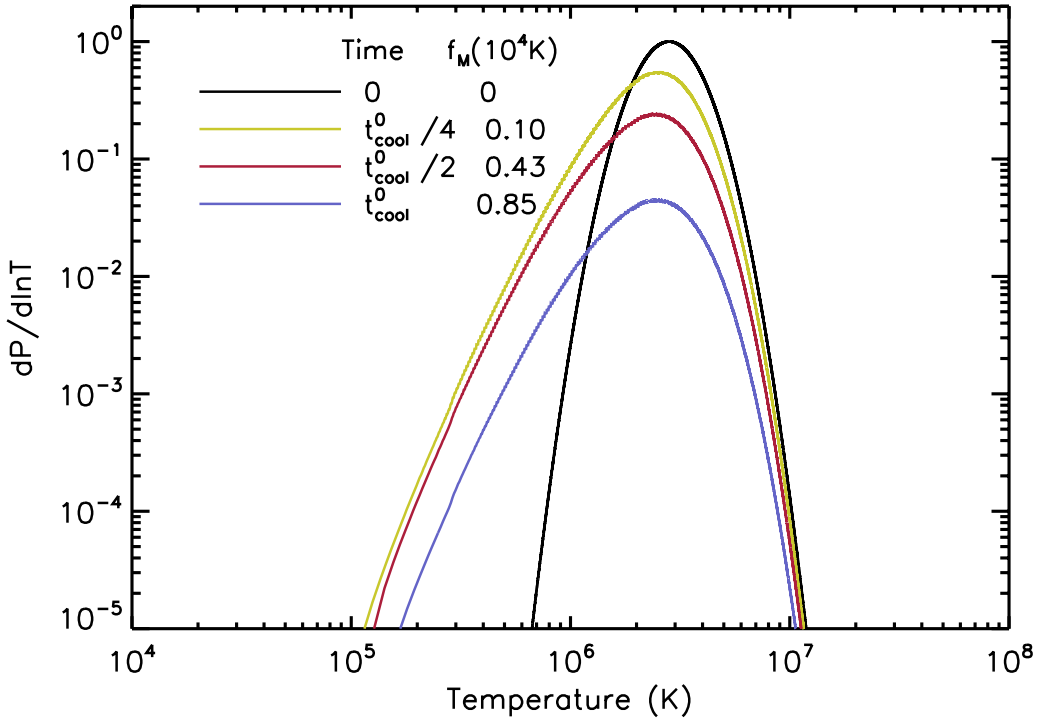

Figure 2.4: Probability distribution function of the gas temperature at different times for isobaric cooling. The initial distribution (black line) is log-normal with a dispersion, $\sigma_{\rm T} = 0.3$, and an initial mean gas temperature, T_0=2.7×10^6 K. The distribution at a time equal to the initial isobaric gas cooling time is plotted in blue, that of half and a quarter of this time in red and green, respectively. In the last column of the legend, we indicate the fraction of the gas that has cooled to 10^4 K within the indicated fraction of the cooling time. For example, in this illustration, after one cooling time, approximate 85% of the gas has cooled to 10^4 K.

In Fig. 2.5, the gas is multiphase for only a few $t^0_{\rm cool}$. The hot gas eventually cools because we have not considered any heating processes. However, the process of fragmentation of the gas could be sustained if there is heating of the hot gas. Even in absence of heating, after expansion the hot gas will eventually mix with the ambient halo gas thus sustaining the hot phase. Possible local sources of heating for the post-shock gas are the radiative precursor of high velocity shocks, thermal conduction, radiation from the surrounding hot medium, and dissipation of turbulence. The mechanical energy input from active galactic nuclei (AGN), winds generated by intense star formation, and other processes can plausibly balance the cooling of the hot gas globally (e.g., Best et al., 2007; Rafferty et al., 2008). Overall, there is more than enough energy, but what is unknown is how and with what efficiency this energy is transferred to the streaming gas. Even though simulations do not capture this process, it has been suggested that the energy from the galaxy is transferred efficiently through turbulent energy cascade and dissipation (Zhuravleva et al., 2014; Banerjee & Sharma, 2014).

A poignant question to ask is can the flowing post-shock gas actually become multiphase while cooling in a halo dynamical time? It is a difficult question to answer in the particular case of accretion streams because it depends on how inhomogeneous the gas is. It will occur if the post-shock conditions are sufficiently inhomogeneous. The gas will become multiphased around when $t_{\rm cool,pe}$ is the same order-of-magnitude as $t_{\rm dyn,halo}$. This justifies where we placed the "multiphase accretion" label in Fig. 2.3. This figure shows that this occurs in the important mass range of $\rm M_{halo}{\sim}10^{11}$ to 10^{13} $\rm M_\odot$. The values of course depend on the relative over-density of the streams (f) and through the characteristics of the halos, on redshift. Halos within this mass range is where the bulk of stars have formed in galaxies. Moreover, because the volume filling factor of the warm gas is likely to be always small, even in the cases where the mass fraction is large, multiphase streams are likely to be difficult to identify observationally. We discuss this further in § 2.5.5.

2.5.3 Consequences of the formation of multiphased, cloudy accretion flows

Turbulence in warm clouds

As the gas fragments, perhaps due to differential cooling and/or thermal instabilities, we assume that some of the initial kinetic energy of the stream is converted into turbulence within the warm component. We parameterize the turbulence after phase separation as the ratio, η, of the turbulent energy density of the clouds and the initial bulk kinetic energy density of the stream. We define this ratio as,

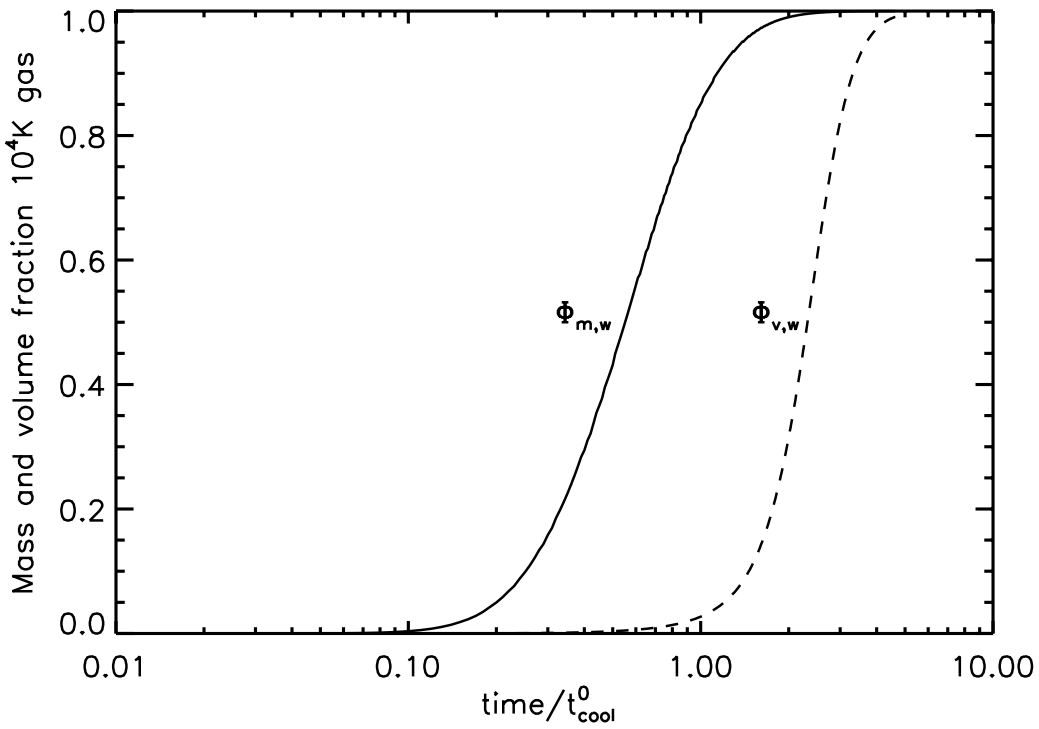

Figure 2.5: The change in the mass fraction, $\phi_{\rm m,w}$, and the volume filling-factor, $\phi_{\rm v,w}$, of the warm, 10^4 K gas as a function of the post-shock cooling time. The time scale is expressed in units of the isobaric cooling time, t^0_{cool} as defined in the text. The values of the pressure and temperature are the same as those used in Fig. 2.4.

$$\eta = \frac{\langle \rho_{\rm w} \rangle_{\rm v} \, \sigma_{\rm turb}^2}{\rho_1 v_1^2} \tag{2.31}$$

where $\langle \rho_{\rm w} \rangle_{\rm v}$ is the volume-averaged density of the warm clouds ($\langle \rho_{\rm w} \rangle_{\rm v} = \phi_{\rm v,w} \ \rho_{\rm w}$, where $\phi_{\rm v,w}$ is volume-filling factor and $\rho_{\rm w}$ is the density of the warm clouds respectively), $\sigma_{\rm turb}$ is the cloud-cloud velocity dispersion, ρ_1 and v_1 are the pre-shock gas density and velocity. We assume that v_1 is equal to the virial velocity, $v_{\rm vir}$. The initial density of the stream is related to the hot halo density, $\rho_{\rm H}$, as $\rho_1 = f \rho_{\rm H}$. The amount of turbulence generated in the post-shock gas is likely determined by as yet poorly understood and undoubtedly complex gas physics. In our model we do not attempt to investigate the complexity involved in this transformation of energy, we simply parameterize the amount of turbulence by η which we allow to be free (see § 2.5.3).

As we briefly alluded to in § 2.5.2, as the turbulent energy dissipates, it reheats the warm clouds, moderating the cooling. The cooling of the clouds will also be moderated by mixing with the ambient halo gas as the stream penetrates deeper into the halo potential (Fragile et al., 2004). Dissipation of turbulent kinetic energy in the hot phase may also contribute to heating the post-shock gas as well as the radiation from the high-speed accretion shock (Allen et al., 2008). The parameter η may be high enough to provide the required heating of the hot gas in the stream through turbulent dissipation and mixing with the halo gas, perhaps instigating thermal instabilities. On the other hand, η must be low enough such that turbulent dissipation and mixing does not prevent instabilities, both thermal and cooling, from growing in the post-shock gas (Banerjee & Sharma, 2014; Zhuravleva et al., 2014). These constraints and considerations may ultimately provide limits on how much or how little turbulence is sustainable in the post-shock gas, but determining these exact values requires further detailed study and will not be considered here.

Mass and momentum budget of the multiphase medium

We assume that as the stream flows into the halo, its mass flowate is conserved during the post-shock expansion and does not mix immediately with the ambient halo gas. This leads to the relation,

$$S \rho_2 v_2 = \rho_1 v_1 \tag{2.32}$$

where ρ_2 is the density after the hot gas has expanded by a factor, S, and similarly, v_2 is its velocity (Fig. 2.1). The expansion factor, S, is defined as the ratio of the initial over the final mass fluxes (per unit surface perpendicular to the flow). The post-shock gas will ultimately reach pressure equilibrium with the halo which implies, $\rho_{\rm w} T_{\rm w} = \rho_{\rm h} T_{\rm h} = \rho_{\rm H} T_{\rm H}$, where $\rho_{\rm w}$ and $\rho_{\rm h}$ are the densities of the warm

and hot components and $T_{\rm H}$ is the temperature of the hot components after phase separation in the post-shock gas.

Before there is any momentum exchange with the halo gas, the momentum of the streaming gas is conserved, implying,

$$S\left(\rho_2 v_2^2 + \eta\rho_1 v_1^2 + P_{\rm H}\right) = \rho_1 v_1^2 + P_1 \tag{2.33}$$

where P_1 is the initial pressure of the stream. We assume the fragmenting gas radiates away its heat until reaching a floor temperature, $T_{\rm w}$=10^4 K. The hot component only cools adiabatically and reversibly (no heat transfer and no entropy increase) expanding after it passed through the shock front, namely, $\rho_{\rm h}^{\gamma} P_{\rm ps} = \rho_{\rm ps}^{\gamma} P_{\rm H}$, where γ is the ratio of specific heats. This approximation holds until the expanding gas reaches pressure equilibrium with the ambient halo gas.

The expansion factor, S, is derived from Eqs. 2.23, 2.32, and 2.33, as,

$$S = \frac{1}{2}\left(\eta + \frac{\gamma-1}{2f}\right)^{-1}\left(1 - \sqrt{1 - 4\frac{\rho_{\rm H}}{\rho_2}\left(\eta f + \frac{\gamma-1}{2}\right)}\right) \tag{2.34}$$

The expansion of the stream is important in our formulation. It leads to the mixing of the expanding post-shock gas with the ambient halo gas. This mixing couples the hot post-shock gas to the larger energy reservoir of the ambient halo gas which acts as a thermostat preventing the gas from cooling, thereby possibly maintaining the pressure necessary to support a sustained shock. As we discussed in § 2.5.2, it is the relative ratios of the thermal cooling time and the expansion time that will influence how the stream evolves.

Cloudy stream disruption

The relative cloud-cloud motions may lead to the warm clouds spreading beyond the original radius of the stream. So instead of the streams being highly collimated as we assumed they are initially (before the virial shock), the flows may de-collimate. This can be thought of as disruption since the warm clouds expand away from the original trajectory of the stream, thus "disrupting" the flow. We define the timescale for disruption as the cloud crossing time of the stream, namely,

$$t_{\rm disrupt} = \frac{r_{\rm stream}}{\sigma_{\rm turb}} \tag{2.35}$$

$\sigma_{\rm turb}$ may be computed from η, f, and the volume-filling factor of the warm clouds, $\phi_{\rm v,w}$. From Eqs. 2.23 and 2.31, assuming pressure equilibrium between gas phases, yields,

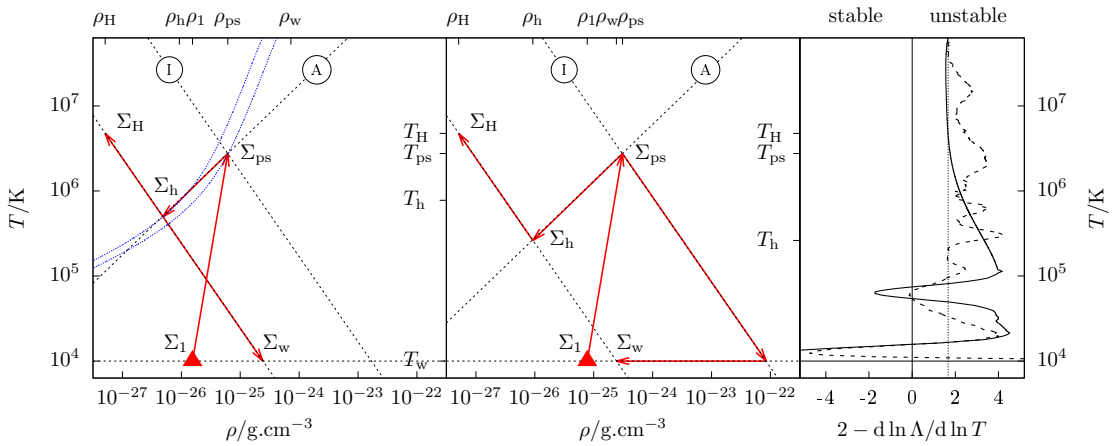

Figure 2.6: *(left and middle)* Sketch of the thermodynamic path for cases *(1)* and *(2)* (see text). Σ_1 (red triangle) indicates the density and temperature of the pre-shock gas. The gas is shocked reaching the point Σ_{ps}. Subsequently, the gas cools adiabatically due to the expansion of the stream until the halo pressure is reached at Σ_h. Two phases separate. For case *(1)*, phase separation occurs at Σ_h, while for case *(2)*, it occurs at Σ_{ps}. In both cases, the hot component mixes with the surrounding halo gas, reaching Σ_H. For case *(1)*, the warm component cools radiatively and isobarically to the point Σ_w. For case *(2)*, the same point is reached but the gas takes a different thermodynamic path. Dashed black lines represent adiabats and isobars labeled A and I respectively. The two blue-dashed curves in the left panel are contours of constant cooling time, $t_{\rm cool} \sim 0.2 t_{\rm dyn,halo}$ (upper curve) and $t_{\rm cool} \sim 0.12 t_{\rm dyn,halo}$ (lower curve). These curves indicate that the cooling time during the expansion remains approximately constant. *(right)* Analysis of the isobaric differential cooling "instability" (Eq. 2.28) of low-, 10^{-3} solar (solid line) and solar-metallicity (dashed line) gas as a function of temperature. When $2 - \mathrm{d}\ln\Lambda/\mathrm{d}\ln T > 0$ the gas can become heterogeneous through accelerated differential cooling.

$$\begin{aligned}\sigma^2_{\rm turb} &= v_1^2(\eta f/\phi_{\rm v,w})(T_{\rm w}/T_{\rm H}) \\ &= \frac{2}{(\gamma-1)}\left(\frac{k_{\rm B}}{\mu m_p}\right)(\eta f/\phi_{\rm v,w})T_{\rm w}\end{aligned} \tag{2.36}$$

Characterized this way, $\sigma^2_{\rm turb}/v_1^2 > \eta$. For a wide range of relative amounts of turbulent energy, stream over-density, and volume-filling factor of the warm gas, the cloud-cloud dispersion be up to $v_{\rm vir}/2$. The dynamical evolution of the stream is determined by the ratio of the disruption and halo dynamical time. If $t_{\rm disrupt} \gg t_{\rm dyn,halo}$, then the warm clouds within the stream will remain collimated as they flow, otherwise, the streams will de-collimate.

2.5.4 A specific case: $10^{13}\,{\rm M}_\odot$ halo at z=2

To gauge whether any of the phenomenology we have discussed is pertinent astrophysically, we calculate the stream characteristics for a single dark matter halo of mass, $10^{13}\,{\rm M}_\odot$, at redshift 2. We chose this halo mass and redshift because in DB06, halos at this mass and redshift were determined to have substantial accretion rates in the "hot mode". Our analysis in § 2.5.2 indicated that this halo mass and redshift would be a revealing illustration of how the impact of expansion and accelerated differential cooling might change the physical characteristics of gas accretion flows (i.e., it would no longer simply be "hot mode accretion"). Both the halo mass and the redshift set the initial stream density and the characteristics of the halo gas. We provide all the characteristics of the halos and initial gas conditions in the Appendix.

Why are streams cloudy?

There are two limiting cases to specifically consider when attempting to understand the development of a biphasic stream. The two cases are: *(1)* $t_{\rm expand} \ll t_{\rm cool,ps}$ and *(2)* $t_{\rm expand} \gg t_{\rm cool,ps}$. In case *(1)*, the warm phase develops only after the expansion has occurred, while in case *(2)* the clouds form before the expansion. We sketch the thermodynamic evolution ("path") of a stream in Fig. 2.6. To make these illustrations, we adopted $f = 30$ and $r_{\rm stream}/r_{\rm vir}$=0.01 for case *(1)*, and $f = 150$ and $r_{\rm stream}/r_{\rm vir}$=0.1 for case *(2)*.

In case *(1)*, clouds fill the entire expanse of the expanded flow. Adiabatic expansion occurs before radiative cooling becomes important, the stream cools and the density of the hot phase declines without a change in entropy. In case *(2)*, the two phase separate before expansion. In both cases, the hot post-shock gas reaches pressure equilibrium and mixes with the ambient halo gas.

These two conditions are of course for the extreme cases, in reality, the gas will have $t_{\rm expand} \sim t_{\rm cool,ps}$ (Fig. 2.3). For these intermediate cases, the thermodynamic

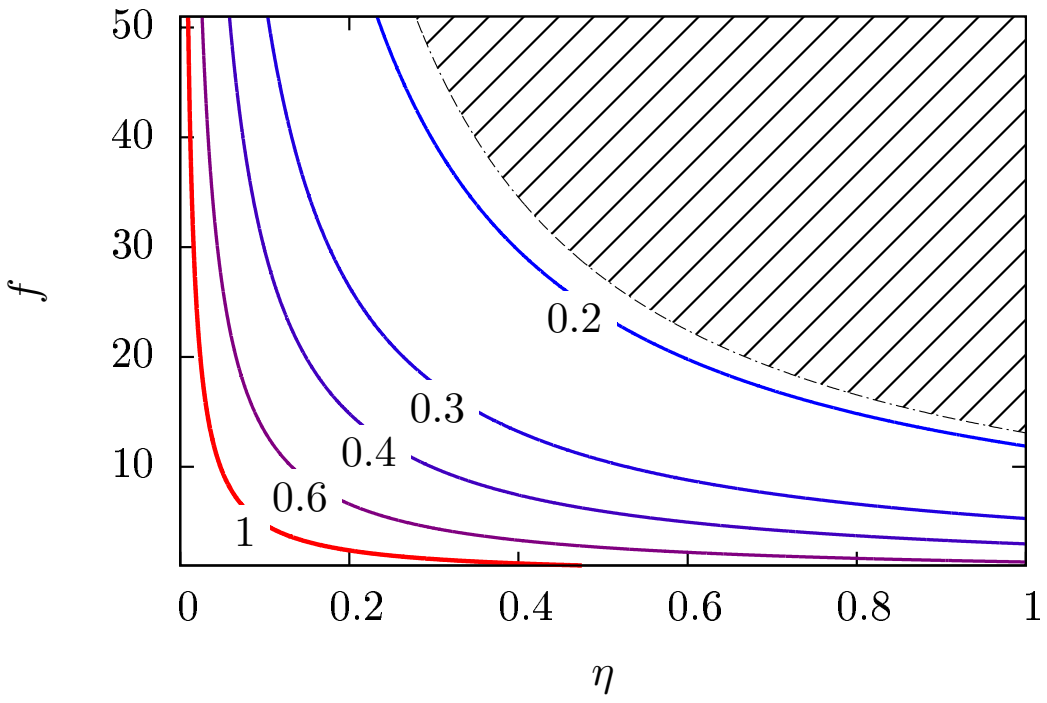

Figure 2.7: Disruption of the flow as a function of the filament over-density, f, and level of turbulence, η. The contours represent constant ratios of $t_{\rm disrupt}/t_{\rm dyn,halo}$ as labeled (cf. Eqs. 2.35 and 2.27). We assume a volume-filling factor of 0.1 (see Fig. 2.5) for the warm clouds and $r_{\rm stream} = r_{\rm vir}/10$. In regions with values less than 1, the streams are "disrupted" (§ 2.5.4). The shaded region indicates regions that are forbidden because for these values of the parameters, the post-shock pressure is less than the halo pressure. We note that because $t_{\rm disrupt} \propto \sigma_{\rm turb}^{-1}$, the contours of constant $t_{\rm disrupt}/t_{\rm dyn,halo}$ are shaped like contours of constant $\sigma_{\rm turb}$ in the same plane. For example, the contour, $t_{\rm disrupt}/t_{\rm dyn,halo}$=0.2, is close to the contour for $\sigma_{\rm turb}$=200 km s^{-1}, which is almost half the initial velocity of the flow.

evolution is more complex, but the clouds reach the same final thermodynamical state. The cooling length at the post-shock temperature is the size over which structures can cool isobarically (i.e., cooling length, $\lambda_{\rm cooling,ps} = c_{\rm ps}\, t_{\rm cool,ps}$). In case *(1)*, the cooling length is much larger than the stream radius, $\lambda_{\rm cooling,ps} >> r_{\rm stream}$, clouds may form over all scales within the stream. In case *(2)*, it is much smaller, $\lambda_{\rm cooling,ps} << r_{\rm stream}$, and clouds may form over a range of sizes smaller than the stream radius. The expansion of the hot gas does not inhibit the growth of thermal and differential cooling instabilities because the decrease in the pressure is roughly compensated by the decrease of temperature along an adiabat in the expression of the cooling time. In other words, for the post-shock temperature, i.e., for the halo mass we have adopted, the gas cooling time remains roughly constant as the gas expands (Fig. 2.6; see also Fig. 2.2). Eventually, the warm phase equilibrates at approximately the halo pressure and the hot phase mixes with the halo gas. We are obviously considering fragmentation on scales much smaller than the scale height of the gravitational potential well and thus we can safely ignore thermal stabilization by convection (Balbus & Soker, 1989; Sharma et al., 2010).

Does the accretion flow disrupt?

The only process we consider in determining whether or not the warm clouds will travel coherently towards the galaxy proper as observed in numerical simulations (e.g. Brooks et al., 2009; Danovich et al., 2015) is the cloud-cloud velocity dispersion. The cloud-cloud dispersion will broaden the stream as it penetrates into the halo. Fig. 2.7 and Fig. 2.8 show contours of $t_{\rm disrupt}/t_{\rm dyn,halo}$ for a constant $r_{\rm stream}$ (Eqs. 2.35 and 2.27). We find that the disruption time is shorter than or approximately equal to the halo dynamical time. Thus it appears that for a wide range of relative turbulent energy densities, stream over-densities, and volume-filling factors of the warm gas, the flows will not simply fall directly into the potential as a highly collimated, coherent streams. In reality, the clouds are dynamical entities, we expect clouds to keep forming through cooling as other clouds are destroyed by hydrodynamic instabilities and heated by dissipation (Cooper et al., 2009).

2.5.5 Discussion

We now discuss broadly how our findings relate to aspects of galaxy formation and evolution.

Are virial shocks persistent?

In our scenario, the existence of a hot phase in hydrostatic equilibrium supports a persistent shock (Binney, 1977; Maller & Bullock, 2004). Cosmological simulations

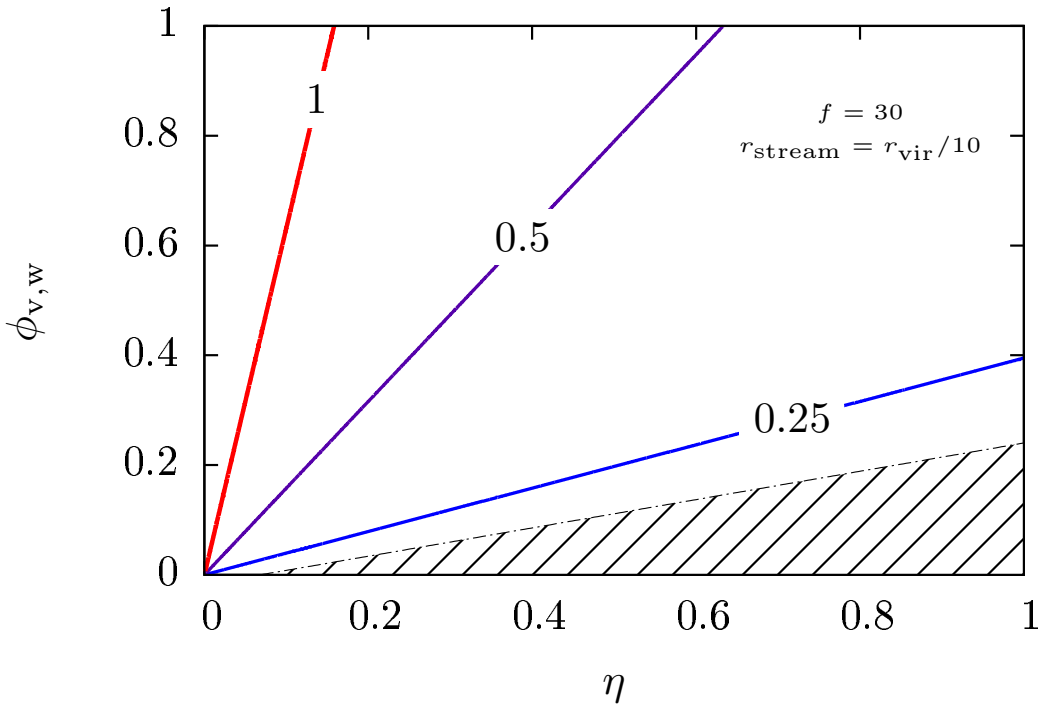

Figure 2.8: Disruption of the flow as a function of the volume-filling factor of the warm gas and level of turbulence. The contours represent constant ratios of $t_{disrupt}/t_{dyn,halo}$ as labelled (cf. Eqs. 2.35 and 2.27). We assume f=30 and $r_{stream} = r_{vir}/10$. In regions with values less than 1, the streams are disrupted. The shaded region has the same meaning as in Fig. 2.7.

appear to show a similar phenomenology as that described in DB06. Depending on the mass of the halo and redshift, streams penetrate at about one to many 100s of $\mathrm{km\,s^{-1}}$ (van de Voort & Schaye, 2012; Goerdt & Ceverino, 2015b) or much greater than the sound speed of the stream, $c_s \sim$10-20 $\mathrm{km\,s^{-1}}$. Simulated accretion shocks are "isothermal" at high Mach numbers and not stable (e.g., Nelson et al., 2016, 2015). Perhaps this uniform isothermality is due to the spatial and temporal resolutions adopted in the cosmological simulations. The scales that simulations must probe are roughly delineated in one-dimensional shock calculations. Raymond (1979) show that atomic shocks with velocities of $\sim$100 $\mathrm{km\,s^{-1}}$ reach their post-shock temperatures within a distance of $\approx$1-10 $\times 10^{15}$ cm in less than $\sim$30 yrs. For higher shock velocities, the spatial and temporal scales will be even shorter (Allen et al., 2008). The gas cools after the shock on timescales that are at most only a couple of orders-of-magnitude longer. In addition, in order to capture the differential cooling and thermal instabilities in the post-shock gas, resolutions much finer than the Field length are required (Koyama & Inutsuka, 2004; Gressel, 2009). Simulations should be specifically designed to capture the multiphase nature of streams penetrating halos to test our scenario by resolving the Field length (Koyama & Inutsuka, 2004). Since the Field length decreases strongly with decreasing temperature, this is most easily done with *ad hoc* floor temperature higher than 10^4 K but lower than the virial temperature as done for simulating thermal instabilities in cool core clusters (McCourt et al., 2012).

The resolution and temporal scales necessary to resolve high Mach number shocks are not achievable in galaxy- or cosmological-scale simulations. To overcome this limitation, numericists use artificial viscosity in the form of a dissipative term either in dynamical equations or dispersion relations, depending on the properties of the gas or the flow (e.g., Kritsuk et al., 2011; Price, 2012; Hu et al., 2014; Beck et al., 2016). Artificial viscosity spreads the shock over several resolution elements enabling simulations to resolve heating and cooling across the shock front. The Reynolds number is inversely proportional to the kinetic viscosity of the fluid. If the flow properties are unchanged but the viscosity increased, the Reynolds number of the flow will be artificially low. Simulations with artificial viscosity have flows with low Reynolds numbers. Simulated low Re flows, $\mathrm{Re} \lesssim 1000$, tend to be laminar. Those with low spatial and temporal resolutions, due to not resolving the Field length and having unrealistical low Reynolds numbers likely fail to produce biphasic turbulent flows (see, e.g., Kritsuk & Norman, 2002a; Sutherland et al., 2003; Koyama & Inutsuka, 2004; Kritsuk et al., 2011; Nelson et al., 2016, for discussion).

Nature of Flows into Galaxies: Observational tests

As a consequence of our assumption that all energetic quantities scale as $v_{\rm vir}$, the cloud-cloud dispersion is a simple linear function of η, f, and $\phi_{\rm v,w}^{-1}$. This relation implies that turbulent velocities of the warm clouds in the post-shock gas are independent of both halo mass and redshift. In principle this means that post-shock streams may be turbulent in any halo at any redshift. The reality is probably much more complex, through both macro- and microscopic gas physics which is not yet well-understood, the 2 parameters, η and $\phi_{\rm v,w}$, likely depend on the accretion velocity and the physical state of the ambient halo gas – both of which undoubtedly depend on redshift and halo mass.

Our scenario has observationally identifiable consequences. If our scenario is realistic, then observations should reveal: *(1)* clumpy, turbulent streams; *(2)* strong signs of the dissipation of turbulent mechanical energy in the warm medium (e.g., Guillard et al., 2009; Ogle et al., 2010; Tumlinson et al., 2011). The situation described in our model where a large fraction of the bulk kinetic energy of the accretion flow is transfered to turbulent motions amongst cold clouds is observed in large-scale galaxy colliding flows, like the situation in the Taffy Galaxies or the Stephan's Quintet, where we see evidence for this energy cascade (Peterson et al., 2012; Cluver et al., 2010). In Stephan's Quintet, two atomic gas filaments are colliding at $\sim$1000 km s^{-1} and yet instead of finding intense X-ray emission from the post-shock gas, most of the bulk kinetic energy is contained in the turbulent energy of the warm molecular gas (Guillard et al., 2009, 2010). Remarkably, roughly 90% of the bulk kinetic energy has not been dissipated in the large-scale shock and is available to drive turbulence. If gas in halos is multiphase and turbulent, then it may be the case as well for accretion streams.

Obviously, a clumpy stream is difficult to identify as such through absorption line spectroscopy and this may explain why streams have not been conspicuously identified so far. This is most obviously seen in Fig. 2.5 where despite a large fraction of the gas is warm, its volume-filling factor is minuscule. Along most lines-of-sight, absorption spectroscopy is expected to sample only the hot, high volume-filling factor halo gas or probe a population of warm ambient halo clouds (Maller & Bullock, 2004; Tumlinson et al., 2011; Werk et al., 2014). The clouds should be looked for in emission. Their emission can be powered by the UV radiation from the galaxy but also through the localized dissipation of turbulent energy and through losses of their gravitational potential energy as they fall into the halo. This may have already been observed in Lyα (e.g., Cantalupo et al., 2014; Martin et al., 2015). In particular, it would be promising to interpret spectral-imaging observations such as those provided by MUSE on the ESO/VLT within the context of our scenario (see Borisova et al., 2016; Fumagalli et al., 2016; Vernet et al., 2017a).

Moderating the accretion rate: Biphasic streams and increased coupling between "feedback" and accretion

In our phenomenological model, two mechanisms moderate the accretion efficiency on to galaxies: *(1)* disruption and fragmentation of the flow; *(2)* interaction between streams and outflows of mass, energy, and momentum due to processes occurring within galaxies (e.g., AGN, intense star-formation).

First, streams potentially become multiphase and turbulent leading to short disruption times resulting in de-collimation. Any de-collimation undoubtedly leads to longer accretion times and thus lower overall accretion efficiencies compared to smooth isothermal streams (Danovich et al., 2015; Nelson et al., 2016). The post shock gas becomes multiphase over a wide range of halo masses at z=2. A fraction of the initial stream mass flow becomes hot gas and ultimately mixes with the surrounding ambient hot halo gas. Thus even accretion streams potentially feed gas into the hot halo which may have long cooling times compared to the halo free fall time (White & Rees, 1978b; Maller & Bullock, 2004).

Second, simulations indicate that the mass and energy outflows from galaxies can interact with streams, regulating or even stopping the flow of gas (e.g., Ferrara et al., 2005; Dubois et al., 2013; Nelson et al., 2015; Lu et al., 2015). Simulated streams are relatively narrow (e.g., Ocvirk et al., 2008a; Nelson et al., 2013, 2016) and generally penetrate the halo perpendicular to the spin axes of disk galaxies and their directions are relatively stable for long periods (e.g., Pichon et al., 2011; Dubois et al., 2014; Welker et al., 2014; Laigle et al., 2015; Codis et al., 2015; Tillson et al., 2015). Feedback due to mechanical and radiative output of intense galactic star formation and active galactic nuclei is observed to be highly collimated in inner regions of disk galaxies (opening angle, $\Omega \sim \pi$ sr, e.g., Heckman et al., 1990; Lehnert & Heckman, 1995, 1996; Beirão et al., 2015). In the case of dwarf galaxies, their outflows are generally more weakly collimated (e.g., Marlowe et al., 1995, 1997; Martin, 1998, 2005). The geometry of the accretion flows and the significant collimation of outflows from galaxies in simulations, result in only weak direct stream-outflow interactions. However, accretion flows in simulations can be moderated or stopped when the halo gas is pumped with mass and energy via feedback to sufficiently high thermal pressures and low halo-stream density contrasts to induce instabilities in the stream and disrupt it; or when the halo gas develops a sufficiently high ram pressure in the inner halo due to angular momentum exchange between the gas, dark matter, and galaxy disk to disrupt accretion flows (van de Voort et al., 2011; Dubois et al., 2013; Nelson et al., 2016).

The processes we have described are generic to flows, whether they are inflows or outflows. It is only the context and timescales that change (Thompson et al., 2016). Just as with the accretion flows modeled here, we also expect the galaxy winds to be highly uncollimated as they flow from the galaxy due to the formation

(and destruction) of turbulent clouds. Thus, the generation of turbulent cloudy media in both accretion flows and starburst-driven outflows will allow for efficient interaction between these two types of flows. This dynamical interaction likely sustains turbulence in the halo compensating for the dissipation. It is perhaps through this interaction that galaxies become "self-regulating" on a halo scale (e.g., Fraternali et al., 2013), and not only on a galaxy scale (e.g., Lehnert et al., 2013, 2015).

While the fate of the turbulent clouds is beyond the scope this paper, the qualitative implication is that the gas accretion efficiency may be moderated through the generation of turbulence in biphasic flows. The fragmented, turbulent nature of the gas in streams and outflows likely makes their dynamical and thermal interaction and coupling efficient. Note that other mechanisms, like the growth of RayleighâĂŞTaylor and Kelvin-Helmholtz instabilities, associated with gas cooling, can also trigger the formation of cold clouds in the surrounding halo (e.g. Kereš & Hernquist, 2009). Moderating the overall gas accretion efficiency onto galaxies may help to alleviate two significant challenges in contemporary astrophysics: the distribution of the ratio of the baryonic to total halo mass as a function of halo mass (e.g. Behroozi et al., 2013), where low mass galaxies have especially low baryon fractions; and the requirement for models to drive extremely massive and efficient outflows to reduce the baryon content of galaxies (e.g., Hopkins et al., 2012, 2016).

2.5.6 Conclusions

We developed a phenomenological model of filamentary gas accretion, "streams", into dark matter halos. We assume both that streams penetrate ambient hot halo gas as homogeneous flows of 10^4 K gas and that they undergo a shock at the virial radius of the halo. The ingredients of the model, those which sets it apart from other phenomenological models of gas accretion, are that we assume the "virial shock" is sustained, the post-shock gas expands into a ambient hot halo gas, and through several mechanisms or characteristics of the shock front, the post-shock gas is inhomogeneous. To gauge whether this model is astrophysically pertinent, we discuss the thermodynamic evolution of a single stream penetrating a dark matter halo of mass 10^{13} $M_\odot$ at z=2. From this analysis, we find that:

- The post-shock gas expands into the halo gas and it can fragment due to differential cooling and hydrodynamic instabilities. Instabilities lead to the formation of a biphasic flow. It is the formation of a hot post-shock phase which mixes with the ambient hot halo gas, ultimately limiting how much of the gas can cool. As a result of the phase separation and the pressure provided by the hot post-shock gas, we argue that the virial shock may be

sustained. However, we have not analyzed the sustainability of the shock in detail in this paper.

- The development of a biphasic medium converts some of the bulk kinetic energy into random turbulent motions in the gas (e.g., Hennebelle & Pérault, 1999; Kritsuk & Norman, 2002a). The turbulent energy cascades from large to small scales and across gas phases. The flows, while retaining significant bulk momentum as they penetrate into the halo, are turbulent with cloud-cloud dispersion velocities that can be up to 1/2 of the initial velocity of the stream.

- For a wide range of turbulent energy densities, our model shows that the stream will lose coherence in less than a halo dynamical time. We emphasize that the turbulent energy density is not in reality a free parameter but is determined by macro- and microscopic multiphase gas physics about which we have only a rudimentary understanding. To understand what processes regulate the amount of turbulence in streams, high resolution simulations of accreting gas need to be made and additional multi-wavelength observations useful for constraining the properties of turbulent astrophysical flows are necessary.

The post-virial shock gas is not isothermal, accretion streams are both hot and cold. The "hot-cold dichotomy" (see DB06) is no longer a simple function of whether or not the shock is stable, but now relies both on the shock occurring and under what circumstances the post-shock gas becomes multiphase and turbulent. However, we have discussed may apply if there is no virial shock provided that inflowing gas is hot and already inhomogeneous (Kang et al., 2005; Cen & Ostriker, 2006). Thus, even in absence of a virial shock, the gas may become multiphased by compression as it falls deeper into the halo potential.

Moderating the gas accretion efficiencies on to galaxies through this and other mechanisms may help to alleviate some significant challenges in theoretical astrophysics. If gas accretion is actually not highly efficient, then perhaps models will no longer have to rely on highly mass-loaded outflows to regulate the gas content of galaxies. It is likely that the underlying physical mechanisms for regulating the mass flow rates and evolution of outflows are very similar to those that regulate gas accretion (Thompson et al., 2016). If so, then observing outflows in detail can provide additional constraints on the physics of astrophysical flows generally. We do not only have to rely on apparently challenging detections of direct accretion onto galaxies.

2.5.7 Parameters in the model

The quantities that are important in setting the initial conditions of the stream-ambient halo gas interaction are the mass, virial velocity, and virial radius of the dark matter halo which we denote as $M_{\rm H}$, $v_{\rm vir}$, and $r_{\rm vir}$. The dark matter distribution is given by a NFW profile with a concentration parameter, c, of 10 (Navarro et al., 1997). The halo is filled by a hot gas of temperature $T_{\rm H}$, which we assume to be equal to the virial temperature of the halo, $T_{\rm vir}$. The density of the hot halo, $\rho_{\rm H}$, is assumed to follow that of the dark matter density with radius, but is multiplied by the cosmological baryon density relative to the dark matter density, $f_{\rm B} = 0.18$. This is $\approx 37 f_{\rm B}\rho_{\rm crit}$, where $\rho_{\rm crit}$ is the critical density of the Universe. The halo pressure, $P_{\rm H}$, is related to $T_{\rm H}$ and $\rho_{\rm H}$. The filling factor of this gas is assumed to be one. We are agnostic about how this hot, high volume-filling factor halo at the virial temperature formed but note that it likely forms by a combination of accretion of gas from the intergalactic medium and heating through the radiative and mechanical energy output of the galaxy embedded in the halo (e.g., Suresh et al., 2015; Lu et al., 2015).

Table 2.1: Halo and gas parameters for example in § 2.5.4

Parameter Name	Symbol	Value
Halo mass	$M_{\rm H}$	$10^{13}\,{\rm M}_\odot$
Baryonic fraction	$f_{\rm B}$	0.18
Redshift	z	2
Virial radius	$r_{\rm vir}$	220 kpc
Virial velocity	$v_{\rm vir}$	440 $\rm km\,s^{-1}$
Critical density	$\rho_{\rm crit}/\mu m_{\rm p}$	7.6×10^{-5} $\rm cm^{-3}$
Number density at $r_{\rm vir}$	n_0	5.1×10^{-4} $\rm cm^{-3}$
Adiabatic index	γ	5/3
Mean particle mass	$\mu m_{\rm p}$	$0.6 \times m_{\rm p}$

The gas accretes through a stream of infalling gas with radius, $r_{\rm stream}$, we assume that it passes through a shock and that the properties of the post-shock gas is given by the standard set of shock equations. We simply scale the density of the accreting stream by a factor, f, which is its density contrast of the background dark matter density at the virial radius multiplied by the cosmological baryon fraction (i.e., $\rho_{\rm H}$). We further assume that there is a temperature floor in the post-shock gas of $10^4\,{\rm K}$. We assumed this temperature mainly because we also assume that the metallicity of the accreting stream is 10^{-3} of the solar value. The gas cannot cool much beyond $10^4\,{\rm K}$ due to it lacking heavy metals (and is likely heated by the meta-galactic flux and the ionizing field of the galaxy embedded in the halo). This assumption, although naive, is also extremely conservative in

Table 2.2: Model variables and their relationships[†] .

Variable Name	Symbol	Equation
Temperature floor	T_0	$= 10^4\,\mathrm{K}$
Initial speed of sound	c_1	$= \sqrt{\gamma k_\mathrm{B} T_0/\mu m_\mathrm{p}}$
Incoming Mach number	$\mathcal{M}_1$	$= v_\mathrm{vir}/c_1$
Density of the halo gas at r_vir	ρ_H	$= \rho_\mathrm{NFW}\left(r_\mathrm{vir}\right) \approx 37.0 \times f_\mathrm{B}\rho_\mathrm{crit}\left(z\right)$
Temperature of the halo gas	T_H	$= T_\mathrm{vir} = \mu m_\mathrm{p} v_\mathrm{vir}^2(\gamma-1)/2k_\mathrm{B}$
Pressure of the halo gas at r_vir	P_H	$= k_\mathrm{B} T_\mathrm{H}\rho_\mathrm{H}/\mu m_\mathrm{p}$
Density of the post-sock gas[a]	ρ_ps	$= (\gamma+1)\,/\,(\gamma-1)\,\mathcal{M}_1^2/\left[\mathcal{M}_1^2 + 2/(\gamma-1)\right]\rho_0$
Pressure of the post-shock gas[a]	P_ps	$= (\gamma-1)\,/\,(\gamma+1)\left[2\gamma/(\gamma-1)\mathcal{M}_1^2 - 1\right]P_0$
Post-shock speed of sound	c_ps	$= \gamma P_\mathrm{ps}/\rho_\mathrm{ps}$
Temperature of the warm phase	T_w	$= T_0$
Density of the warm phase	ρ_w	$= \rho_\mathrm{H} T_\mathrm{H}/T_\mathrm{w}$
Density of the hot phase (post-expansion)	ρ_h	$= \rho_\mathrm{ps}\left(P_\mathrm{ps}/P_\mathrm{H}\right)^{1/\gamma}$
Temperature of the hot phase (post-expansion)	T_h	$= \rho_\mathrm{H} T_\mathrm{H}/\rho_\mathrm{h}$
Volume-averaged density of the warm phase	$\langle\rho_\mathrm{w}\rangle_\mathrm{v}$	$= \phi_\mathrm{v,w}\rho_\mathrm{w}$
Volume-averaged density	ρ_2	$= \phi_\mathrm{v,w}\rho_\mathrm{w} + (1-\phi_\mathrm{v,w}\rho_\mathrm{h})$
Expansion factor of the post-shock stream[b]	S	$= \left(1-\sqrt{\Delta}\right)/\left[(\gamma-1)/f + 2\eta)\right]$
Velocity dispersion of the warm clouds	σ_turb	$= \sqrt{2k_\mathrm{B}T_\mathrm{w}\eta f/(\gamma-1)\phi_\mathrm{v,w}\mu m_\mathrm{p}}$
Halo dynamical time	$t_\mathrm{dyn,halo}$	$= r_\mathrm{vir}/v_\mathrm{vir}$
Cooling time of the phase $\Phi \in \{\mathrm{ps}, \mathrm{w}, \mathrm{h}\}$	$t_{\mathrm{cool},\Phi}$	$= k_\mathrm{B}\mu m_\mathrm{p} T_\Phi/\rho_\Phi\Lambda\left(T_\Phi\right)$
Expansion time of the post-shock gas	t_expand	$= 2\gamma r_\mathrm{stream}/c_\mathrm{ps}$
Disruption time of the turbulent warm phase	t_disrupt	$= r_\mathrm{stream}/\sigma_\mathrm{turb}$
Isobaric cooling length $\Phi \in \{\mathrm{ps}, \mathrm{w}, \mathrm{h}\}$	λ_cooling	$= c_\Phi t_{\mathrm{cool},\Phi}$

Notes.
[(†)] A graphical representation of many of these variables is shown in Fig. 2.1.
[(a)] Standard normal shock equation from the Rankine-Hugoniot jump conditions.
[(b)] The equation assumes $\Delta = 1 - 4\left[\eta f + (\gamma-1)/2\right]\rho_\mathrm{H}/\rho_2$

that this implies the post-shock gas will have one of the longest possible radiative cooling time (see Sutherland & Dopita, 1993; Gnat & Sternberg, 2007). We use the cooling curve, $\Lambda(T)$, from Gnat & Sternberg (2007) to compute the cooling times in the post-shock gas. We assume that the temperature of the gas in the stream before passing through the shock is also 10^4 K (T_1). At those temperatures and very low metallicity, we assume that no molecules form, so that the adiabatic index of the gases is always that of a monatomic gas, namely $\gamma = 5/3$.

The parameters we use in the model, given our assumed mass and redshift are given in Table 2.1. We enumerate for completeness and clarity all variables used in our analysis in Table 2.2.

2.5.8 Idealized model of a time-evolving multiphase medium

I implemented a numerical model to follow the differential cooling of an initially slightly heterogeneous medium. The width of the initial log-normal distribution of the temperatures, δ, is the determinant factor for growing a multiphased medium. I made simple analytic approximations for the time evolution of mass- and volume fraction of cool gas. Then I correlated the parameters of the analytical function with the initial distribution and draw preliminary physical conclusions. I further show how these correlations may be constrained by the output of our main model and state physical limitations. Afterwards, I implement a turbulent heating source, followed by the implementation of a scheme resembling a typical expansion of the pressurized gas in the hot halo.

Approximation of the time evolution of inhomogeneous gas

I developed a simple model for the evolution of an initially slightly inhomogeneous medium to a multiphase (warm+hot) medium. Assuming

- no cosmological context;
- gas is perfect with adiabatic index $\gamma = 5/3$;
- pressure is homogeneous at all times;
- cooling is isobaric ($\mathrm{d}P/\mathrm{d}t = 0$);
- temperatures (and thus densities) are initially log-normally distributed,

we can numerically compute the thermal evolution of the distribution. This can be done either by a sampling-based or a discretized distribution function-based, finite-difference method.

The log-normal distribution is usually relevant to isothermal turbulent media (Passot & Vázquez-Semadeni, 1998), but we chose the simplest one knowing that when the effective adiabatic index is more (less) than one, power-law tails should appear at low (high) densities. This is defined by the probability distribution function:

$$\mathrm{pdf}(T) = \frac{1}{T\delta\sqrt{\pi}} \exp\left(-\frac{\log(T/T_i)^2}{2\delta^2}\right) \tag{2.37}$$

where T_i is the initial peak temperature and δ is the initial dispersion.

The sampling-based method can be described as the following. Given a pressure P, we sample N values $\tilde{T}_i$ ($i \in \mathbb{N}$, $1 \leq i \leq N$) from a normal probability law. These values represent the temperatures of N particles, through $\tilde{T}_i = \log(T_i)$, only coupled by their common pressure. Their densities are derived from the law of perfect gases. Each has a specific energy $e_i = (\gamma - 1)k_\mathrm{B}T_i/\mu m_\mathrm{p}$, subject to a (discrete-)time evolution:

$$\forall\, i,\ \log_{10} e_i(t + \Delta t) = \log_{10} e_i(t) - \Delta t / t_{\mathrm{cool},i}(t) \tag{2.38}$$

and similarly, due to the constant pressure,

$$\forall\, i,\ \log_{10} \rho_i(t + \Delta t) = \log_{10} \rho_i(t) + \Delta t / t_{\mathrm{cool},i}(t) \tag{2.39}$$

where the cooling time of a particle i at time t is defined by:

$$t_{\mathrm{cool},i}(t) = \frac{4\gamma\mu m_\mathrm{p} k_\mathrm{B} T_i(t)}{(\gamma - 1)\rho_i(t)\Lambda(T_i(t), Z)} \tag{2.40}$$

Say that we split the distribution, at any time, in two sets, depending on the value of the temperature T relative to an arbitrary threshold $T_c = 10^4\,\mathrm{K} + \epsilon_T$, where $\epsilon_T \ll T_c$. Below this value lies the warm component, above it lies the hot one. We are then able to follow the time evolution of the warm mass fraction, as well as its volume-filling factor. The initial dominant cooling time, $t_{\mathrm{cool},0}$, is the one corresponding to the peak value of the distribution.

The warm mass fraction is defined by:

$$\phi_{\mathrm{m,w}}(t) = \#\{i | T_i(t) < T_c\}/N \tag{2.41}$$

and the hot one is simply $\phi_{\mathrm{m,h}} = 1 - \phi_{\mathrm{m,w}}$. A perfect illustration of this fraction can be found in Fig. 3 of Kritsuk & Norman (2002b). The volume-filling factor of the warm component is:

$$\phi_{\mathrm{v,w}}(t) = \frac{\sum_{\{i|T_i(t)<T_c\}} 1/\rho_i(t)}{\sum_{\{i\}} 1/\rho_i(t)} \tag{2.42}$$

and the hot one is simply $\phi_{\mathrm{v,h}} = 1 - \phi_{\mathrm{v,w}}$.

Running this code for $N' = 10$ values of δ in [0.01,1], the curves of each fraction is plotted against time. As distribution cools, the process slows down, i.e. the absolute value of time derivatives of mass fractions decrease. Thus we adopt as a time variable the logarithm of t divided by the characteristic time, the initial cooling time of the mean of the PDF in temperature, $t_{\mathrm{cool},0}$. Denoting $\Theta = \log_{10}(t/t_{\mathrm{cool},0})$, we found an excellent fitting function defined with the two parameters by:

$$\Phi_{\Theta_{1/2},\Delta} : \Theta \mapsto \frac{1}{2}\left[1 + \mathrm{erf}\left(\frac{\Theta - \Theta_{1/2}}{\sqrt{2}\Delta}\right)\right] \tag{2.43}$$

where erf is the error function:

$$\mathrm{erf}(x) = \frac{1}{\sqrt{\pi}} \int_{-x}^{x} e^{-u^2} du \tag{2.44}$$

then the following approximation is found:

$$\phi_{*,\mathrm{w}}(\Theta) \approx \Phi_{\Theta^*_{1/2},\Delta^*}(\Theta) \tag{2.45}$$

where $* \in \{\mathrm{m}, \mathrm{v}\}$ denotes a quantity pertaining to the mass or the volume, and $\Theta^*_{1/2}$ and Δ^* are functions of the initial dispersion of the log of temperatures δ. The former is the log-time at which the fraction reaches 50% and the latter is the lag between ∼31% and ∼69%.

Fitting the two parameters

I will apply this calculation to the previously discussed specific halo with a mass of $10^{13}\,\mathrm{M}_\odot$ at $z = 2$. The input parameters must then match the post-shock physical quantities. With the following initial conditions:

- $P/k_{\mathrm{B}} = 5.8\,10^4\,\mathrm{K.cm}^{-3}$
- $\mathrm{pdf}(\log(T)) = \mathcal{N}(2.7\,10^6\,\mathrm{K}, \delta)$
- $Z = 0$

Results are shown in Fig. 2.5.8 for $\delta = 0.01, 0.1, 0.3, 0.5$. Eq. 2.45 is fitted for different values of $\delta \in [0.01; 1]$, and for both $\phi_{*,\mathrm{w}}$, yielding relations $\Theta^*_{1/2}(\delta)$ and $\Delta^*(\delta)$, that are well fitted by affine functions:

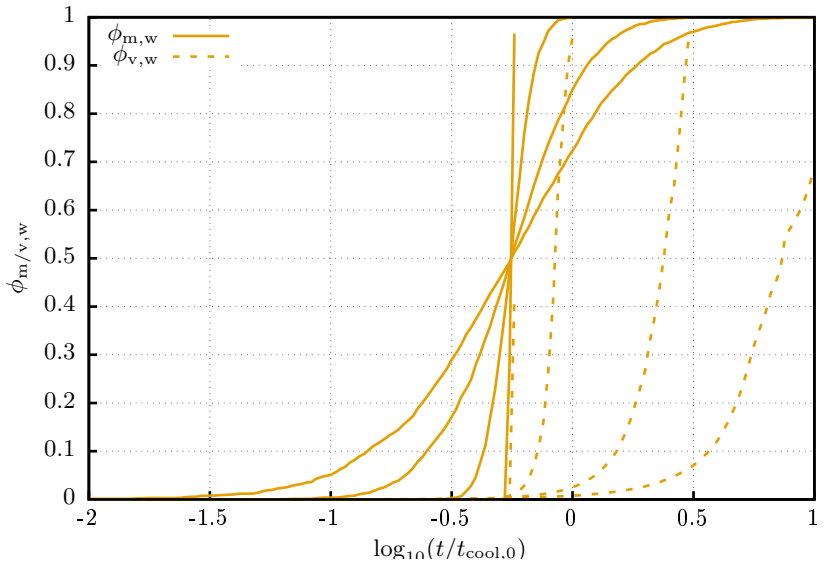

Figure 2.9: Evolution of the warm gas fractions for different values of δ.

$$\Theta^{\mathrm{m}}_{1/2} \approx -0.255 \tag{2.46}$$

$$\Delta^{\mathrm{m}} \approx 0.854\delta \tag{2.47}$$

$$\Theta^{\mathrm{v}}_{1/2} \approx -0.264 + 2.19\delta \tag{2.48}$$

$$\Delta^{\mathrm{v}} \approx 0.438\delta \tag{2.49}$$

These relations can be summarized as:

- $\Theta^{\mathrm{m}}_{1/2}$ is independent of δ, so that the warm mass fraction reaches 50% at a fixed time. That is, half the mass has cooled after $\sim$0.55 times the initial dominant cooling time, no matter the exact initial dispersion of the PDF.
- Δ^{m} is proportional to δ, so the higher the initial dispersion, the sooner the medium becomes multiphase and the longer it takes to cool completely.
- $\Theta^{\mathrm{v}}_{1/2}$ increases with δ, so that the warm mass fraction reaches 50% with a delay compared to the increase in the mass fraction. This delay increases linearly with δ. It implies that during the timelag, the warm mass fraction is much higher than the volume-filling factor.
- Δ^{v} is proportional to δ, implying the same conclusion as for Δ^{m}. Note that the volume-filling factor reaches 1 at a faster rate than the mass fraction, since $\Delta^{\mathrm{v}}/\Delta^{\mathrm{m}} \approx 1/2$.

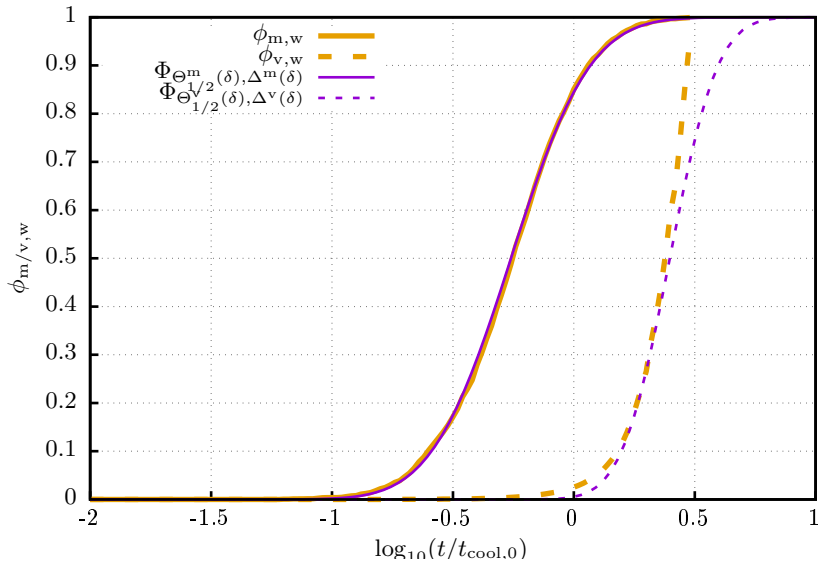

Figure 2.10: Evolution of the warm fractions against the log of normalized time. Fits with Φ functions are shown.

When $\delta = 0$, i.e. the distribution is a Dirac, the mass fraction and the volume-filling factor of the warm phase abruptly jumps from 0 to 1 at $\Theta = \Theta^{\mathrm{m}}_{1/2} = \Theta^{\mathrm{v}}_{1/2}$. This latter condition is not reflected by the independent linear fits and we shall correct that by adjusting the terms of order 0 in both Θ^*_0 expressions with a mean value:

$$\Theta^{\mathrm{m}}_{1/2} \approx -0.260 \tag{2.50}$$

$$\Theta^{\mathrm{v}}_{1/2} \approx -0.260 + 2.19\delta \tag{2.51}$$

Constraining the two parameters

It is possible to relate those functions to the known densities of our expanded, multiphase, turbulent medium, namely ρ_{w} and ρ_{h}, with the previously derived equation:

$$\left(\phi^{-1}_{\mathrm{v,w}} - 1\right)\rho_{\mathrm{h}} = \left(\phi^{-1}_{\mathrm{m,w}} - 1\right)\rho_{\mathrm{w}} \tag{2.52}$$

and solving it for (δ, Θ), after having replaced the ϕ's with their Φ approximations.

$$\frac{\phi^{-1}_{\mathrm{v,w}} - 1}{\phi^{-1}_{\mathrm{m,w}} - 1} = \frac{\rho_{\mathrm{w}}}{\rho_{\mathrm{h}}} = \text{const.} \tag{2.53}$$

may be translated in:

$$\frac{\Phi_{\Theta^{\rm v}_{1/2}(\delta),\Delta^{\rm v}(\delta)}(\Theta)^{-1}-1}{\Phi_{\Theta^{\rm v}_{1/2}(\delta),\Delta^{\rm v}(\delta)}(\Theta)^{-1}-1}=f(\Theta,\delta)=\text{const.} \tag{2.54}$$

and, as surprising as it may be for such a complicated expression, the locus of $f(\Theta,\delta)$ =const. is a line in the (Θ,δ)-plane:

$$\delta=\alpha\left(\Theta-\Theta^{\rm m}_{1/2}\right)\approx\alpha\log_{10}\left(\frac{1.82\,t}{t_{\rm cool,0}}\right) \tag{2.55}$$

with α a coefficient depending on the ratio $\rho_{\rm w}/\rho_{\rm h}$. This dependence is nonlinear but, again, the function can be numerically interpolated.

What does it mean? If we know the density ratio, there is a one-to-one map between the initial dispersion and the time it took to grow this multiphase medium.

Note that there are important caveats.

Pressure evolution – In our model, the gas has expanded so that a perfectly isobaric transformation should not apply. However, this is a realistic way of gaining conservative information on the time the process took and on the initial (post-shock) dispersions. Indeed, the loss of pressure by mechanical adjustment to the environment should slow down the cooling so that the times obtained by the method described above are lower bounds to a more physically accurate estimate of the cooling time.

Stationarity – Our model explicitly states that the processes are stationary, eventually reaching an asymptotic multiphase state. Here in this sort theoretical study, the whole medium must always end up cool. This can be balanced by a turbulent heating term which stops the cooling at a certain asymptotic mass fraction. Given the order of magnitude of the times considered, an other important ingredient should be added that compensates the cooling—namely the cosmic expansion.

2.5.9 Further: more realistic conditions

Since we wanted to describe the evolution of a cylindrically symmetric flow representing an IGF, we may want to implement additional constraints and processes. Here are two major propositions on mechanisms that could be implemented to obtain more realistic results, in particular for expanding post-shock streams.

Mimicking the expansion – Pressure equilibrium with the ambient halo must be reached. Ideally, without radiative cooling, we expect it to be adiabatic and reversible. To mimic the physical situation, we should write the equations for the expansion so that a vanishing cooling rate implies the adiabatic law for gases ($P\propto\rho^{\gamma}$). A more physically robust model would include spatial gradients—the outer envelope first expands and the rarefaction wave propagates toward the

axis into the medium, at any instant, leading to a pressure field with a cylindrical geometry. Moreover, the initial conditions should not represent a purely cylindrical discontinuity (there would be unrealistic shocks propagating in the filament and the halo) but perhaps at its most basic level, a layered model that would smooth the radial profiles, using knowledge gained from the simulation (see Chap. 3).
Radiative loss and spatial scales – Imposing a constant pressure is valid as long as the expansion and the cooling occur one after the other. When they are concurrent, the pressure drops along with the radiative losses. The parcel of gas under this condition either exerts or receives no mechanical work, in which case its average density is conserved, or work is done and it must be accounted for. In a sense, this is scale-dependent, so that the former case corresponds to smallest space scales, the latter to larger ones; their separation is governed by time ratios. For thin cylindrical shells, the sound-crossing time is much shorter than the thermal evolution timescale and the pressure loss is only due to the radiative loss, without work being exchanged between neighboring shells. The outer shells would experience such a work exchange because of higher pressure gradients with their neighbours. One must also account for the fact that the expansion is initially fast and slows down to an asymptotic mechanical equilibrium: the sound-crossing time also evolves.

2.6 Concluding remarks

We have developed a phenomenological model for the evolution of the gas stream immediately following a virial shock. However, in several ways, the model left important open questions. These questions are:

- Is there a heating process that prevents the hot post-shock gas from cooling significantly? In Section 2.5, we mention mixing with the hot halo gas and turbulent heating as such possible processes. These two processes need to be investigated with numerical simulations.

- How strongly do outflows and inflow couple? Such a coupling is a natural way of regulating or moderating galaxy growth. Through the expansion of the post-shock gas and warm clouds will amplify its cross section outflows from the galaxy hosted within the halo. The physics behind such coupling and its efficiency should be investigated numerically.

- Are there any observational tests of our scenario? Current observations may already provide observational constraints but we are still missing an interface our scenario and observables. Phenomenological and numerical studies

should be "post-processed" to compute intensity of cooling lines and absorption columns. For example, the gas which is cooling into the warm clouds and its subsequent passage into the halo, may be a relatively prodigious producer of Lyα photons (see Vernet et al., 2017b, for example).

- What are initial physical conditions of gas penetrating halos from cosmic filaments? For the stream to become bi-phasic, the temperature and/or density of the post-shock gas must be initially inhomogeneous. It is the degree of this inhomogeneity that sets the timescale over which the medium becomes bi-phasic. Determining this requires us to investigate the thermodynamics of the filament *before* it penetrates the halo. We discuss this further in the next chapter relying on numerical simulations and analogy with the development presented here.

Chapter 3

Structure and dynamics of intergalactic filaments at $z \approx 2$

Abstract

By means of an adaptive mesh-refinement code, we performed a zoom-in simulation of a specific halo and extracted the data pertaining to one of its accreting intergalactic filaments. After having presented the need for a simulation, we shortly describe the code RAMSES. We address the common view of an IGF as a pure cylinder and detail the radial and angular properties of its gaseous component. Some key quantities are studied as they evolve along the filament and we derive a refined paradigm to study IGFs, as well as consequences regarding their fate after entering the target halo. We finally made use of the accessible data to extrapolate some subgrid physical processes which the simulation must have missed.

Contents

3.1 First motivations

After having devised a frame in which our phenomenological model applies (see Chap. 2), constraining the free parameters was the new issue. One way to constrain at least the overdensity factor f and the stream radius $r_{\rm stream}$ was to use a numerical simulation. To obtain values as realistic as possible, cosmological conditions had to be set initially. And to be able to extract the relevant quantities, a focused zoom-in was needed. This is why we decided to get closer to Yohan Dubois, who presented us the code Ramses.

An in-depth analysis of an intergalactic filament revealed a great richness of information that could be advantageously related to our problems. The analogy we found between halo accretion and filament accretion has proven to be more profound than initially thought: the very processes involved in our phenomenological modelling, namely thermal fragmentation and turbulence, were as likely to occur in the filamentary context. This convinced us to clarify and organize our findings.

3.2 Rationale

We exposed in the introduction the importance of intergalactic filaments (IGFs) as a major channel for the material needed to build galaxies. The study of the so-called "cold-mode" accretion (eg. Birnboim & Dekel, 2003; Kereš et al., 2005; Dekel & Birnboim, 2006; Ocvirk et al., 2008b; Dekel et al., 2009) was mainly focused on the thermal state of the gas when it has already entered the accreting halo and its possible fate if and when it reaches the hosted galaxy. On the other hand, following the initial theoretical works[1] from Hoyle (1951); Peebles (1969); Doroshkevich (1970); White (1984), further investigations were made about the effect of a tidal torque on filaments (may they bind galactic halos or even cluster halos) and the results on the halo spin and galactic rotation by deposition of angular momentum (eg. Pichon et al., 2011; Powell et al., 2011; Stewart et al., 2011; Libeskind et al., 2013a,b; Stewart et al., 2013; Danovich et al., 2015; Tillson et al., 2015; Codis et al., 2015). As well, some of their internal rotational structure in the form of a quadrupole of vorticity has been detailed from numerical simulations (eg. Pichon & Bernardeau, 1999; Laigle et al., 2015; Codis et al., 2015).

As far as filamentary structures are concerned, the most advanced field so far is that of interstellar filaments (ISFs), where gas radiatively cools and is further confined gravitationnally (eg. Heitsch, 2013b,a; Gómez & Vázquez-Semadeni, 2014) or by turbulent motions of the ISM (eg. Padoan et al., 2001; André et al., 2010). This advance is mainly due to the possibility of observing molecular gas in these

[1] Those works contitute the Tidal Torque Theory, or TTT.

structures (Nutter et al., 2008; André et al., 2010; Schmalzl et al., 2010; Arzoumanian et al., 2011; Hill et al., 2011; Juvela et al., 2012). The main difference between IGFs and ISFs is the role of the cooling: it initiates the condensation of ISFs whereas it is induced by the gravity-driven condensation of IGFs.

This knowledge is however a great benefit. It allowed a discrimination and a refinement of previous theories owing to cylindrical stationary structures especially in the case of an isothermal gas but also in polytropic cases (eg. Chandrasekhar & Fermi, 1953; Stodólkiewicz, 1963; Simon, 1963; Ostriker, 1964a; Fridman & Polyachenko, 1985). Of course, the isothermal case is well adapted to ISFs, but could fail in a complete description of IGFs where the thermal equilibrium is much longer ot reach. The polytropic case is more general (the isothermal case is recovered when the polytropic index tends to $\pm\infty$) and we will test the consequences of the related Lane-Emden equation in our data.

More precisely, the state of the cold core needs to be investigated further, as it is the basis of any cold mode accretion. The conditions under which such a core may collapse due to radiative cooling have been studied by Gray & Scannapieco (2013) by relating the densities and metallicities of the gas with the redshift. The consequences on the DM-gas decoupling, as well as linear masses of gaseous filaments were statistically derived from a cosmological simulation at $z \approx 5$ by Harford et al. (2008); Harford & Hamilton (2011).

The gas dynamics in IGFs, its thermal evolution from its outskirts to its "axial" core and the possible phenomena that would be missed by the simulation but traced through large scale clues, all remain to be inquired into. In order to complete the current knowledge, we will bring some answers to the four questions:

- Is the cylindrical description accurate? Under which conditions?
- What are the typical scales of a quantitative description of an IGF?
- What is the physical state of the gaseous IGF before the halo-entry?
- Do its dynamics affect its thermal state?

3.3 Numerical method

We here present the numerical means used to accurately time-integrate a limited set of physical equations, relevant to the evolution of the Universe, and down to the desired scale. The recording of successive states of the integration let us choose an accurate and realistic basis for a numerical study of IGFs.

3.3.1 The Ramses code

Ramses is a code initially designed and programmed by Romain Teyssier (Teyssier, 2002). It is remarkable by its association of an N-body simulation to describe the evolution of a set of dark matter particles with a grid whose local resolution may adapt dynamically and increase in regions of interest—namely an adaptive mesh refinement—to describe the evolution of fields pertaining to gas physics: density, pressure, velocity components, and metallicity. The numerical scheme used to integrate the hydrodynamic equations employs a high-order Godunov solver with total variation diminishing interpolation of cell-centered quantities at interfaces of cells in order to solve one-dimensional Riemann problems. It is designed to ensure the conservation of physical quantities: mass, momentum, energy, and, if needed, chemical abundances, and so on. It is also very efficient in capturing shocks, which is an ubiquitous phenomenon in astrophysics.

The refinement consists in dividing locally the side of a mesh cell by two—which means splitting each tridimensional cubic cell in eight smaller cubes to reach one higher level of refinement—for each cell of gas whose mass crosses a predefined ceiling value. When matter condenses, the mass in the cell increases up to the ceiling, then is split in eight until further condensation, so that the mass of a cell of any level is comprised in a relatively narrow interval, all cells having the same mass, in a factor of eight.

3.3.2 Cosmological simulation

We performed first a dark matter-only cosmological simulation. Cosmological parameters for this simulations include the Hubble constant $H_0 = 70.3\,\mathrm{km.s^{-1}.Mpc^{-1}}$, a matter-to-total mass-energy ratio $\Omega_\mathrm{m} = 0.276$, a flat Universe (so $\Omega_\Lambda = 1 - \Omega_\mathrm{m} = 0.724$), a baryonic fraction $f_\mathrm{b} \approx 0.1603$, an amplitude of the initial matter power-spectrum $\sigma_8 = 0.811$. Physical parameters specify that the side of the cubic box is $L = 100\,\mathrm{Mpc}.h^{-1}$ in comoving coordinates, i.e. $L \approx 142.2\,\mathrm{Mpc}$ with our choice for H_0. Numerical parameters were set so that the boundary conditions for the simulation box are periodic conditions. The primary, coarse resolution is set to $\Delta x \approx 556\,\mathrm{kpc}$ and this corresponds to a 256^3 3-d grid, which we will refer from now on as *level 8*, since $2^8 = 256$. Snapshots of the simulation were output from initial redshift of $z_\mathrm{ini} = 100$ down to $z_\mathrm{fin} = 0$.

The retained output for this study corresponds to an equivalent redshift of $z = 2.121$. A code used to detect halos and subhalos was then run on the outputs. This program is HaloMaker (Tweed et al., 2009), set up to find halos with Adaptahop (see the appendix of Aubert et al. (2004)). It provides a halo tree with their masses and equivalent virial parameters. From this catalogue, we selected a halo of $12.6\,10^{11}\,\mathrm{M_\odot}$ at redshift $z \approx 2$.

3.3.3 Zoom-in

Using one of the software tools provided with Ramses, namely *geticref*, we managed to extract the identity of all dark matter particles contained in a sphere of radius 3 times the virial radius of the desired halo and sharing the same center. The initial positions of all particles being known, it is then possible to determine the envelope of the initial region of space that will condense to form the said halo. Using the software tool MUSIC (implementation and algorithm, see Hahn & Abel (2011)), a new set of initial conditions was produced, so as to reach the refinement *level 12* in the region of interest. This time, gas is present, cooling follows the interpolated function from Sutherland & Dopita (1993) for a pristine gas (i.e. metal-free) and with no star formation.

A run is then launched with a maximal refining *level 17*. Let us recall that the finest cells have then a size corresponding to a $(2^{17})^3$ simulation, which is 348 pc of side .

From this new simulated data, we extract again a catalogue of halos with HaloMaker. Inside the region of interest, we noticed that the higher resolution, and especially the finer particles, allowed for fragmentation so that the mass initially contained in the targetted halo has split into several smaller ones. The halo we selected has a mass of $2.78\,10^{11}\,\mathrm{M}_\odot$. Its evaluated size is $r_{\mathrm{halo}} = 190.34\,\mathrm{kpc}$ and the virial radius given by the code is 58.5 kpc. This discrepancy already shows that the detected halo is not spherical. The first value has been used as unitary in all computations.

3.4 Study in cylindrical geometry

We here consider the studied filament in cylindrical coordinates. This geometry may seem obvious when tackling objects like filaments, but it would also be naive, as we will see, to model filaments as purely cylindrically symmetric regions. As matter falls onto the filament and itself and its environment are pulled by a halo gravitational well, all cylindrical coordinates are relevant, because we expect the filament to be at the intersection of sheet-like structures. The possible coordinate separation and the departure from symmetry are then tested.

The radius from the axis is denoted r. The "altitude", i.e. the distance to the center of the halo, is ζ. The azimuthal coordinate is θ. The adjective "transverse" is used whenever ζ is fixed, while "longitudinal" stands for functions depending on ζ only.

The use of cylindrical coordinates (r, θ, ζ) first requires defining a frame of reference. After having done so (3.4.1), we then set limitations helping define correct projections of the simulated data (3.4.2).

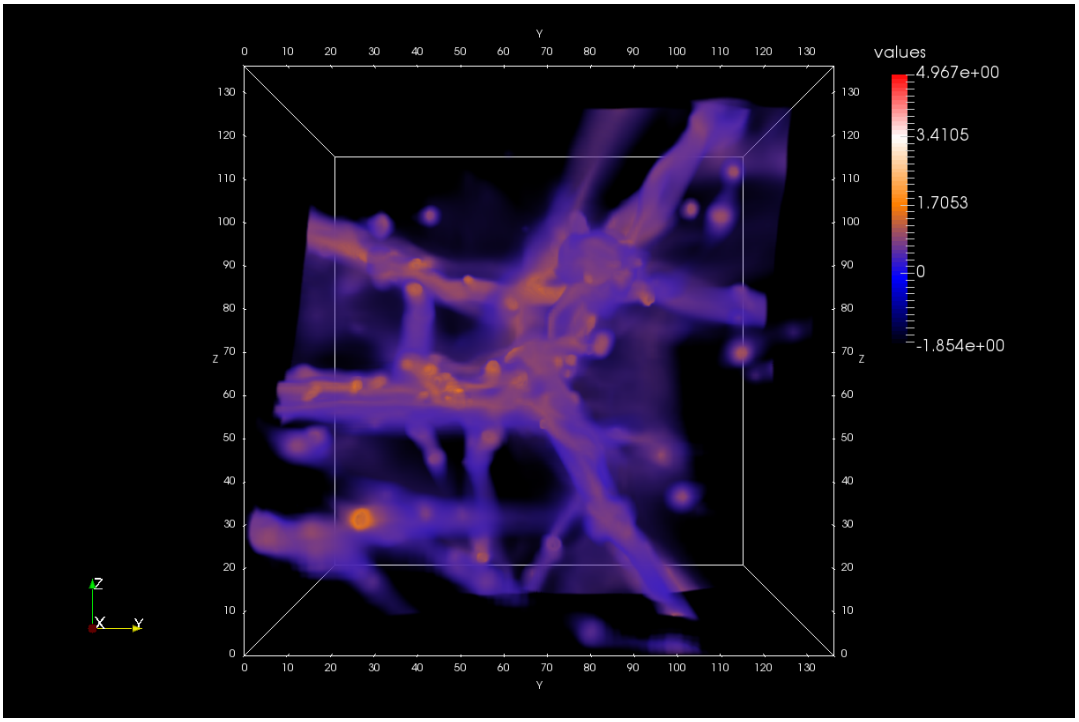

Figure 3.1: A view of the halo, with emphasis on the densities characteristic of IGFs. The cube has a side of 381 kpc and densities in the color bar range from 10^{-30} to $10^{-22}\,\mathrm{g.cm^{-3}}$, from which is only displayed a thin band around one to a few $10^{-28}\,\mathrm{g.cm^{-3}}$.

3.4.1 Choice of a reference frame

Simplest theoretical expectation: axis as a halo-halo linear bond – Filaments are by nature denser regions of space connecting even denser nodes, i.e. halos. Dynamical considerations lead to a simple definition: halo centers lie at points where the gravitational acceleration converges from all directions; between two neighbouring halos must exist a saddle-node where convergence is bidimensional and the last dimension is that of a diverging field; filaments are extensions of this saddle-node until they reach the fixed points of halos.

Choice of an origin – The most natural way of setting the origin of the cylindrical frame is to use the *detected center of the nearest halo accreting* the studied filament. Following this choice, the axis of our frame is a ray emerging from the halo and the ζ coordinate may be interpreted as a distance from the halo center. This fits with studies of halos where the relevant coordinate is the spherical radius.

Deviation from linearity – Contrary to the simplicity of a cylindrical frame, filaments have no reason to be perfect straight lines, since the whole environment is *a*

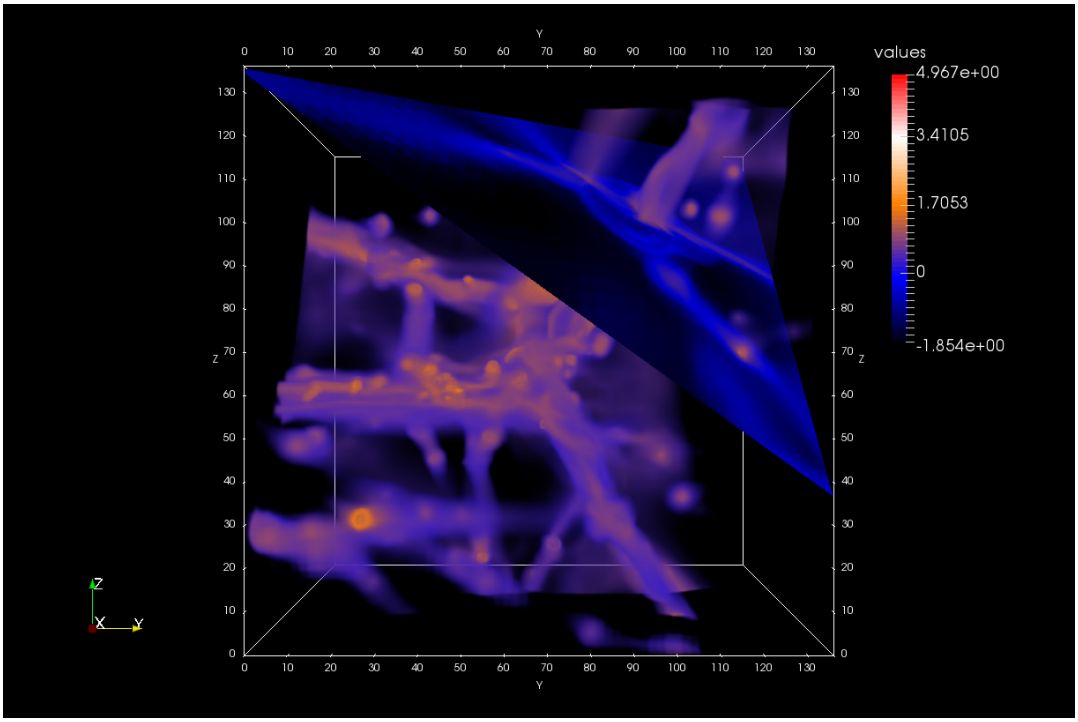

Figure 3.2: The same view as Fig. 3.1, but with a visible slice in the later examplified filament.

priori highly heterogeneous and the corresponding vector fields highly anisotropic. Despite this deviation, the interpretation of our results does not suffer from it. A finer approach would consider arcs and an even finer one would track the most probable sites for saddle-nodes with a gradient-based method. For a first study, such a refinement is not needed however. We explain further how to control the amplitude of this deviation.

3.4.2 Studying slices of data

Projecting data is quintessential to multidimensional analysis. The way the data are originally distributed has a crucial impact on optimizing the projection method. But optimization is a tedious task that can be partly skipped, whenever its benefits are in fact negligible. This is the balance we sought for.

Desired accuracy Orders of magnitude and scaling relations – One of our main goals being to establish not only narrow ranges of values for physical quantities, but also their gradients and ultimately the possible scaling laws relating them, so as to discriminate between mutually incompatible theoretical predictions

Avoiding the trap of a deceptively high precision – Firstly, the resolution of the simulation is a frontier. Even excellent methods for interpolating the data will not create additional relevant values. Secondly, even high-precision values varying at the scale of the resolution are neither to be fully trusted as a physically exact variation. Keeping these two considerations in mind, we may design methods of analysis that are both reliable enough and not resource-consuming.

Width of the slice We simply look now for a discretization step in the ζ dimension. Since the axis of the frame is arbitrary, transverse slices are taken along planes that are arbitrarily tilted in comparison with the simulation grid. An excessively thin slice would thus have few to no chance to uniformly capture data points. Moreover, the slices need to contain enough points to enhance the inevitable signal-to-noise ratio resulting from discretization. If too big a cell is cut by the slice but its center falls out of the slab, the space it occupied will be considered empty, damaging the analysis. In a way, we could say that the wider the slice, the smoother the projected fields. And on the other hand, the wider the slice, the more it will capture fluctuations, artificially blurring gradients.

The best estimate for the width $2\delta\zeta$ took into account the density of data and the fact that maps should noticeably be different between ζ and $\zeta + \delta\zeta$. Its value has been taken to be $\delta\zeta \approx 7.14\,\mathrm{kpc}$.

Assigning a corrected origin to the slice Having cut a slice, and given the fact that the filament itself is not perfectly linear, a local centering is needed. To give a proper origin in the planar frame, we use a simple method called *shrinking disk*. The principle is to evaluate the 2D coordinates of the barycenter of all points in the 3D slice and then iteratively reduce the size of the disk, evaluate the new barycenter, and so on. Doing so, from a radius of 150 kpc down to the smallest size of a grid cell in that slice (say 350 pc), dividing each radius by 1.1, the loop converges to a density peak inside the slice of filament.

It is possible then to retrieve all detected centers, slice by slice, to draw a polygonal chain that matches more closely the density valley. However, this method does not accurately correct the bias introduced by the linear approximation for the filament axis. This is because the direction of the planes is still taken constant and equal to the initial halo-halo bond direction, rather than parallel to the local line element.

3.5 Anatomy of a transverse slice

3.5.1 Structure and scales

The first thing to remark about filaments is their structure. To highlight it, transverse maps are a good means. After having detailed the distribution of matter, we will present scalar properties of the dynamics.

Density field

The supporting figure of this subsection is Fig. 3.3, made of four color maps. To exemplify the structure, we chose a transverse slice taken at 343 kpc from the center of the closest halo, which corresponds to about 1.8 times its virial radius. The colors correspond to rounded values instead of continuously varying ones, so that a color change draws a constant-value contour-line.

Dark matter The lower-left panel shows the dark matter distribution, as well as three circles used as guides to the eye. They are centered on the slice origin, defined in the way described above. Their radii are equally spaced: 30, 90, and 150 kpc.
Structuration void–sheet–filament – The contours are far from isotropic outside of the innermost circle and above 90 kpc from the origin, three lobes are apparent: two are roughly aligned in an east-west direction, while the one at south-east seems to host a dense blob. The latter is common to all the transverse slices, meaning that there is a lighter companion filament, that merges with the main one after their plundging in the halo. The former ones indicate the presence of a dense "corridor", also found in every slice, thus corresponding to a dense sheet-like structure. The least dense regions on the map are then the ones commonly referred to as voids.
Typical densities – The closest to the origin of the figure, the more isotropic are the DM density contours. The region which is apparently relevant to a filamentary description is inside the 90 kpc-radius circle. For the selected halo and at the given altitude, the densities inside this disc range from a few 10^{-29} to a few $10^{-28}\,\mathrm{g.cm^{-3}}$, with a relatively low gradient. These values are to be compared to the critical density of the Universe at $z \sim 2$, which is slightly less than $10^{-28}\,\mathrm{g.cm^{-3}}$. The DM overdensity is therefore to be compared to $\Omega_{\mathrm{DM}}\rho_{\mathrm{crit}} \approx 2.4\,10^{-29}\,\mathrm{g.cm^{-3}}$, thus comprised in a range $1 - 10$, indicating that the condensation is rather smooth.
Analogy with halos – If it was a slice cutting through a halo, we could think of a radially decreasing density with filamentary extensions. We can propose the following analogy; a filament is a dense cylindrical structure connected to other filaments by less dense, radially extended sheets in the same way halos are spherical

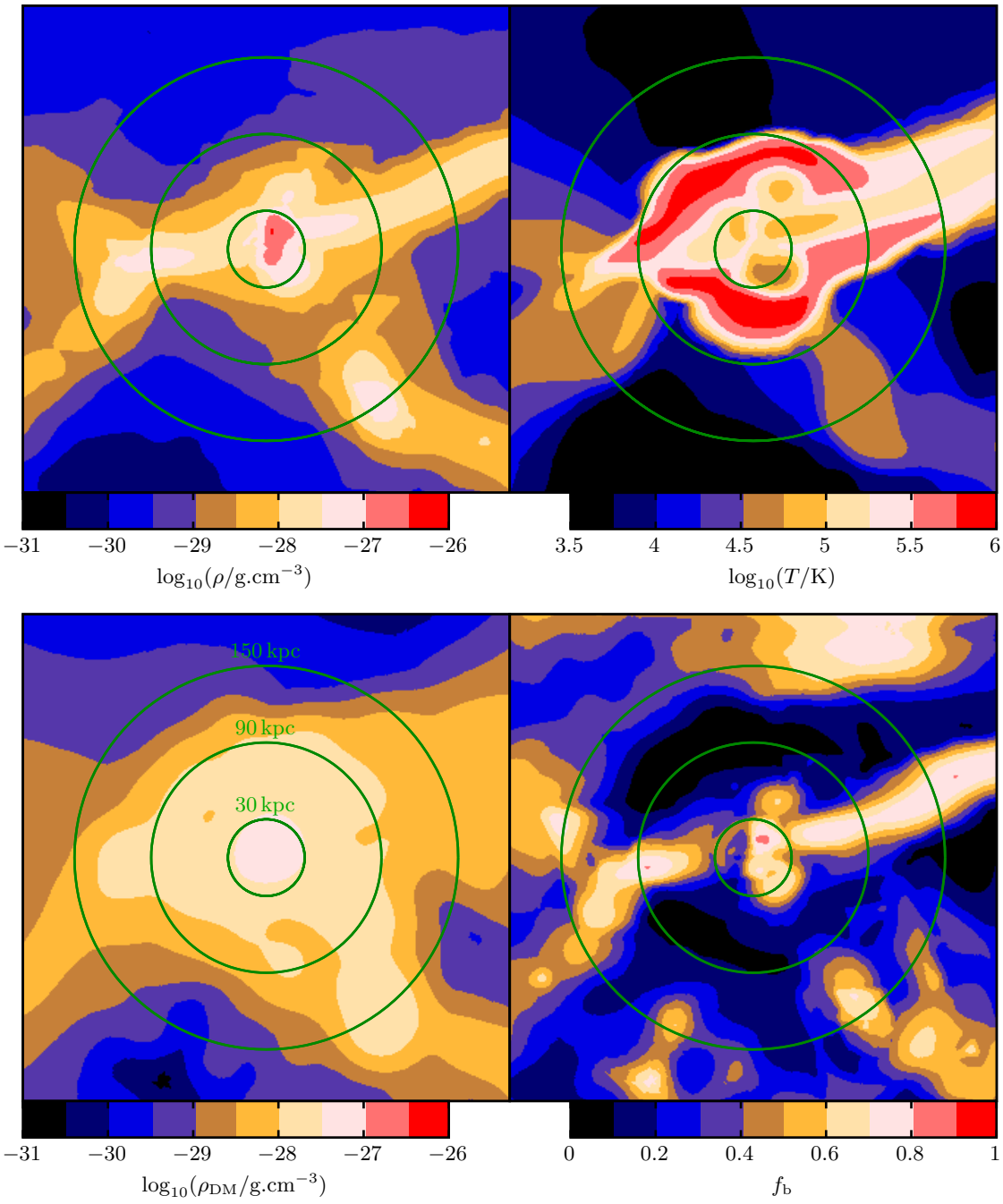

Figure 3.3: Maps of a transverse slice of an IGF, at $\zeta/r_{\rm halo} = 1.8$, i.e. at 343 kpc from the center of the closest end-point halo. Dimensions are $380 \times 380\,{\rm kpc}^2$. Marked are three circles as guides to the eye, whose radii are, as written in the bottom-left map, 30, 90, and 150 kpc. *Top-left:* gas density. *Top-right:* gas temperature. *Bottom-left:* dark matter density. *Bottom-right:* Baryonic fraction. The filament structure is clearly far from purely cylindrical, due to the importance of converging walls.

dense structures connected to other halos by less dense, radially extended filaments. This analogy is to be completed further and this will prove fruitful in understanding the dynamics and growth of filaments.

Gas The upper-left panel shows the gas distribution. The three same circles as before are shown.
Sharper structuration – The anisotropies of DM density are recognizable, except that they are much sharper. The east-west sheet, the companion filament as well as the continuation (western) of a dilute sheet aligned with the one crossing the companion (south-western) are visible. As opposed to the DM distribution, the most isotropic contours lie within a radius of 30 kpc and exhibits two small lobes, perpendicular to the sheet direction. We will further explain these.
Typical densities – Inside the innermost circle, densities range from a few 10^{-29} to up to a few $10^{-27}\,\mathrm{g.cm^{-3}}$ at the computed origin. This already indicates much stronger radial density gradients than DM. The presence of a much denser, tiny (3 kpc radius) region in slices of altitudes down to less than one virial radius follow what we will call the "dense axial core", or simply "core" of the filament. Compared to $\Omega_\mathrm{b}\rho_\mathrm{crit} \approx 4.57\,10^{-30}$ g.cm^{-3}, this represents an overdensity ranging from 10 to 1000.

Baryonic fraction The lower-right panel shows the baryonic fraction, defined as $f_\mathrm{b} = \rho/(\rho + \rho_\mathrm{DM})$, where ρ and ρ_DM are the locally computed densities of gas and dark matter, respectively. Note that the smoothing that resulted from the DM density computation is important to this representation, as sharp DM clumps would have dominated it otherwise.
Interpreting f_b – The values of the baryonic fraction need to be compared with the cosmic value. This value is a constant all along the cosmological run of the simulation and had been set to $f_\mathrm{b} = 0.1603$. On the figure, the black and dark blue regions exhibit a value lower than the cosmic one. The discrepancy between the local and the cosmic values is to be seen as the consequence of a decoupling of gas and dark matter. This decoupling happens whenever the gas is subject to physical processes which do not occur for dark matter, such as shocks or radiative cooling, as we are about to see from temperature maps.

Temperature field

Three important features are to be remarked in the top-right panel of Fig. 3.3, the one representing the temperature field in the selected transverse slice.

First, the structure voids–sheets–filament is as clear as in density maps. Voids appear cold ($< 10^4$ K), walls are hotter (up to a few 10^5 K). This is consistent with a scheme where the condensation is associated with compression and thus heating.

More, the rightmost sheet, which displays the highest density, appears hotter than its other counterparts, indicating that it must have resulted from a stronger compression through its own gas accretion.

But a strong gradient in temperature, around 90 kpc of radius, makes the filament highly contrasted: a strong shock (density and temperature ratios accross hint at $\mathcal{M} \sim 10 - 15$) propagates outwards into the gas from voids. Closer to the center, the post-shock medium gets cooler and a four-fold structure of a $10^{4.5} - 10^5$ K gas sits there. It will be found later in other fields (see Figs. 3.4, 3.14, 3.15).

Still consistently with the staged condensation aforementioned, the region where one expects the highest convergence is so compressed that a shock has formed, and further condensation is allowed by the subsequent loss of pressure due to radiative cooling. This is in agreement with the baryonic fraction map panel—where the post-shock medium extends, gas pressure is so high that it is prevented to collapse at the same rate DM does, but cooling, as a net pressure leakage term, favors a "secondary" condensation which leads to a higher baryonic fraction close to the axis.

As envisioned by Birnboim et al. (2016) in their cylindrical case, the gas accreting on the IGF can endure a shock. However, we would not try to apply their stability criterion in our case since our flow greatly differs from the one they assumed. Theirs is purely cylindrical while our accreting sheets break the symmetry and the shock fron continuity as well, and theirs is homologous while ours is not even purely radial just beind the shock (see Fig. 3.4).

Nevertheless, we can keep from that work the idea that only the dimension of the accreting object changes from a sheet, to a filament, to a halo. This reinforces the analogyi set out above, according to which a filament is subject to the same kind of accretion-related phenomena as a halo, only with a different dimensionality. Like halos, filaments may be surrounded by a shocked corona exhibiting a relative lack of baryons whereas a central region would host an overrepresentative fraction of the like.

Dynamics

The upper-left panel of Fig. 3.4 is a colormap of the radial velocity field. The bright green contours help identify where it changes sign, that is where the flow is converging on one side and diverging on the other. Outside 90 kpc, the flow is purely falling in towards the filament. Inside that radius, a quadrupolar structure, reminiscent of, and in fact analogous to the one seen in the temperature color map. It displays two facing regions where the flow converges and two other facing ones where it diverges. The four meet at the detected center of the filament. The constant inflow counteracts the central cooling, contributing to support the enclosing shocked gas.

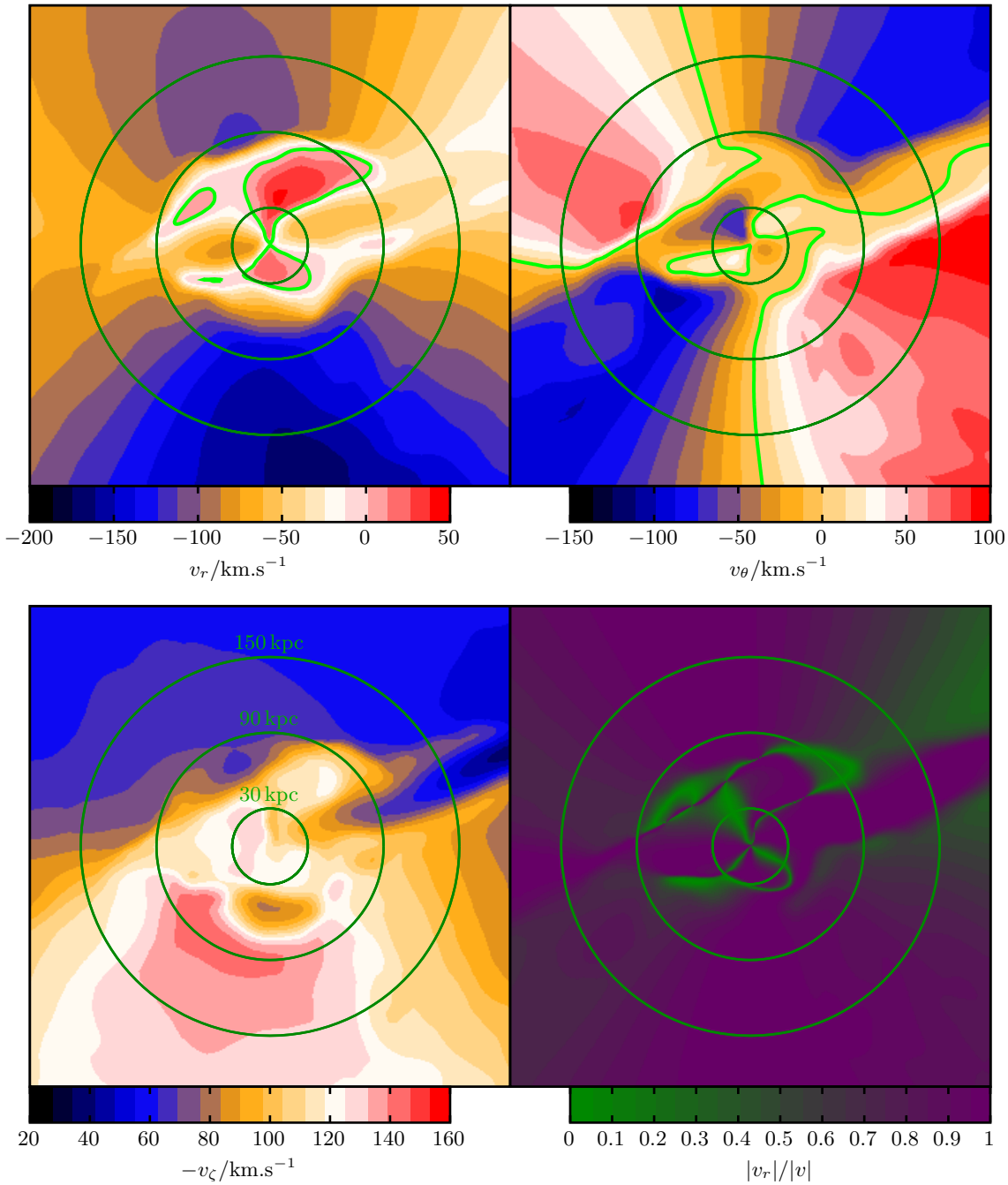

Figure 3.4: Maps of a transverse slice of an IGF, at $\zeta/r_{\rm halo} = 1.8$, i.e. at 343 kpc from the center of the closest end-point halo. Dimensions are $380 \times 380\,{\rm kpc}^2$. Marked are three circles as guides to the eye, whose radii are, as written in the bottom-left map, 30, 90, and 150 kpc. *Top-left:* Radial component of the velocity field. Bright green contours follow the loci where it changes sign. *Top-right:* Orthoradial component of the velocity field. *Bottom-left:* Infalling speed toward the halo. *Bottom-right:* Fraction of the absolute radial velocity component over the norm of the total velocity.

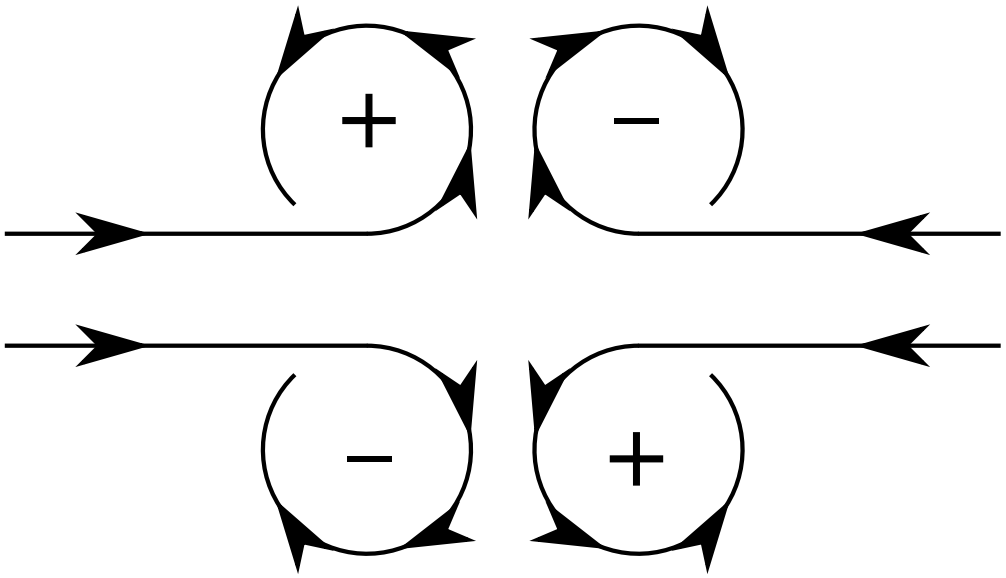

Figure 3.5: Stylized view of two converging, unidimensional jets bouncing, giving rise to a quadrupolar vorticity structure.

The upper-right panel of the same figure is the counterpart of the one described above: it represents the azimuthal velocity field, the positive (rep. negative) sign corresponding to the counter-clockwise (resp. clockwise) motion. Outside 90 kpc, the field seems to be divided in two and its vanishing contour (also in bright green) can be considered the locus where gas is equally attracted by two opposing structures, which appear to be the two pairs of accreting sheets. Inside 90 kpc of radius, the quadrupolar structure is visible but even clearer inside 30 kpc.

The lower-right panel is the colormap of a composite field, that of the ratio of the absolute radial component to the norm of the velocity. Greener colors (i.e. closer to 0) indicate that the azimuthal component dominates, whereas the more purple colors (i.e. closer to 1) stand for a radially dominated field. The two denser sheets accreting on the filament are noticeable through the fact that their dense inner slab is characterized by a purely radial inflow, while their vicinity is marked by a gradient from radial (accretion from void to filament) to orthoradial (accretion from voids to the sheets). This latter gradient is stronger further away from the filament, where its gravitational influence is lower. The inner quadrupolar structure has a clearer explanation with this panel: gas flows in from two opposite directions, splashes in the two perpendicular directions and the surrounding accretion flow imposes that four recirculation vortices form.

This qualitative description perfectly fits with that of Laigle et al. (2015) who determined that “the vorticity in large-scale structure is mostly confined to, and

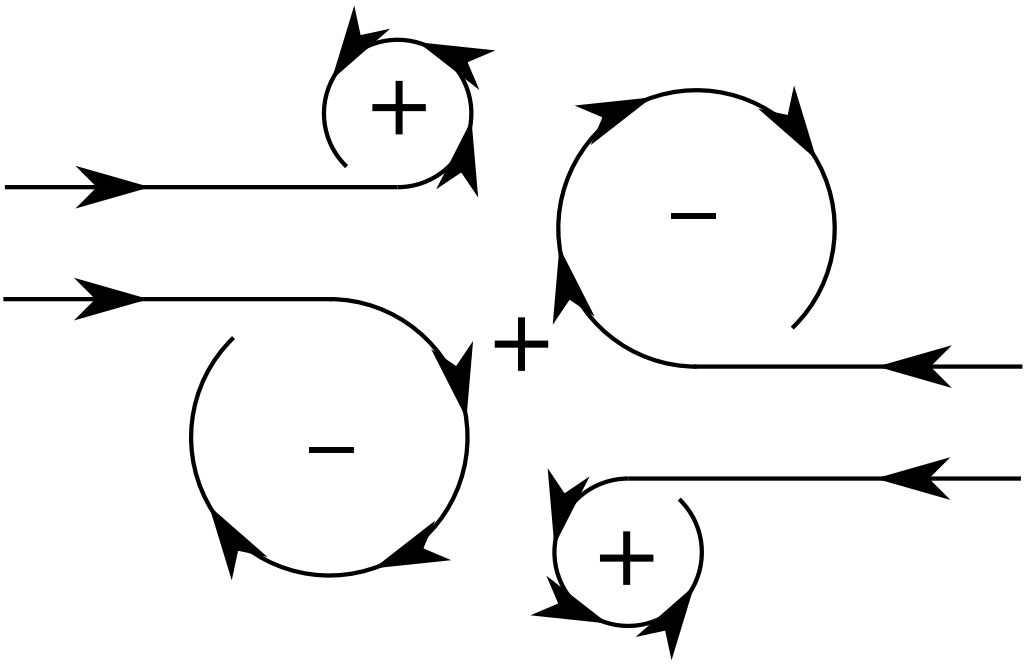

Figure 3.6: Stylized view of two converging, unidimensional jets bouncing, giving rise to a quadrupolar vorticity structure, with an impact parameter.

predominantly aligned with, their filaments" and that "the cross-sections of these filaments are typically partitioned into four quadrants with opposite vorticity sign". This is not surprising when one considers IGFs to be lower-scale versions of ICFs. Figure 3.5 presents a stylized view of two sheets meeting a producing that kind of quadrupolar structure.

Note however that there is a slight asymmetry in the structure. In fact, the two sheet-like inflows that converge in the center are not exactly aligned. This misalignment, or impact parameter, must result in a non-zero overall angular momentum. The whole rotation reinforces the vortices of the same sign whereas it should reduce those of opposite sign. This is shown, in a stylized way, in Fig. 3.6.

From the three panels described above, we can also see that the shock (see Fig. 3.3, upper-right panel) has an effect on the direction of the post-shock velocities. Indeed, as already seen, the two main shock fronts are almost nowhere purely normal to the flow, implying deflections of flowlines.

The lower-left panel of Fig. 3.4 is a colormap of the axial velocity field. More precisely, its sign is positive and corresponds to a fall towards the halo marking the end of the studied IGF. The field seems to be divided in two halves, the division being marked by the two aligned and opposite major sheets: the upper one falls slowlier ($\sim 50\,\mathrm{km.s^{-1}}$) than the lower one ($\sim 100 - 15\,\mathrm{km.s^{-1}}$). Close to the shock

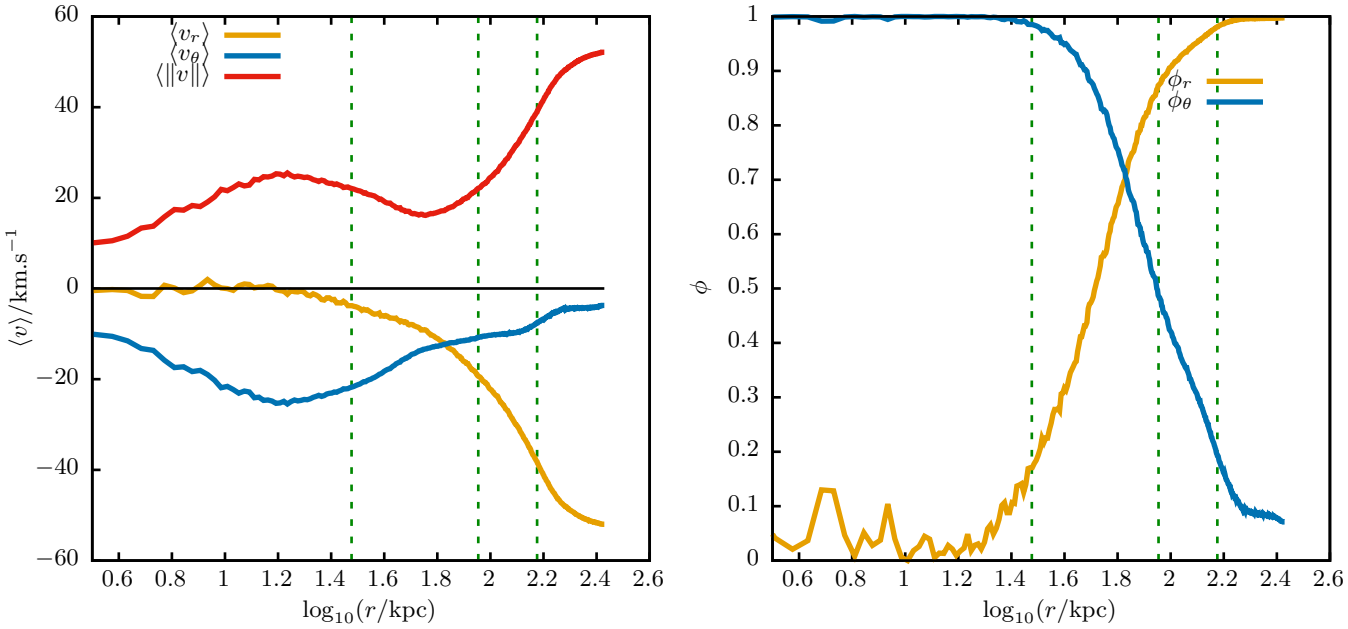

Figure 3.7: *Left*: Evolution of the radially mass-averaged velocities. Shown are the averaged radial (orange) and azimuthal (blue) components, as well as the norm (red) of the velocity field. *Right*: fraction of the radial (orange) and complementary azimuthal (blue) components in the total norm. The vertical green dashed lines indicate the three guides at 30, 90 and 150 kpc.

fronts, anomalies are found: those strong gradients of v_ζ may indicate an already present vorticity directed parallel to the mapped plane. Is it a hint to a growing Kelvin-Helmholtz instability on the void-filament surfaces? Such an instability and in this precise context is currently researched, for example with the series of papers beginning with Mandelker et al. (2016).

Let us recall Fig. 3.6. Does it really apply to our filament? To see that, we performed a radial, mass average of the radial and azimuthal components of the velocity field in the transverse plane. Each is defined as follow. For a collection of N particles, indexed by i and affected with masses, radial positions and velocities $m_i, R_i, \mathbf{v}_{ii\leq N}$, we define, on a disc of radius r, the mass-averaged radial velocity $\langle v_r \rangle(r)$ and as:

$$\langle v_r \rangle(r) = M(r)^{-1} \sum_{R_i<r} m_i \mathbf{v}_i \cdot \mathbf{u}_r \tag{3.1}$$

with $M(r)$ the mass inside the considered disc: $M(r) = \sum_{R_i<r} m_i$ and $\mathbf{u}_r$ the radially directed unit vector.

The lefthand panel shows that the total norm of the mass-averaged velocity, being a proxy to the kinetic energy, strongly decreases while approaching the center. Its steeper decline is in the region containing the shock. That energy is dissipated by viscous forces and the resulting heat then radiated away. The radial component is everywhere negative, which is a signature of a flow converging at all scales. This is what allows us to read and interpret this plot from the large to the

small scales. Its absolute value follows the same decline as the total norm from 300 kpc down to about 12 kpc. Alike, the azimuthal (or orthoradial) component is everywhere negative. This implies that at any scale, the flow is globally rotating clockwise. This confirms the sketch of Fig. 3.6. The righthand panel explains the drop of radial component at 12 kpc: whatever may be the dissipative effects, the convergent flow is converted into a rotative flow as we approach the origin.

Even if a radial only study erases all anisotropies, this is still an important feature of the gas flow: rotation may stabilize the gas against its collapse.

3.5.2 Accretion rates

A good test of the cylindrical approximation, apart from the qualitative appreciation of transverse colormaps, consists in plotting the accretion rates at different radii and as a function of the azimuthal coordinate θ. In a perfect cylindrical geometry, these plots would be vertical lines. To compute such accretion rates, we opted for simplicity. Instead of binning angularly, we simply projected, for each point of the transverse slice, the product of the density by the radial velocity. It is then a mass flux through a rectangular section whose area is the product of the slice's width by the pixel width.

Figure 3.8 reports, in logarithmic scales, those quantities. The points are taken in three rings of radial width 10 kpc and of central radii 150, 90, and 30 kpc. At 150 kpc, the accretion is clearly not cylindrical and we can determine the entry regions of sheets. A black horizontal line serves as a guide to discriminate between accretion from voids and from denser structures. The highest peak corresponds to the companion filament. At 90 kpc, the peaks have dampened and the main accreting sheet dominates. Some blue points are found close to the angle π, meaning that there is a tiny angular sector of outflow. At 30 kpc, two main contributions to the inflow are found, separated by two outflows: this is precisely the vortical quadrupole which is responsible for that. The fact that the angular spans are not all equal hints at the asymmetric picture of Fig. 3.6.

We can now say that the mass flows inwards are neither invariant under rotation nor does the cylindrical accretion (from voids) prevailing.

3.5.3 Unsteady, out-of-equilibrium

Radial binning – Only the radial coordinate (i.e. distance to the axis) has been retained to produce radial profiles. The loss of angular information then erases a lot of the inner filament structuration (eg. the vorticity quadrupole), but aims at finding a more general, detail-blind model that may subsequently help designing idealized and toy models.

Choice of a slice – The selected slice is at $\zeta \approx 343\,\mathrm{kpc}$ (recall that $r_{\mathrm{vir}} \approx 60.8\,\mathrm{kpc}$).

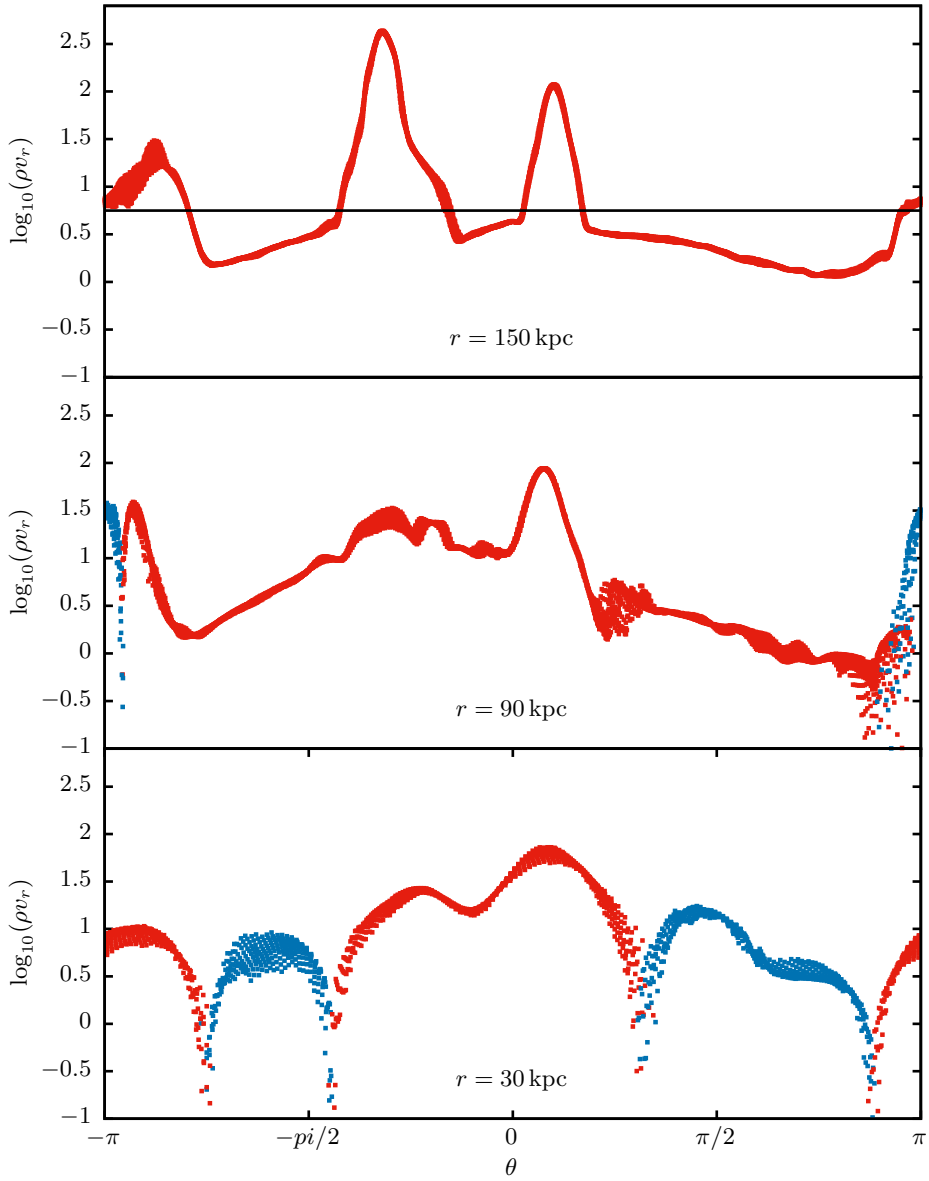

Figure 3.8: Mass inflow azimuthal profiles in a transverse slice of an IGF, at $\zeta/r_{\mathrm{halo}} = 1.8$, i.e. at 343 kpc from the center of the closest end-point halo. Represented is product of the density times the radial velocity in $\mathrm{M}_{\odot}.\mathrm{kpc}^{-2}.\mathrm{yr}^{-1}$ (logarithm), at three radii, in rings of width $\delta r \approx 3\,\mathrm{kpc}$. Red points are for radially converging flows and blue points for radially escaping flows. *Top:* $r = 150\,\mathrm{kpc}$. The horizontal line gives an arbitrary value to discriminate between sheets and voids. *Middle:* $r = 90\,\mathrm{kpc}$. *Bottom:* $r = 30\,\mathrm{kpc}$. This illustrates the fact that the asymmetrical structure due to inflowing sheets tends to disappear as the radius is decreased.

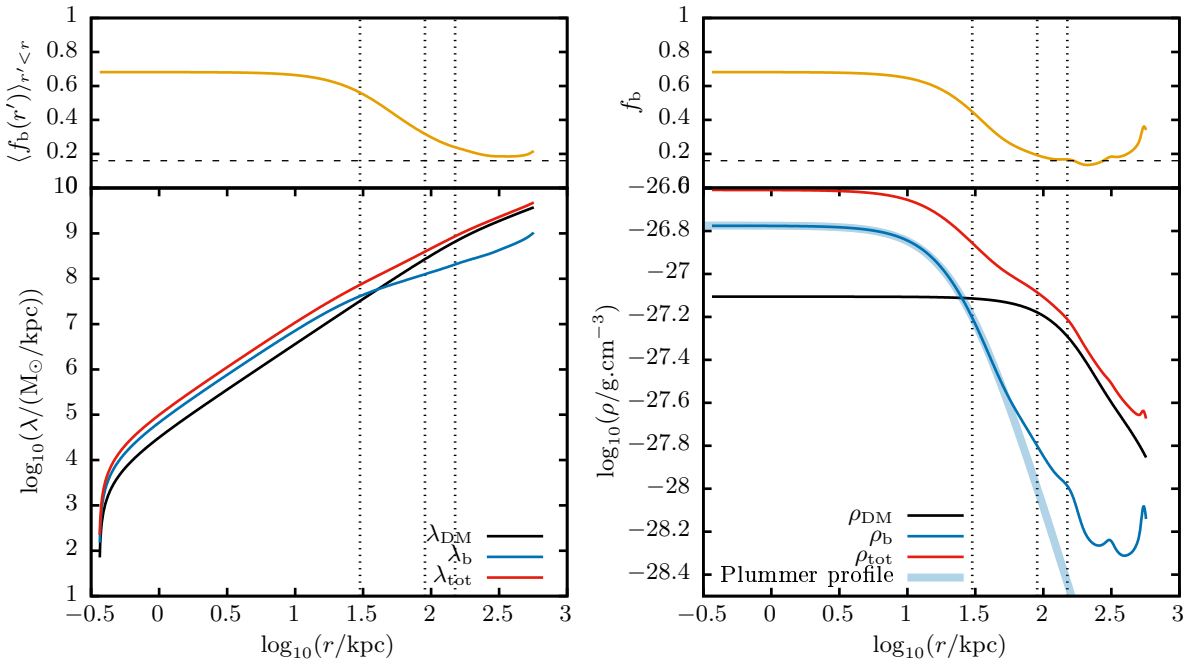

Figure 3.9: Radial profiles of the cumulated linear mass (*left*) and the density (*right*) at $\zeta = 343\,\mathrm{kpc}$. Radii are given in log. Above is plotted the average baryonic fraction inside a ring of given r (*left*) and the baryonic fraction at each radius r (*right*) with a horizontal dashed line representing the cosmic value. The grey dotted vertical lines correspond to the illustrative measures of $r \in \{30, 90, 150\}\,\mathrm{kpc}$. In light blue is shown a fit of the gas profile by a Plummer profile with parameters $\rho_0 = 1.68\,10^{-27}\,\mathrm{g.cm^{-3}}$ and $r_0 \approx 24\,\mathrm{kpc}$ (see text for details).

Mass and density profile

Fig. 3.9 present the mass and density radial profiles of the selected transverse slice. The radii go below the highest resolution scale of $\sim 110\,\mathrm{pc}$ because of the projection effect of a thin slice tilted from the simulation grid axes. We kept these bins because, even if it may appear too ambitious, the profiles are rather consistent at these low scales. The histograms are made of 20 bins and have been produced using 8608 cells (total $8.87\,10^8\,\mathrm{M_\odot}$) of gas and 1706 dark matter particles (total $4.28\,10^9\,\mathrm{M_\odot}$).

As is often the case with polar or cylindrical geometries, the choice of a center is crucial to the radial profiles. For the transverse maps, we used the shrinking disk method, computed with all masses, gas and DM. Here, since one of our goals is to compare with self-gravitating models of gaseous filaments, we let the code set the origin based on gas masses only.

To produce these profiles, interpolation was needed. Like for transverse maps, the discrepancy between data representations is a challenge. Let us recall that gas is computed on a grid whose axes are not align with those of the slice and dark matter is a cloud of mass points. To emulate a filled space, we used the same technique as for maps: both gas and DM are considered mass points and we operated a convolution of the resulting distribution with an adaptive gaussian, bidimensional kernel.

Projecting the distribution of points, indexed by i, on the radial component only requires a transform of the kernel $\kappa_i(r)$:

$$\begin{aligned}\kappa_i(r) &= \frac{1}{2\pi\sigma_i^2} e^{-\frac{r^2+r_i^2}{2\sigma_i^2}} \int_0^{2\pi} e^{\frac{r r_i \cos(\theta)}{\sigma_i^2}} \mathrm{d}\theta \\ &= \frac{1}{\sigma_i^2} e^{-\frac{r^2+r_i^2}{2\sigma_i^2}} I_0(\frac{r r_i}{\sigma_i^2})\end{aligned} \tag{3.2}$$

where r_i and σ_i are the positions and adapted spreadings of the distribution, and I_0 is a modified Bessel function of the first kind and of order 0.

Such an interpolation allows for an oversampling of the radial bins. But are the results physical? We compared different samplings to understand the effects of our choices. First, a linear interpolation of the cumulative mass gives very noisy results, polluted by the dark matter discrete distribution. The fact that DM acts on the flow through its potential (inverse square law) is not accounted for in this case. Then, the choice of the kernel size matters. We scaled it, as would seem natural, with the simulation size of cells: $\sigma_i = \alpha \Delta x_i$. The applied coefficient α spreads the densities. Increasing its value obviously smooths the profile but also changes amplitudes. Above $\alpha = 5$, the profile does not change anymore. We thus retained this value.

Of course, some features may be smoothed out but the smoothing factor being proportional to the resolution length, which in turn is shorter at small radii, the general behavior of the profiles is preserved in logspace representation. The binning was chosen to be regular in logspace, totalling 1000 bins. It even reinforces the continuity of the density field close to the center, since it would have been highly fluctuating due to the small samples in inner shells.

Typical linear mass range – The linear density of our filament at this altitude give us a typical range of values: from $r \approx 30\,\mathrm{kpc}$ to $r \approx 150\,\mathrm{kpc}$, the linear mass is comprised in the interval $3\,10^7 < \lambda/\mathrm{M}_\odot.\mathrm{kpc}^{-1} < 10^9$.

Density profiles – On the other hand, density seems to fall with a power-law of slope ~ -1 after a central plateau. Gas density itself declines with an exponent ~ -2. The gas density profile itself resembles a Plummer-like profile, with a plateau below a characteristic radius (here between 3 kpc and 10 kpc) and a power-law decline. This cylindrical profile is inspired by Ostriker (1964b), where

the following law was proposed:

$$\rho = \frac{\rho_0}{\left(1 + \left(\frac{r}{r_0}\right)^2\right)^{p/2}} \tag{3.3}$$

where the plateau is set at a value of ρ_0 up to a radius of r_0 at which it bends down with an asymptotic slope p. This was developed from the Lane-Emden equation[2] for an isothermal gas in cylindrical geometry, with $p = 4$.

The idea to fit our data with an other exponent is consistent with the fact that the gas we study is not the sole source of gravitational potential, that it is certainly not isothermal but maybe evolving from or towards such a case, and that a rotation parameter, function of the radius, may alter the slope by supporting the gas. The gas density profile is well fitted by such a profile, with $\rho_0 = 1.68\,10^{-27}\,\mathrm{g.cm^{-3}}$, $r_0 = 23.89\,\mathrm{kpc}$ and $p = 2.070$.

Dark matter also seems to follow such a profile, with a much broader plateau. This is a signature of the impossibility for DM to condense through dissipation. The lag betwwen the knees of gas and DM explains the decreasing of the baryonic fraction.

DM-gas decoupling – The baryonic fraction f_b helps understanding the importance of gas physics. When below ∼20 kpc of radius, the baryonic fraction is higher than the cosmic value. At 30 kpc it reaches 50%. Then it decreases toward the cosmic value, reached around 90 kpc, and finally increases again up to 150 kpc. Above 300 kpc, an other dense structure is met. Clearly this indicates a decoupling of gas and dark matter inside the filament. While the gas may condense, dark matter particle fly through the space without collision.

Existence of a core – The existence of a plateau at low radii helps defining a dense core. But an explanation for this phenomenon still remains to be found. To understand the fact that the gas has neither completely collapsed due to cooling nor has it been prevented from collapsing, we must investigate two families of processes—namely, the confinement and the support forces.

3.6 Anatomy of longitudinal structures

3.6.1 Longitudinal slices

In the previously shown figures of transverse slices, the natural coordinate system from the cylindrical geometry would reduce to polar coordinates (r, θ), ζ being a given constant. Setting the center as the origin and the x-axis a the reference, angles θ are completely defined. In each slice, we took a "sliver", that is a thin beam along a given direction θ, from each transverse slice. The sliver data array is built by linear interpolation of accordingly rotated transverse slices. We juxtaposed them to build a longitudinal slice corresponding to θ. The width of the sliver was set to match the resolution of transverse slices, that is 365 pc. Each sliver is represented vertically on the longitudinal maps with the width of each transverse slice, that is 7.14 kpc, and is made of 200 data values, i.e. having a (vertical) resolution of 2.9 kpc.

Having done so brings one advantage and one disadvantage. Using the centered transverse slices aligned all those centers in the longitudinal slices, making the filament appear rather straight. This straightness is an artifact. The advantage resides in the setting aside of environmental effects that bended the IGF and thus ensures the visibility of a continuity in longitudinal structures. The drawback is the exact other side of the coin: the hidden bendings could have proven useful to trace either a regular pattern (such as an instability possibly originated from vorticity) or its effects on the internal structure. Such curvature effects are still to be investigated.

Figures 3.10 and 3.11 show longitudinal slices constructed the way described above. They count in total four columns, each for a given angle, and three rows, each for a different field: entropy, temperature, and density. The chosen angles are irregularly spaced: $\theta \in \{\pi/8,\ \pi/2,\ 11\pi/16,\ \pi/33,\ \pi/32\}$. They correspond, respectively, to the following directions of the exemplified transverse map (the one at $\zeta = 343\,\mathrm{kpc}$): that of the most strongly accreting sheet, that crossing the most shocked medium expanding in the voids, that containing the western converging entry point, and that which crosses the interesected companion filament. The trace of the previously marked circles in the transverse maps are here highlighted by green dashed horizontal lines, as if they were generatrices of three coaxial

[2]The Lane-Emden equation describes a hydrostatic equilibrium. It is a rewriting with non-dimensional variables of the combined hydrostatic and Poisson equations. Its two parameters are n, the polytropic index, and N, the spatial dimension of the problem. Only a few exact solutions are known and other numerically integrated solutions have been tabulated and published (cf. Ostriker, 1964a). It has been extensively studied, for example by G. Horedt (Horedt, 1970; Viala & Horedt, 1974a,b; Horedt, 1983, 1986a,b, 1987a,c,b; Oproiu & Horedt, 2008), who published a book specifically dedicated to polytropes in astrophysics: Horedt (2004).

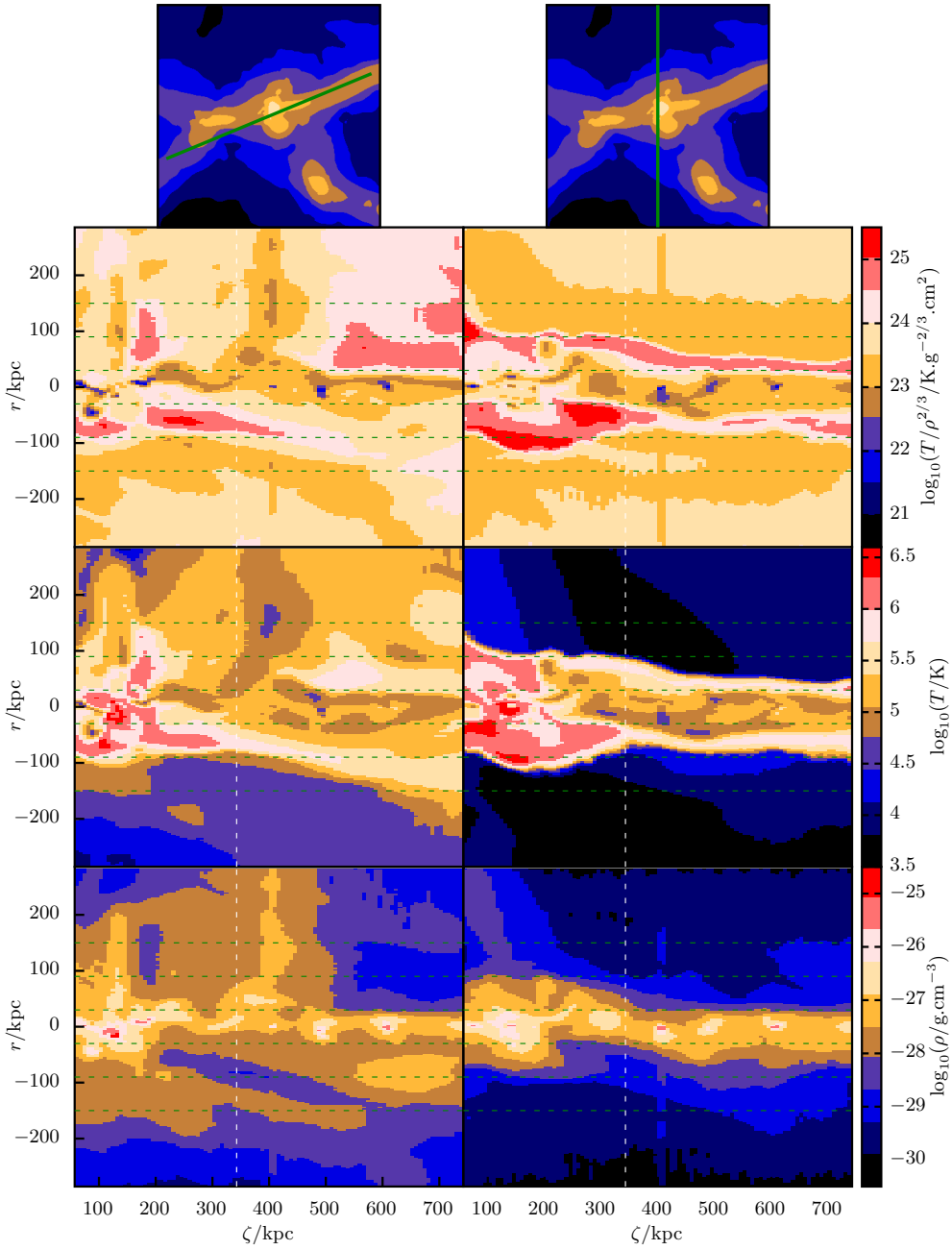

Figure 3.10: Maps of a longitudinal slice of an IGF, at different slicing angles. Dimensions of each map are $\Delta\zeta = 704$ and $\Delta r = 570\,\mathrm{kpc}$. The rows show three fields. From top to bottom: the density, the temperature, and the entropy. The columns show two different sclicing angles. From left to right: $\theta = \pi/8$ and $\theta = \pi/2$, each being illustrated by the green solid lines in the top transverse slices. Horizontal dashed lines correspond to the three circles of transverse slices. The vertical white dashed line corresponds to the exemplified slice.

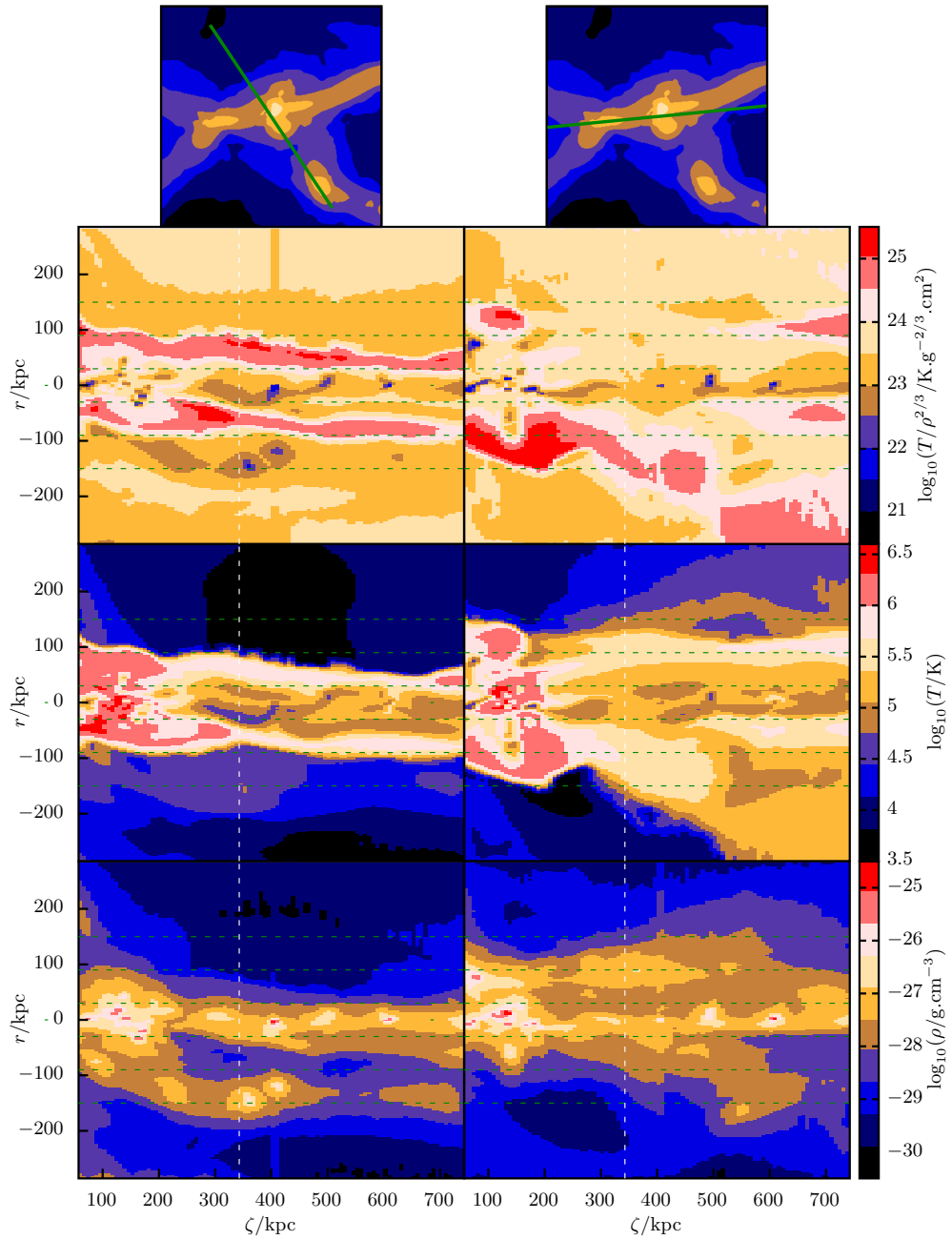

Figure 3.11: Maps of a longitudinal slice of an IGF, at different slicing angles. Same as Fig. 3.10 but for angles $\theta = 11\pi/16$ and $\theta = 33\pi/32$.

cylinders.

The simple view of a filament as a tube is found in the longitudinal slice at $\theta = \pi/2$ (right-hand column of Fig. 3.10). The dense core has an almost constant radius of ~ 30 kpc and is embedded in a larger tube of shocked gas of radius $60-90$ kpc. Two peculiarities are already remarkable: at the halo radius (190 kpc), an accreting subhalo is encountered. It is still interesting to see that its own gaseous halo is in direct continuity with the filament gas. Note that its own shocked gas (over 10^6 K) would be found in transverse cuts between $\zeta = 240$ kpc and $\zeta = 300$ kpc, where the condensation of the subhalo may not be the cause of this shock stronger than at higher altitudes. A strongly shocked envelope may develop at the filament edges with voids and invade the filament: this can explain the presence of a virial-like shock in filaments from other numerical works, with an external origin and propagating outside-in.

The second noticeable feature is the presence of small condensates along the axis of the filament. The entropy map is clearer: five spots of very low entropy are aligned; they have sufficiently condensed to strongly contrast with their gaseous environment. Their apparent radius is close to 30 kpc.

This is reminiscent of, at higher scales, galaxies forming in the cosmic web, or at much lower scales, stars forming in interstellar filaments. This common behavior has been studied in Freundlich et al. (2014), where a dispersion relation is derived to describe this pattern emerging from a gravitational instability in a self-gravitating, rotating cylinder.

The other angles of longitudinal slices (left-hand column of Fig. 3.10 and Fig. 3.11) show that what has been learnt from the one transverse slice studied above is almost generic, all along the filament. Indeed, its environment does not vary much in structure with the altitude ζ. The main accreting sheet is almost always found at the same angle $\theta = \pi/8$, except maybe above $\zeta = 485$ kpc, where it may be slightly tilted. The filament companion is at about $\theta = 11\pi/16$ all along too, and it merges with our IGF exactly in the accreting subhalo, close to $r_{\rm vir}$. We can propose the following hypothesis for the formation of that subhalo: a small structure had condensed in the IGF and gravitationally attracted the companion, with the help of the spherical geometry of the potential of the main halo, that naturally tends to make falling objects converge. The entry point where two sheets merge is also constant in position, at $\theta = 33\pi/32$.

3.6.2 Linear masses

Linear masses are of interest, as they are often assumed constant along IGFs and their value can be considered one of the main input parameters in models (correlated with the central density and exponent of a Plummer profile). Figure 3.12 presents the linear mass λ of the filament as a function of the altitude ζ. The

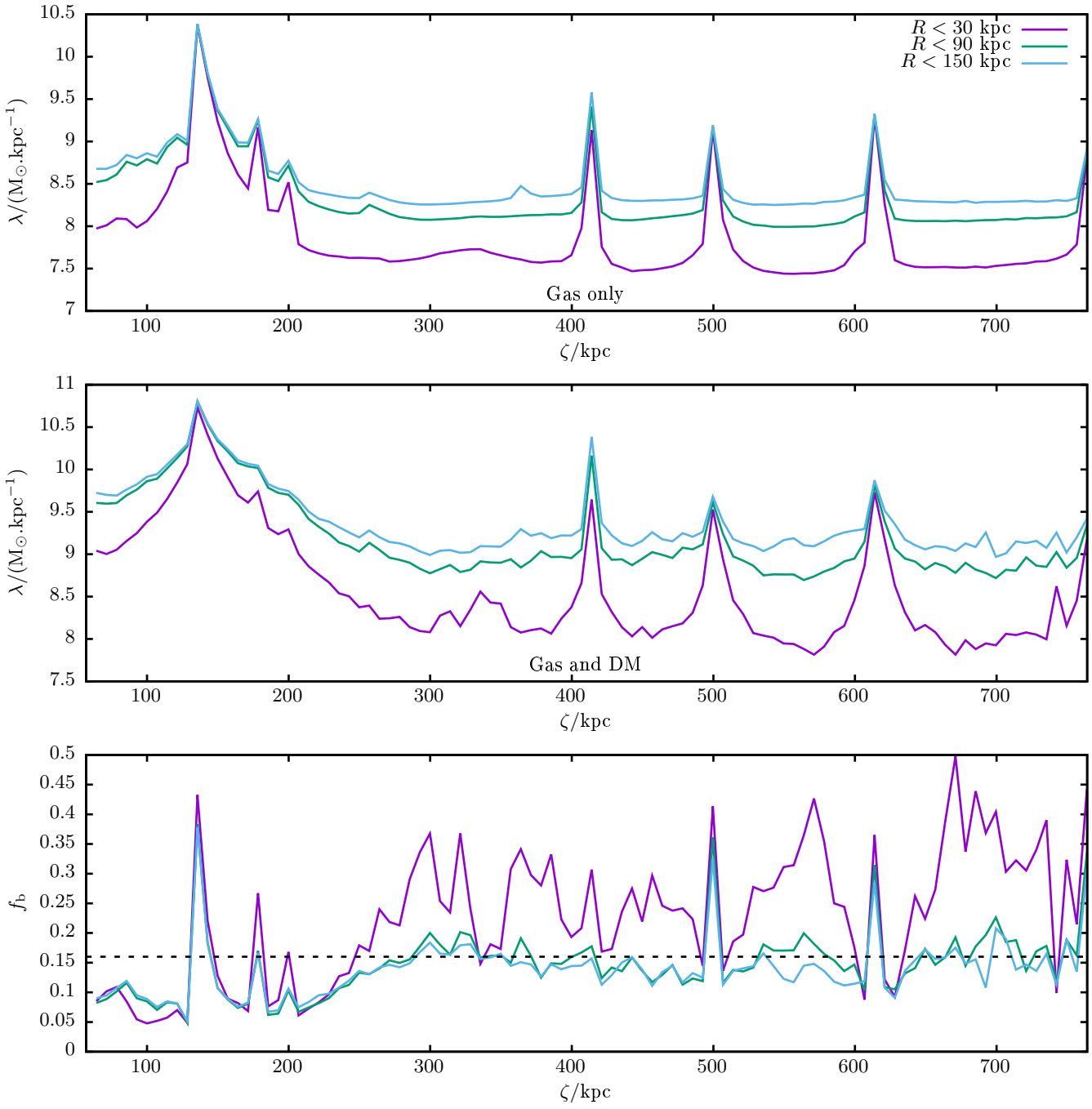

Figure 3.12: Linear mass λ, in $M_\odot$/kpc as a function of the altitude ζ, taken for each slice at radii $r = \{30, 90, 150\}$ kpc. *Top:* linear mass of the gas only. *Middle:* linear mass of all matter. *Bottom:* baryonic fraction at th three radii.

masses of gas only varies smoothly and the positions of localized condensates are rather clear. The ground value for the filament is close to $10^7\,\mathrm{M}_\odot/\mathrm{kpc}$ of gas inside the cylinder of radius 30 kpc, and $\sim 10^8\,\mathrm{M}_\odot/\mathrm{kpc}$ in cylinders broader than 90 kpc. At 150 ± 60 kpc, the accreting subhalo is visible.

Total matter linear masses show that all condensates have a halo-like structure, more extended than their gaseous component. The baryonic fraction shows that above 30 kpc of radius, it is very close to the cosmic value, except in the core of some condensates and in the subhalo. Inside 30 kpc of radius, however, f_b oscillates between the cosmic value and $35-45\%$, indicating that the gas occupies a dominant role close to the axis. This also means that it experienced a "secondary" condensation almost everywhere due to radiative cooling. This noisy behavior may be explained by the combination of the partly arbitrary nature of the centering in each slice, and the fact that the density peak may oscillate (for example due to the vicinity of the four vortices).

A notable feature appears at $\zeta \approx 336$ kpc. Inside the 30 kpc disc, there seems to be an aggregate of dark matter which corresponds to a slight local increase in the gas linear mass. It is also correlated with a relatively low baryonic fraction (more precisely, it is the cosmic value) compared to the neighboring values. Finally, it is seen on the longitudinal maps (Figs. 3.10 and 3.11) that an dense pocket, analogous to those surrounding other condensates, extends around 320 kpc. This may be a new condensate in formation.

3.6.3 Characterizing the condensates

The condensates appear at the following altitudes: 336 (in formation?), 414, 500, 614 and, extrapolating the rightmost linear mass increase, 769 kpc. Their relative spacings is not constant but decreases with ζ. This does not enable us to define a typical wavelength to compare to the Jeans length or even to models of rotating cylinders, like in Freundlich et al. (2014). If the intervals depend on ζ, and since they must have formed through a gravitational instability, they must be linked to quantities involved in such instabilities and that evolve with ζ. We can suspect the accretion rate on the IGF from the sheets and voids, the imparted torque, and the tidal stretching imposed by the IGF's ending halos. More investigation is needed, especially through outputs at previous redshifts.

They are best seen by use of transverse slices. Fig. 3.13 shows the entropy field of four slices whose altitudes ζ match with the positions of maximal linear mass enumerated previously. What is striking is that the condensates show two orders of magnitude in entropy less than their immediate environment. They seem to form close to the meeting point of the two sheet-like flows, but all present low-entropy lobes, extending into one of the four central vortices, and each time a vortex that has the same sense of rotation as that determined by the impact factor

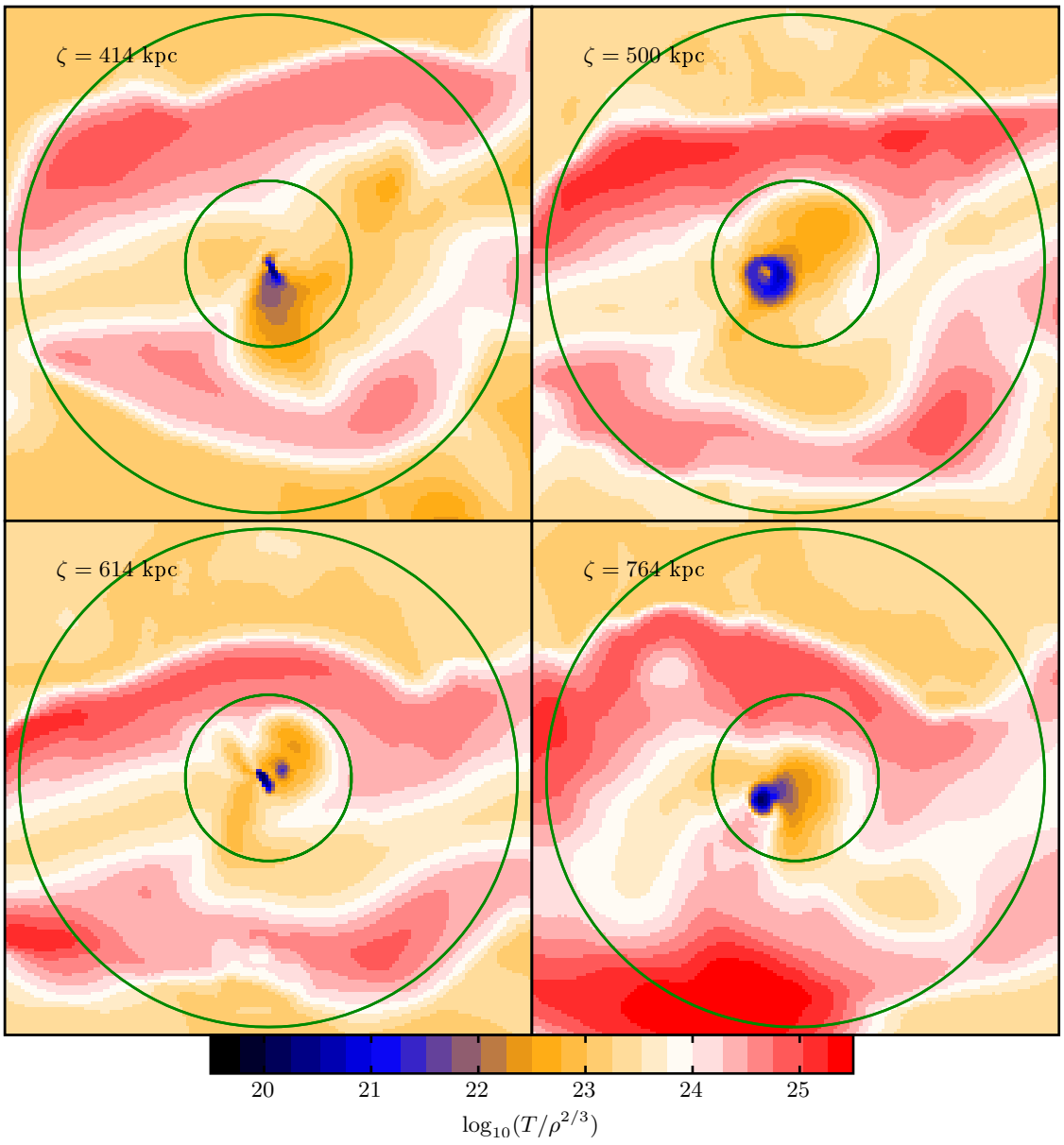

Figure 3.13: Maps of four transverse slices of an IGF, at $\zeta \in [414, 500, 614, 764]$ kpc, from the center of the closest end-point halo. Dimensions are $190 \times 190\,\mathrm{kpc}^2$. Marked are two circles as guides to the eye, whose radii are 30 and 90 kpc. The represented field is the logarithm of $T/\rho^{2/3}$, used as a proxy to the entropy. The condensates are distinguished by their very low entropy.

between the sheets (here the clockwise sense). We hypothesize that either they formed inside the vortices and migrated, leaving a trace behind; or they formed in the more central region (which should also host a weak vortex) and the strongest neighboring vortex sucked its cool gas in. In both cases it must be a region of low shear and high compression. The first hypothesis is however more consistent with the dynamics described in Laigle et al. (2015), as sketched in their figure 11.

An other interesting fact concerns the shape of the condensates. At 414 and 614 kpc, they look elongated in a north-west to south-east direction, which suggests that they are tridimensional oblate structures whose spin is perpendicular to the filament's axis. The two other slices show, on the contrary, two shapes closer to circles, letting us think of either a disk whose spin is parallel to the main axis, or a sphere cut by the slice. More investigation is needed to see if, like in inter-cluster filaments that carry haloes of masses $10^{11} < M_{\rm H} < 10^{13}\,{\rm M}_\odot$, the spin is correlated with the shear tensor, as suggested by Libeskind et al. (2012). Laigle et al. (2015) studied systematically a number of ICFs and derived a correlation between the spin-filament and the spin-vorticity alignments with the mass of the halo. They derived probability distributions for the cosine of the relevant angles. The spin and the filament are misaligned (almost perpendicular) for high masses and it tends to align descending from 10^{13} to 10^{12} ${\rm M}_\odot$. From there, where the alignment was found to be maximal, the angle between the two directions increased again while descending from 10^{12} to 10^{11} ${\rm M}_\odot$. Since our condensates barely reach 10^9 ${\rm M}_\odot$, we can not rely on these correlations to explain our case.

We looked closer at the first condensate, the one lying at $\zeta = 414$ kpc. Using a principal component analysis to study it in a geometry closer to spherical, we could derive radial information. Cumulative mass profiles indicated that the mass, corresponding to a sphere with an average density 200 times higher than the critical one, is 2 10^9 ${\rm M}_\odot$. The associated radius is 12 kpc in the PCA space, which roughly corresponds to the width of a transverse slice. Gas largely dominates its matter content up to a radius of about 2 kpc and settles in accordance with the cosmic baryonic fraction at about $3 \times r_{200}$. Note however that, even if the sample of particles and grid cells is sufficient to derive smooth statistics, the numerical resolution of the central part of the condensate is the highest. This means that no further refinement occurred below about 1 kpc of radius.

An other remarkable feature is seen in the temperature-density distribution. Although it is clear that gas cools while converging, inside a sphere of a few kpc, the distribution follows a compression which is asymptotically adibatic while approaching the center of mass. This is not a physical effect and rather reflects the artificial polytropic equation of state applied by Ramses to avoid producing singularities when conditions are met to form stars. Since we did not turn the star formation routine on, we only get this signature of a likely star-forming gas in the

inner shells. The study of the virialization by comparing pressure, gravitational and centrifugal forces on spherical shells is therefore compromised by this artificial bias.

If more appropriate parameters are given (higher resolution and star formation), a fraction of the 10^9 $M_\odot$ of gas will end up into stars. This would enrich the IGF gas with metals, critically enhancing its cooling. The scales of masses and sizes point toward a forming dwarf galaxy. It is noticeable, in the sense that IGF could therefore be considered as channels for dense gas, but also dwarf galaxies, directed toward a somehow typical halo.

3.7 Beyond simulation: modelling subgrid features

Numerical simulations are of immeasurable help to researchers, as it is the integration of a number of coupled differential equations that would not be easily solved analytically otherwise. But first, the "cooking" depends on the ingredients put in, that is, a finite set of approximate physical laws relying on an other finite set of assumptions. May the numerics get close to the boundaries of the assumed ranges and regimes, it would be highly dangerous to credit the results with full validity. Second, integrating numerically means using discrete spaces of values. This generates quantization errors which can propagate and self- or cross-amplify during a run. Good codes like Ramses are designed to minimize and keep the errors controlled. However, apart from numerical errors, discretization also annihilates some interesting physical phenomena: scales interactions are damped, and scales outside of the computed scale range are inexistant.

The case of phenomena emerging from small scales are of prime importance here. It is known that instabilities such as cristallizing fronts in solid physics or even the Kelvin-Helmholtz instability in fluid physics, as well as a huge number of pattern-generating instabilities, find their structure in self-amplified modes, because of a local resonance in the phase space close to the instability's onset. When such modes have a time-frequency (resp. space-frequency) higher than allowed by the time-step (resp. resolution), the instability either does not grow or only the boundary modes grow, at an artificially slow rate, and notwithstanding the missing nonlinear interactions with the missing modes.

Falling into this category is the thermal fragmentation, where the cooling of a fluid with a perturbed pressure, density or temperature field increases the amplitude of perturbations. In the astrophysical plasmas we are interested in, very localized peaks can appear, for example due to compressive intermittent turbulence, especially in the supersonic case. But if the small scale outliers are smoothed out by resolution, no seed can be numerically found to grow cold clouds in a hotter backgrounds, or at wrong rates and wrong sizes.

Talking about turbulence, all many theories[3] describing it rely on scaling paradigms. Seeing it as a "cascade" of large structures breaking into smaller ones, like Kolmogorov in 1941, leads to a transfer of energy from a scale to a lower one, ultimately dissipating it at the lowest ones. This seminal idea has been refined over and over but the basic principle remained the same. It stood because it provides a satisfying explanation to the (fractal) structuration of a flow in which energy is injected at some scale, and ultimately dissipated in the form of heat. More, if flow structures "resonate" or, said otherwise, self-organize, energy is transferred to higher scales, and this sets up a "reverse cascade".

In astrophysical flows, the kinetic energy may be injected at the scales characterizing the flow themselves, but also at scales that characterize small-scale phenomena impacting the flow, like hydrodynamical or thermal instabilities. Thus, missing small scales lead first to the wrong delay between the energy injection and its transformation into heat, and second, to the possible absence of turbulent modes emerging from small-scale instabilities due to reverse cascades.

We adopt here a particular approach. Our aim is to get, from results whose scales are limited in range, clues to underlying processes owing to subscale physics. It follows the way modellers design so-called "subgrid models", implemented as subroutines that are run to phenomenologically mimick missing processes, with the sole knowledge of gridded quantities and their (discrete) derivatives. We will hence try to extrapolate the plausible subgrid features from our simulation data, based on a simple analytical criterion for the growth of a multiphase medium, in Subsection 3.7.1, and with simple scaling arguments for the existence of subresolution turbulence in Subsection 3.7.2.

3.7.1 Multiphase medium?

Out-of-equilibrium differential cooling

Radiative cooling being more efficient for higher densities and depending on the ionic composition of the gaz, and thus its temperature (and history), a heterogeneously dense, or hot, or pressurized medium may undergo a differential cooling, in that some of its compounding regions may cool at different rates. When these discrepancies tend to self-amplify, small perturbations may grow so that, from slightly heterogeneous, the medium becomes multiphase.

At thermal equilibrium, heating and cooling terms balance each other. Close to this equilibrium, a phase separation may occur and that case is designated *thermal instability*. Among the many works dealing with it, Sharma et al. (2012a) derived a typical time for the instability to grow under isobaric conditions, depending on

[3] We refer the reader to Landau & Lifshitz (1987) for the early, albeit deeply insightful, developments of the theory of turbulence.

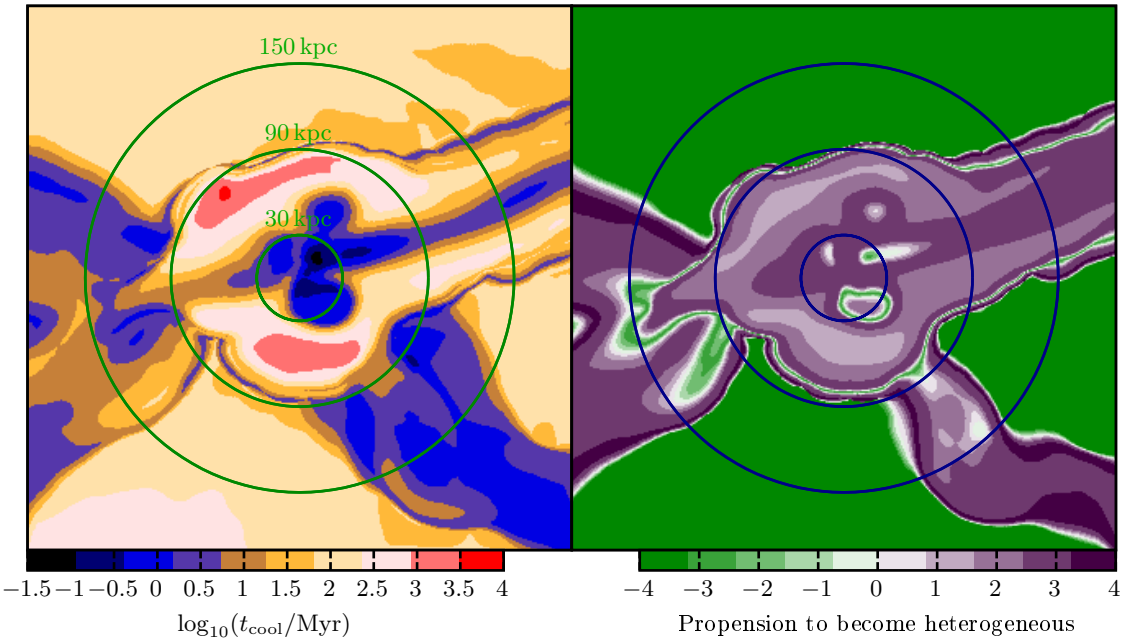

Figure 3.14: Maps of a transverse slice of an IGF, at $\zeta/r_{\rm halo} = 1.8$, i.e. at 343 kpc from the center of the closest end-point halo. Dimensions are $380 \times 380\,{\rm kpc}^2$. Marked are three circles as guides to the eye, whose radii are, as written in the ooling times in millions of years. *Right:* Propensity to become heterogeneous by use of the index defined in the text. When the value is positive, the accelerated differential cooling is active. The higher the value, the stronger the effect.

the inverse of the density contrast. When this time gets to infinity, i.e. the growth rate vanishes, the instability does not occur. This situation is met when

$$\frac{{\rm d}\log\Lambda}{{\rm d}\log T} = 2 \tag{3.4}$$

where Λ is the effective cooling power per unit density. The equation itself carries less information than the typical rate, as we lose the quantitative value, but changing the equal sign into a less-than sign constitutes a qualitative criterion for the propension to increase density gradients.

Even if the heating provided by metagalactic fluxes are present into our numerical computation, it is not sufficient to balance the cooling at densities that characterize the interior of filaments. It is therefore inaccurate to look for a possible thermal instability there. Nevertheless, a self-amplified differential cooling may act on relevant timescales. The use of the aforementionned criterion (Eq. 3.4) is still useful to determine whether a medium is likely to become multiphase. The quantitative information will then simply come from the cooling time of the gas.

We projected in Fig. 3.14 two fields for the already exemplified transverse slice. The left-hand panel shows the cooling time of each pixel, while the right-hand one shows the value of the spread to Eq. 3.4, i.e. $2 - {\rm d}\log\Lambda/{\rm d}\log T$, as a proxy for

the propension to become heterogeneous. Using the panel of Fig. 3.4 relevant to the infalling speeds, we can roughly say that the filament falls at $\sim 100\,\mathrm{km.s^{-1}}$. The slice being at $\zeta = 343\,\mathrm{kpc}$ and the virial radius of the accreting halo being $r_{\mathrm{halo}} = 190\,\mathrm{kpc}$, the approximate time to enter the virial sphere is $\sim 1.5\,\mathrm{Gyr}$. This indicates that, apart from any other process that may affect the gas, line and recombination emissions may significantly cool the gas before the entry everywhere exept in the shock-heated regions. Looking at the right-hand panel, almost all of the dense structures such that the filament and its feeding sheets may develop a multiphase medium. Notice that the densest central peak and a ring bounding one of the four vortices are however prevented from it.

This sole slice then suffices to indicate that except from the dense core, the four tubular cooler structures are prone to undergo a phase separation before entering the virial sphere. That statement makes the scenarii for an IGF cold core more intricate, but the consequences would greatly modify the envisioned accretion of warm gas through the halo: compression effects, mixing, boundary instabilities, survivability of the dense matter, would all need to be considered as volume and mass fractions of each phase. We refer the reader to Chapter 2 for a broader discussion about the possibly fragmented nature of IGF gas when entering the halo.

Toward a subgrid modelling

A look at higher slices reveals that the inside of the vortex tubes are in such a situation far above the virial radius. But a more rigorous approach needs to include the local density contrasts. If well represented by a measure of the dispersion of the density distribution on a given test volume, one could compute a phase separation time at the scale corresponding to the test volume.

The smaller the scale, the narrower the density dispersion. A subgrid model could make use of a simple extrapolating scheme to lower scales and virtually grow separate phases with the associated scales for the cooler, denser blobs and the associated timescales for their growth. We did not get further on implementing it, but leave it as a track for future refinement of plasma simulations.

There exists a tight connection between the existence of density fluctuations and the turbulent nature of the flow. The next subsection may then be fully complementary in understanding the scale-dependence of density fluctuations.

3.7.2 Turbulent precursors

Turbulence has often been studied in regimes that are not fully relevant to astrophysical situations. For example, perfectly stationary statistics of the flow describing quantities only apply on some timescales, i.e. when the injection rate

can be considered almost constant and when the cascade is fully developed down to the viscous scale. In the class of problems we try to address, even the injection scale itself may vary on a dynamical time.

To track down the possible wrongful absence of turbulent action in simulated data, one must first establish the relevant scales. Considering the processes that give birth to turbulent motions is the key. The first one we must think of pertains to the classical view of a multiscale vortical fragmentation, i.e. the so-called solenoidal turbulence[4]. It is commonly defined as one component of a turbulent flow, more precisely the divergence-free part. The other component is termed compressive turbulence and is defined, as is mathematically natural when decomposing such a vector field, as the purely divergent flow, i.e. the rotational-free part.

Solenoidal turbulence arises when rotation of particle cells is locally enhanced, that is where shear is strong enough to overcome the dissipative effect of viscosity and where nonlinear terms (namely the advection term of the Navier-Stokes equation for momentum, in hydrodynamics) allow for a stimulation of other spatial frequency modes to grow. The Kelvin-Helmholtz instability is an example among other ones. Let us write the rotational of the Navier-Stokes equation first divided by the density:

$$\frac{\partial \omega}{\partial t} + (v \cdot \nabla)\,\omega + (\nabla \cdot v)\,\omega - (\omega \cdot \nabla)\,v = \frac{\nabla\rho \times \nabla p}{\rho^2} + \nabla \times \left(\frac{\nabla \cdot \tau}{\rho}\right) + \nabla \times \left(\frac{f}{\rho}\right) \quad (3.5)$$

where v is the velocity field, $\omega = \nabla \times v$ is the vorticity field, ρ is the density field, p is the pressure field, τ is the viscouss stress tensor, f is the resultant field of all body forces acting on the particle cell, the vector notation is omitted, the parentheses enclosing an operand-free nabla sign ∇ is itself an operator. The equation applies at any point in space and at any time.

Two terms are able to play the role of a source in Eq. 3.5. These are the first and the third of the right-hand side. The third may represent a forcing term, at which is affected a typical injection scale. The other one is called the baroclinic term. It measures the baroclinity, i.e. the misalignment of the gradients of density and pressure.

On the left-hand side of the same equation, lies a term proportional to the vorticity itself, and to the divergence. Facing the time derivative, and assuming that the divergence evolves more slowly than the vorticity, it acts as a first-order term. Where the flow diverges, it dampens the vorticity, whereas where the flow converges, it amplifies vorticity.

In a Kolmogorov-like development, one would average Eq. 3.5 *on a given scale*, exhibiting the dependence of each term on the said scale, using a Fourier expansion

[4]The vast majority of literature about turbulence aiming at understanding human- or Earth-scale flow motions, that is that of liquids and a stratified atmosphere, it concerns incompressible flows. Hence, the term solenoidal is never used therein,

to eliminate differential operations. The forcing term would only be relevant at one scale, and the assumption of stationarity of the spectra would be made. The study of turbulence attributes a great importance to the characterization of the forcing.

To estimate its scale, we will make use of the two fields previously proved relevant, the divergence and the rotational of the flow, mapped on the two upper panels of Fig. 3.15. The units of the colorbar is, strictly speaking, a frequency, or the inverse of a time. Here that dimension is of no interest and only the contrasts are to be taken into account. As is not so surprising, regions of strong convergence (i.e. where the divergence is negative) are found along the shock fronts and where the two inflows meet. On the other hand, the sites of strong shear (i.e. where the absolute value of the vorticity is high) ar along those two inflows, where it slips against the accreting gas previously shocked.

Notice the sign of the vorticity. Its alternation while turning around the center is reminiscent of the quadrupolar vortical structure. It is also in accordance with those rotative tubes where found. The shearing regions seem to span over around 90 kpc each. The compressed regions extend over a total length comparable with the perimeter of the 90 kpc circle, which corresponds to the same order of magnitude as for shear.

Between this estimated injection scale and the maximal resolution scale, there are a number of scales $\log_{10}(90\,\mathrm{kpc}/348\,\mathrm{pc}) \approx 2.4$. This is clearly low to consider a cascade which follows scaling laws such as those found in literature, since they should span a wider range of scales to even develop.

The lower-right panel of Fig. 3.15 shows the logarithmic value of the baroclinic term. A first look at the colorbar makes it remarkable that the term varies over almost nine orders of magnitude. Then we need to add a technical but crucial point. The baroclinic term as computed here is a local contribution to the vorticity increase, but on a tighter mesh than the actual simulation output. This is thus to be considered as a virtual value everywhere the grid is in fact looser. However, interpolation must have smoothed the fields and thus attenuated the gradients; what is shown is thus a lower limit. It appears to be much higher in regions where Fig. 3.4 involves bending of flowlines. It fills almost all of the filament inside a radius of 90 kpc, and, marginally, at the edges of the main accreting sheet.

Finally, the lower-left panel of Fig. 3.15 is the projection of the local Mach number, in the barycentric frame computed as in the above sections. Shocks are strong at the filament-void edges ($\mathcal{M} \gtrsim 10$) and at the edges of the main accreting sheet, while they are weak at the entry of other sheets into the filament. Since the regions where the flowlines are bent appear as prone to generate vorticity at pixel-scale, and since such a bending occur right after a curved shock, the shocks in the voids, which imply a strong deflection, are a source of vorticity in their

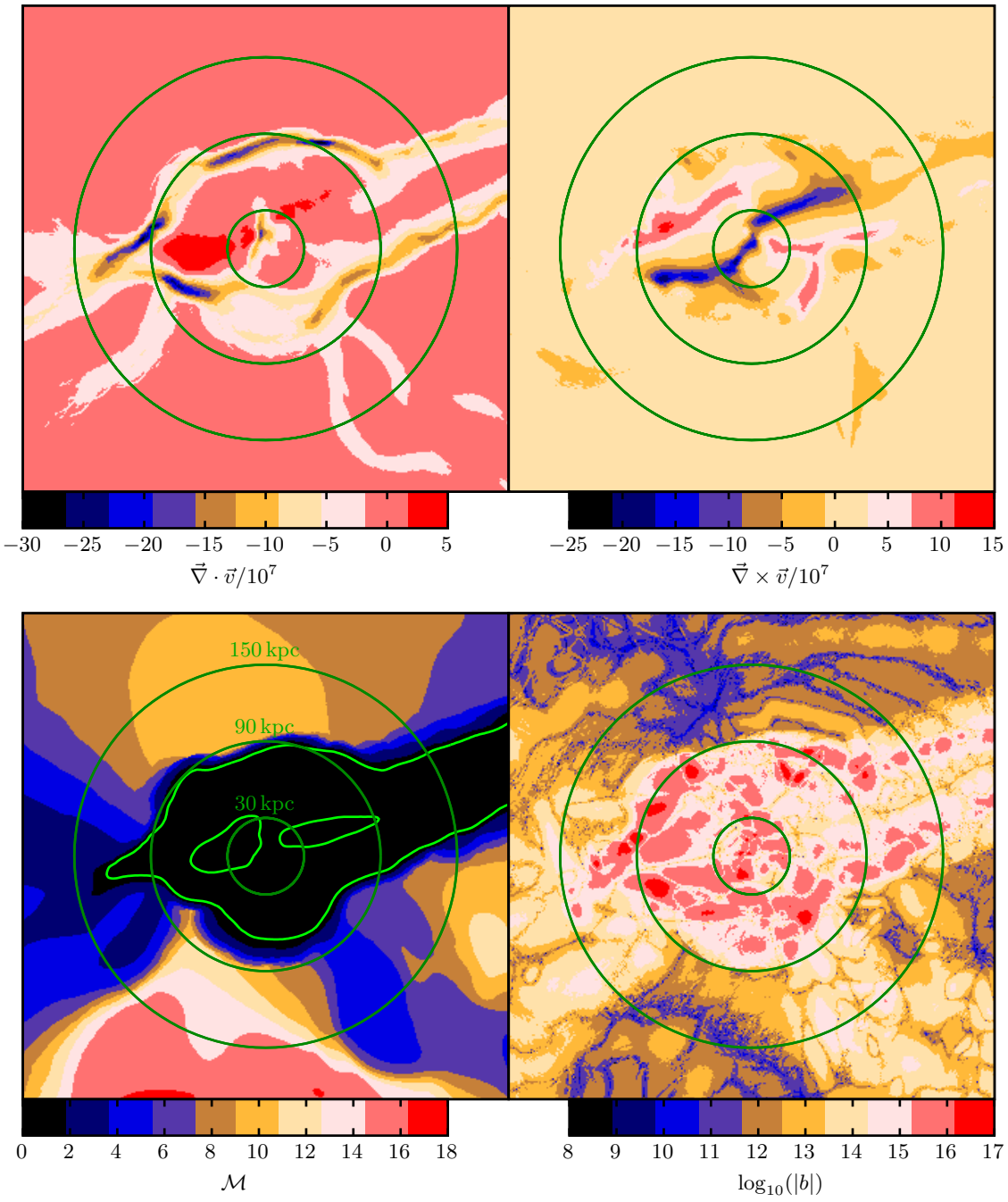

Figure 3.15: Maps of a transverse slice of an IGF, at $\zeta/r_{\rm halo} = 1.8$, i.e. at 343 kpc from the center of the closest end-point halo. Dimensions are $380 \times 380\,{\rm kpc}^2$. Marked are three circles as guides to the eye, whose radii are, as written in the bottom-left map, 30, 90, and 150 kpc. *Top-left:* Divergence of the flow. *Top-right:* Vorticity of the flow. *Bottom-left:* Mach number in the flow, the green line is the sonic contour ($\mathcal{M} = 1$). *Bottom-right:* Baroclinic contribution to the vorticity equation.

respective post-shock regions. The flow is accelerated (see the positive divergence in the upper-left panel) above the sound speed in two zones inside the filament: they correspond to the penetration (see upper-left panel of Fig. 3.4) of the highest accretion channels from the sheets, bordered by the strong shear layers (see the upper-right panel of Fig. 3.15). They become subsonic again where they meet, close to the center.

Note that the impact parameter already described and schematically drawn in Fig. 3.6 will lead to a structuration of vortices of different scales. The flow should then evolves towards a tessellation respecting alternating vorticity signs, in the same way one would construct a system of gearings. This tessellation is, on a first approach, giving rise to a fractal bidimensional flow, i.e. solenoidal turbulence. The central region of convergence is itself very likely to host a turbulent cascade.

In the assumption of a purely cylindrical geometry, one can trace random motions through the second moment of its radial distribution. In the same way observers infer turbulent motions in molecular clouds, we studied a velocity dispersion as a function of the radial size of the domain over which it is computed. We mass averaged the squared components of the velocity to obtain dispersion values $\sigma(r)$. For a collection of N particles, indexed by i and affected with masses, radial positions and velocities $m_i, R_i, \mathbf{v}_{i i\leq N}$, we define, on a disc of radius r, the mass-averaged velocity $\mathbf{v}_r$ and the dispersion $\sigma(r)$ as:

$$\begin{aligned} \mathbf{v}_r &= M_r^{-1} \sum_{R_i<r} m_i \mathbf{v}_i \\ \sigma^2(r) &= M_r^{-1} \sum_{R_i<r} m_i \|\mathbf{v}_i - \mathbf{v}_r\|^2 \end{aligned} \tag{3.6}$$

with M_r the mass inside the considered disc: $M_r = \sum_{R_i<r} m_i$.

Applied to the exemplified transverse slice, we plot the blue curve of Fig. 3.16. On the same figure is plotted an equivalent Reynold number, defined as

$$Re = \frac{\rho \sigma r}{\eta(T)} \tag{3.7}$$

with $\eta(T)$ the viscosity taken from Spitzer's formula for highly ionized plamas (Spitzer, 1962):

$$\eta(T) = 2.2\,10^{-15}\,\frac{T^{5/2}}{\log \Lambda_i}\,\mathrm{g.cm^{-1}.s^{-1}} \tag{3.8}$$

where Λ_i is the ion Coulomb integral. Following Roediger et al. (2013), we chose to simply set $\log \Lambda_i = 40$, even if this is slightly wrong when the gas is cooler than a few 10^4 K. Our goal is not to define an accurate value for the Reynolds number but rather obtain a rough one, whose order of magnitude and radial variations can be interpreted. The corresponding curve in Fig. 3.16 is shown in orange.

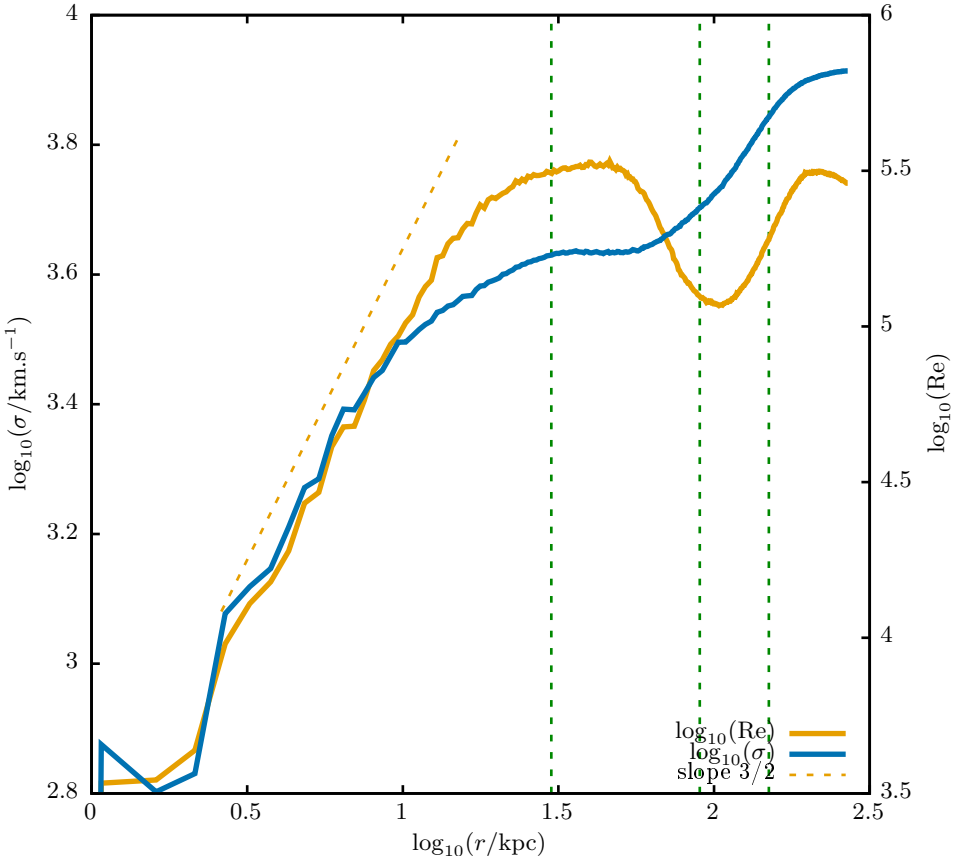

Figure 3.16: Velocity dispersion and corresponding Reynolds number averaged on concentric circles as a function of their radii, in a slice at $\zeta/r_{\text{halo}} = 1.8$, i.e. at 343 kpc from the center of the closest end-point halo. The dashed tilted line indicates a $3/2$ power-law. Green dashed vertical lines correspond to the radii of the concentric circles of transvers slices.

As far as the RMS velocity is concerned, no clear power-law appears. As expected from its cumulative nature, by definition, it increases with the size of the disc on which it is measured. At very low radii, $r < 3$ kpc, the dispersion is minimal and, even if the first bins are not very populated, it appears to be at least 500 km.s^{-1}. About 300 kpc from the center it reaches almost 10,000 km.s^{-1}, which gives an average slope of ~ 0.4.

On the other hand, the Reynolds number displays more interesting features. First, it varies on over an order of magnitude, from a few 10^5 to almost 10^7, indicating a regime that should be far from laminar at small scales. It increases up to $r \approx 30\,\mathrm{kpc}$, decreases up to $r \approx 90\,\mathrm{kpc}$ and increases again up to a little more than $r \approx 150\,\mathrm{kpc}$. Values above that radius are less reliable since, as seen in transverse maps, the cylindrical geometry is far from adequate. The condensing region $30\,\mathrm{kpc} < r < 90\,\mathrm{kpc}$ is also a mixing region and the Reynolds number increases during convergence. This is in agreement with what we suggested above, based on color maps of turbulent precursors. One must still be careful: it is not an indicator of a fully developed turbulence, as two distant points in a disc of given scale may not interact in a time shorter than other dynamical times.

Regardless of the regime of accretion (supersonic, dilute from voids, or subsonic, dense from sheets), the condensation of gas into a filament must convert a substantial fraction of the incoming ram pressure into small-scale vortices.

The **compressive turbulence**, on the other hand, is more difficult to trace thanks to such maps. This is unfortunate because this is the component that may, coupled with the radiative cooling, the most strongly affect the homogeneous nature of the flow. But we may consider this mode as wave turbulence, i.e. a structured mixing of acoustic and non-linearly interacting pressure waves. The only clues we can highlight with these data are the irregularity of the shock fronts and the irregular back-propagation of pressure waves from the condensation region (inside 30 kpc). Two processes might dampen them significantly: viscosity, of course, and radiative cooling, whenever it is sufficient to decrease pressure at a higher rate than the waves would increase it.

3.8 Main results

Numerical simulations have been used to investigate in detail the gas thermodynamics and kinematics during the formation and evolution of a cosmological filament. The intergalactic filament mainly forms via gas accretion through intersecting sheets. This accretion is anisotropic and the gas dynamics has many characteristics similar to that of turbulent flows. Important to this is the generation of vorticity due converging sheets of gas not being well aligned. The gas in these converging flows has a cooling time shorter than the dynamical time. Its

temperature range is such that the differential cooling discussed in Chapter 2, should also apply during the formation of filaments. The thermodynamics of the filament during its formation is, in many ways, analogous to what occurs during the formation of gaseous halos. This finding substantiates our assumption made in Chapter 2 that filaments have the initial temperature, velocity, and density structure necessary to seed the growth of inhomogeneities for forming multiphase accretion streams. Thus even if the resolution of our numerical simulations can not account for all physical processes relevant to small-scale perturbations, several clues lead us to think that the gaseous filaments may be multiphase and turbulent before entering the halo.

Interestingly, we found that the closer we moved toward the axis of symmetry of the filament, the higher the baryonic fraction, indicating strong condensation of the gas. As part of this investigation, we discovered that dwarf-sized halos with high density gaseous cores formed in a quasi-regular pattern close to the filament axis.

Chapter 4

Perspectives

Contents

4.1 Extending the results

We found during this thesis work, new theoretical properties of filamentary, gaseous flows accreting into galactic halos. Even in the admittedly over-simplified view of filaments as homogeneous and laminar flows (Chap. 2), a sustained shock close to the entry into the halo must have several consequences on the post-shock characteristics of the flow. Instead of an "isothermal" radiative shock which would result in a subsequent laminar flow of cold gas or a completely disrupted flow of hot gas mixing with the ambient halo, depending on characteristic cooling and dynamical timescales, the flow may and likely will be subject to instabilities. Due to its geometry, the post-shock stream will expand in the halo as it cools. This leads to a wider range of phenomena, including perhaps the creation of a turbulent biphasic medium flowing into the halo.

When studied with a numerical simulations at redshift 2 (Chap. 3), these filaments appear to be very likely to be confined, spinning (vorticity), turbulent and multiphase. Overall, the collimation of the flows, and any spinning or large-scale vorticity they may have, may result in filaments like those we assumed in our phenomenological modeling. As we also showed, a virial shock undergone by the filament would potentially amplify the turbulent multiphased nature of the post virial shock flow. This amplification may well occur even if there is not a virial shock but only a compression at around the virial radius of the halo. This is something that needs to be investigated but suggests that a shock at the boundary is not the decisive factor in the development of the multiphased turbulent stream.

The implications of our results for our understanding of the characteristics of gas accretion into galaxies are myriad and important. Having multiphase and turbulent accretion streams under certain conditions must affect the nature of the circumgalactic medium of galaxies. For example, streams of this nature would have a higher potential of interaction with even highly collimated galactic outflows. Such interaction may further moderate the accretion efficiency of cold gas onto galaxies. Since filamentary accretion is thought to be the major channel of supplying gas to galaxies necessary for sustaining their growth over cosmic time, if the gas accretion rate is moderated through the development of multiphased turbulent streams, then our understanding of the entire balance of inflows, star formation and outflows must be incomplete. Thus our results are opening new insights into how galaxies get their gas and sustain their growth. This is somehow more complex than what was thought up until recently but moderating accretion rates does help to alleviate some drawbacks of the findings about "cold flows" in the context of galactic halos as we outlined in Chapter 2.

More effort should be expended to further include a broader range of physical processes in low resolution, cosmological scale simulations. To reach this goal of understanding the generation of a turbulent and multiphase medium requires,

at least initially, a more detailed, higher resolution modelling of the coupling between dynamical and thermal energy conversion (dissipation and motion due to induced local pressure gradients) in idealized simulations. Such modelling will provide us with insights into the hot and cold fractions as well as the typical, randomly distributed, velocities of cold clouds in the post-shock gas and what physical mechanisms determine things like the fraction of hot and cold post-shock gas. Moreover, we can generalize the context of halo entry from a sustained planar shock to any form of compression, especially from the study of the origin of this sudden compression even in the absence of a high Mach shock. Numerical simulations with significantly higher resolution will also help building statistics and obtaining general relations between the cosmic context and the filamentary flow's nature.

With this general outline in mind, we now present **some** details of what is to be done next.

4.2 Tracks for modelling

We have derived a model based on two methods: a phenomenology derived from timescale ratios, and estimates from a set of conservation equations. We showed that a sustained shock in an IGF would be followed, for sufficiently massive halos, that the filament's identity may "rupture" through expansion, thermal fragmentation, turbulent dispersion and (very probably) mixing. Completing this model with other simple phenomenology, we will be able to narrow down less arbitrary and more realistic non-dimensional parameters that will lead to a better understanding of the effect of a filament's disruption on the gas accretion rate onto galaxies and on the properties of the circum-galactic medium.

4.2.1 Relating density and velocity fluctuations

As seen in our numerical study (Chap. 3), the incoming gas, before its entry in the halo, is very likely to be already turbulent and multiphase. Relating this result to our phenomenological model, we may rewrite our conservation equations so as to take into account both pre-shock and post-shock fractions ($\phi_{\mathrm{m,w}}$ and the like) and turbulence (σ). The first objective is to find analytical boundaries in the parameter space which delimit regimes where the shock is expected either to amplify or dampen the multiphase and turbulent nature of the flow.

The next step consists of assuming that the fluctuations in the velocity field, accounting for the gas turbulence, and those of the density field, accounting, among other things, for the density dispersion of the hot component, are tightly connected. This is explained by our stating the following hypotheses that:

1. the condensation of a warm phase *induces* turbulent motions,
2. the compressible component of turbulence *stimulates* the phase separation (these first two items are in fact interrelated),
3. the solenoidal component of turbulence *mitigates*, on average, the density peaks,
4. the turbulent dissipation *heats up* the gas,
5. the radiative cooling always *acts* as the gas evolves with time with the rate depending on temperature and density,
6. the processes 1 to 5 balance each other, resulting in a *quasi-static* evolution.

We will now focus on the numerical integrator described in §2.5.8 and the modifications implied by these new hypotheses. In that new simple case, at each timestep, the density distribution, i.e, the hot post-shock component has a density dispersion, in log, δ, which can be used to derive the turbulent velocity dispersion ($\sigma \propto \mathcal{M}_{\rm rms}\sqrt{T}$) for the next timestep. How are they be related?

Relating δ and $\mathcal{M}_{\rm rms}$

If we assume that the initial dispersion of densities is related to the trans- or supersonic turbulence, we can try to apply the density variance–turbulent Mach number relation

$$\delta \approx \log(1 + (b\mathcal{M}_{\rm rms})^2) \tag{4.1}$$

with b a constant of order unity and $\mathcal{M}_{\rm rms}$ the root-mean-squared Mach number (eg. Passot & Vázquez-Semadeni, 1998; Audit & Hennebelle, 2010; Price et al., 2011; Molina et al., 2012).

This relation had been empirically found and theoretically derived for isothermal, supersonic cases, but we will use it as an approximately appropriate guess for $\mathcal{M}_{\rm rms} = \sigma_{\rm ps}/c_{\rm ps}$. If the compressive modes dampen rapidly, we can take a fiducial value of $b = 1/3$, while a mix of compressive and solenoidal modes yields $b \approx 1/2$ (see previous references).

First approach: turbulent decay only

In a first approach, we can consider that the shock front perturbations are the driver and that the ensuing flow hosts a spontaneously decaying turbulence. Thus, hypothesis 1 would not apply and the turbulent Mach number at each timestep would only result from the dissipation of previous timesteps. Only the initial RMS Mach number is derived from the variance in the initial density.

The turbulent dissipation rate is the inverse of its characteristic time, which is the ratio of the turbulent specific energy (σ^2) to the specific dissipation power ($n\sigma^3/L_{\rm dissip}$) at any given time. This can be expressed as:

$$t_{\rm dissip} = \frac{L_{\rm dissip}}{\sigma} \tag{4.2}$$

where $L_{\rm dissip}$ is a typical dissipation length, usually taken as the typical injection length scale. However, doing so is justified in the case of a homogeneously driven turbulence.

The time evolution of σ is given by:

$$\mathrm{d}\log(\sigma) = \frac{\mathrm{d}t}{2t_{\rm dissip}} \tag{4.3}$$

and at each timestep we may calculate the RMS Mach number by dividing σ by the dominant sound speed in the hot medium.

Turbulent motions dissipate into heat at a rate given by the inverse of its characteristic time, defined by the ratio of the thermal specific energy to the specific dissipation power:

$$t_{\rm heat} = \frac{L_{\rm dissip} k_{\rm B} T}{n\sigma^3} \tag{4.4}$$

Since turbulent dissipation is a heating source, a new characteristic time may be constructed to reflect the thermal evolution:

$$t_{\rm therm} = \left(\frac{1}{t_{\rm heat}} - \frac{1}{t_{\rm cool}}\right)^{-1} \tag{4.5}$$

relevant for each particle, and varying with time. When it is negative, cooling prevails, whereas when positive, heating dominates. The time evolution of the thermal specific energy is now:

$$\mathrm{d}\log(e) = \frac{\mathrm{d}t}{t_{\rm therm}} \tag{4.6}$$

Eqs. 4.3 and 4.6 are then implemented into their discretized versions in the way Eqs. 2.38 and 2.39 were written.

I already attempted such an implementation and it led, in effect, to long-term saturation of the mass fraction in some cases, where the turbulence is slightly subsonic. No report of this work is currently in progress and so no conclusions can be provided mostly because of the lack of a systematic study of the effect of the two fundamental parameters: b, and $L_{\rm dissip}$.

4.2.2 Even further

The shock transition itself could be more accurately modelled. Breaking the assumption that the shock is planar and stationary should inform us about the transition parameter η and about the shock stability itself. First, we would study oblique- symmetric, concave, convex and perturbed shocks and derive turbulent amplitudes by staying close to the derivation of the Richtmyer-Meshkov instability (Richtmyer, 1960; Meshkov, 1969). The origin of the shock itself should be investigated, either by means of an analytical model of an inward-propagating strong compression and with a numerical simulation of an idealized filament.

We also discussed exploring the parameter space of galaxy mass, redshift, halo environment, etc on the stability of the shock. Doing so, it is possible to find regions wherein our phenomenological modeling is invalid. This constitutes an interesting and somehow general way of constraining the relevance of our combination of hypotheses. Indeed, crossing some bounding surfaces of the parameter space questions the assumption of stationarity. If the flow is not stationary, would it result in losing or reinforcing the necessary lower supporting forces for sustaining the virial shock? In the first case, the disruption of the filamentary warm flow would vanish, the same way as with the unstable shock from Dekel & Birnboim (2006), but for more complex reasons. In the second case, that we could call overstability, it would result in the disappearance of the collimated flow at the edge of the halo. An even more subtle but perhaps more realistic possibility is that the shock oscillates, alternating between under- and over-stable phases, due to the halo pressure evolving as the flow penetrates deeper. Determining a stability criterion for a fully 3-dimensional shock is another avenue we must consider.

There are also interesting avenues through which the accretion efficiency onto the galaxy proper may also be estimated. A first attempt was made to model the emission of clouds from a single source point for various limiting solid angles and various dispersion of a Maxwellian distribution of velocities, free-falling into an NFW potential. The amount of "clouds" reaching the sphere of radius 10% of the virial sphere (representing the galaxy) is always around 20% of the initial mass after one dynamical time, and this is only weakly affected by the initial average angular momentum. Adding a distribution of sizes and masses, as well as corresponding probabilities of collision, evaporation or stripping (eg. Maller & Bullock, 2004) would strongly improve may predictions for the mass acquisition rate of warm gas by the galaxy and has the gas balance in galaxies.

4.3 New avenues for simulations

While modelling involves a refinement and an increase in the number of hypotheses, the numerical simulation used in Chap. 3 relies only on a small set of first principles (or approximations), which provides a complementary avenue for understanding various phenomena of accretion flows. Tuning parameters in numerical simulations may help alleviate some doubts about what we modelled, while the model will help in deciding what is to be numerically investigated. A lot can be made with this work as a starting point. We now try to orient ourselves towards further developments that may be important for our developing understanding of the formation of filaments and accretion flows.

4.3.1 Further numerical processing

Finding scalings An effort must be made to automate the detection and the tracing of intergalactic filaments in our data set. This can be done with the help of numerical tools such as DisPerSe (see eg. Sousbie et al. (2011); Sousbie (2011)). By building a catalogue of filaments, characterized by the masses of the halos they flow into, we could systematically extract quantitative properties such as their average Plummer exponents, their average linear density of condensates as well as their average wavelength, their ability to thermally fragment and the level of expected turbulence they have. Such a halo-mass dependent characterization would not only reveal a possibly scale-invariant physics, but would also serve as input into more robust modelling on cosmological scales.

Time evolution A logical development would benefit from additional outputs from simulations, such as more redshifts, to determine whether our findings are still valid at higher redshifts, when the filamentary accretion onto galaxies is thought to be most vigorous for all halo masses. The study of earlier snapshots would allow for a deeper insight on dynamics and mass growth of filaments, their stability and their ability to condensate warm gas as a function of time, and why, if it is the case, they progressively lose their dominate role of supplying gas relative to mergers after redshift 1.

4.3.2 Further numerical experiments

Increasing resolution The next step may appear obvious. It consists in increasing the resolution of the simulation. The finer the grid, the closer we would get to reveal fragmented fields such as velocity of turbulence and density/temperature for a multiphase medium. This will also allow us to determine more accurate radial profiles, leading to a better understanding of the stability of filaments and their

detailed large scale density distribution. Adaptive mesh refinement, the refining condition needs to be changed to understand specific aspects of the characteristics of filaments. For example, if boundaries of the filaments are to be understood, refining on density gradients, instead of density itself, is of the essence. On the other hand, if rotational effects are to be investigated, such as for understanding the development of turbulence in flows, refining on regions of higher vorticity is the pertinent choice (see Kornreich and Scalo for example).

Running finer physical models Numerous phenomena have been omitted in our zoom-in simulation. An obvious one is the formation of stars in the filament. Considered time-consuming and possibly without consequence on high-redshift filaments, we did not let the gas trigger small scale condensations which may form into star clusters. Apart for artificially pressurizing the densest structures, it has the disadvantage of not allowing the "pre-enrichment" the intergalactic medium with metals. And even if the filaments penetrate the halo gas with enough momentum to keep their bulk free from metals, a boundary mixing layer could well form a cooler sheath resulting in an increased warm mass fraction. And if stars may form in some substructures of the filaments, they could also "self-enriched" with metals, which would be a game-changer for galactic models.

The second missing ingredient that could affect filaments is the magnetic field. With an MHD simulation, plasmas in IGFs would experience weaker shocks and the vorticity structures would interact with the magnetic field so as to amplify it. The radiative cooling would also be altered, for ion collisions would occur at different rates and energies.

4.3.3 Deriving observational constraints

With the use of spatial and thermodynamic conditions, assuming for example a collisional equilibrium, spectra of the gas radiative emission could be computed so as to obtain constraints on observations aiming at finding intergalactic filaments. In particular, emissions would be rather different if the medium is homogeneous or heterogeneous. In the latter case, small, dense, cold clouds would represent a high mass fraction but a low volume-filling factor, thus diluting their spectral signature, whereas the highly volume-filling, hot ambient gas would not emit much because of its very low density and low efficiency of emission. Not only the spectral lines would be mixed in the case of a heterogeneous medium, but their intensity would be lower.

Bibliography

Alatalo K., et al., 2015, Star Formation Suppression in Compact Group Galaxies: A New Path to Quenching?, ApJ, 812, 117

Allen M. G., Groves B. A., Dopita M. A., Sutherland R. S., Kewley L. J., 2008, The MAPPINGS III Library of Fast Radiative Shock Models, ApJS, 178, 20

Anderson M. E., Bregman J. N., 2010, Do Hot Halos Around Galaxies Contain the Missing Baryons?, ApJ, 714, 320

André P., et al., 2010, From filamentary clouds to prestellar cores to the stellar IMF: Initial highlights from the Herschel Gould Belt Survey, A&A, 518, L102

Appleton P. N., et al., 2013, Shock-enhanced C^+ Emission and the Detection of H_2O from the Stephan's Quintet Group-wide Shock Using Herschel, ApJ, 777, 66

Arzoumanian D., et al., 2011, Characterizing interstellar filaments with Herschel in IC 5146, A&A, 529, L6

Aubert D., Pichon C., Colombi S., 2004, The origin and implications of dark matter anisotropic cosmic infall on ˜L_* haloes, MNRAS, 352, 376

Audit E., Hennebelle P., 2010, On the structure of the turbulent interstellar clouds . Influence of the equation of state on the dynamics of 3D compressible flows, A&A, 511, A76

Balbus S. A., Soker N., 1989, Theory of local thermal instability in spherical systems, ApJ, 341, 611

Banerjee N., Sharma P., 2014, Turbulence and cooling in galaxy cluster cores, MNRAS, 443, 687

Beck A. M., et al., 2016, An improved SPH scheme for cosmological simulations, MNRAS, 455, 2110

Behroozi P. S., Wechsler R. H., Conroy C., 2013, The Average Star Formation Histories of Galaxies in Dark Matter Halos from z = 0-8, ApJ, 770, 57

Beirão P., et al., 2015, Spatially resolved Spitzer-IRS spectral maps of the superwind in M82, MNRAS, 451, 2640

Benson A. J., Bower R. G., Frenk C. S., Lacey C. G., Baugh C. M., Cole S., 2003, What Shapes the Luminosity Function of Galaxies?, ApJ, 599, 38

Best P. N., von der Linden A., Kauffmann G., Heckman T. M., Kaiser C. R., 2007, On the prevalence of radio-loud active galactic nuclei in brightest cluster galaxies: implications for AGN heating of cooling flows, MNRAS, 379, 894

Binney J., 1977, The physics of dissipational galaxy formation, ApJ, 215, 483

Birnboim Y., Dekel A., 2003, Virial shocks in galactic haloes?, MNRAS, 345, 349

Birnboim Y., Padnos D., Zinger E., 2016, The Hydrodynamic Stability of Gaseous Cosmic Filaments, ApJ, 832, L4

Blumenthal G. R., Faber S. M., Primack J. R., Rees M. J., 1984, Formation of galaxies and large-scale structure with cold dark matter, Nature, 311, 517

Borisova E., et al., 2016, Ubiquitous Giant Lyα Nebulae around the Brightest Quasars at z$\sim$3.5 Revealed with MUSE, ApJ, 831, 39

Borthakur S., Heckman T., Strickland D., Wild V., Schiminovich D., 2013, The Impact of Starbursts on the Circumgalactic Medium, ApJ, 768, 18

Bouché N., Lehnert M. D., Péroux C., 2006, The missing metals problem - II. How many metals are in z˜= 2.2 galaxies?, MNRAS, 367, L16

Bouché N., et al., 2016, Possible Signatures of a Cold-flow Disk from MUSE Using a z$\sim$1 Galaxy-Quasar Pair toward SDSS J1422-0001, ApJ, 820, 121

Brooks A. M., Governato F., Quinn T., Brook C. B., Wadsley J., 2009, The Role of Cold Flows in the Assembly of Galaxy Disks, ApJ, 694, 396

Bryan G. L., Norman M. L., 1998, Statistical Properties of X-Ray Clusters: Analytic and Numerical Comparisons, ApJ, 495, 80

Cantalupo S., Arrigoni-Battaia F., Prochaska J. X., Hennawi J. F., Madau P., 2014, A cosmic web filament revealed in Lyman-α emission around a luminous high-redshift quasar, Nature, 506, 63

Cen R., Ostriker J. P., 2006, Where Are the Baryons? II. Feedback Effects, ApJ, 650, 560

Chandrasekhar S., Fermi E., 1953, Problems of Gravitational Stability in the Presence of a Magnetic Field., ApJ, 118, 116

Cluver M. E., et al., 2010, Powerful H_2 Line Cooling in Stephan's Quintet. I. Mapping the Significant Cooling Pathways in Group-wide Shocks, ApJ, 710, 248

Codis S., Pichon C., Pogosyan D., 2015, Spin alignments within the cosmic web: a theory of constrained tidal torques near filaments, MNRAS, 452, 3369

Cooper J. L., Bicknell G. V., Sutherland R. S., Bland-Hawthorn J., 2009, Starburst-Driven Galactic Winds: Filament Formation and Emission Processes, ApJ, 703, 330

Cornuault N., Lehnert M., Boulanger F., Guillard P., 2016, Are Cosmological Gas Accretion Streams Multiphase and Turbulent?, preprint, (arXiv:1609.04405)

Danovich M., Dekel A., Hahn O., Ceverino D., Primack J., 2015, Four phases of angular-momentum buildup in high-z galaxies: from cosmic-web streams through an extended ring to disc and bulge, MNRAS, 449, 2087

Davis M., Efstathiou G., Frenk C. S., White S. D. M., 1985, The evolution of large-scale structure in a universe dominated by cold dark matter, ApJ, 292, 371

Dekel A., Birnboim Y., 2006, Galaxy bimodality due to cold flows and shock heating, MNRAS, 368, 2

Dekel A., et al., 2009, Cold streams in early massive hot haloes as the main mode of galaxy formation, Nature, 457, 451

Dekel A., Zolotov A., Tweed D., Cacciato M., Ceverino D., Primack J. R., 2013, Toy models for galaxy formation versus simulations, MNRAS, 435, 999

Doroshkevich A. G., 1970, Spatial structure of perturbations and origin of galactic rotation in fluctuation theory, Astrophysics, 6, 320

Dubois Y., Pichon C., Devriendt J., Silk J., Haehnelt M., Kimm T., Slyz A., 2013, Blowing cold flows away: the impact of early AGN activity on the formation of a brightest cluster galaxy progenitor, MNRAS, 428, 2885

Dubois Y., et al., 2014, Dancing in the dark: galactic properties trace spin swings along the cosmic web, MNRAS, 444, 1453

Edge A. C., et al., 2010, Herschel observations of FIR emission lines in brightest cluster galaxies, A&A, 518, L46

Emonts B. H. C., et al., 2016, Molecular gas in the halo fuels the growth of a massive cluster galaxy at high redshift, Science, 354, 1128

Fall S. M., Efstathiou G., 1980a, Formation and rotation of disc galaxies with haloes, MNRAS, 193, 189

Fall S. M., Efstathiou G., 1980b, Formation and rotation of disc galaxies with haloes, MNRAS, 193, 189

Ferrara A., Scannapieco E., Bergeron J., 2005, Where Are the Missing Cosmic Metals?, ApJ, 634, L37

Field G. B., 1965, Thermal Instability., ApJ, 142, 531

Fragile P. C., Murray S. D., Anninos P., van Breugel W., 2004, Radiative Shock-induced Collapse of Intergalactic Clouds, ApJ, 604, 74

Fraternali F., Marasco A., Marinacci F., Binney J., 2013, Ionized Absorbers as Evidence for Supernova-driven Cooling of the Lower Galactic Corona, ApJ, 764, L21

Freundlich J., Jog C. J., Combes F., 2014, Local stability of a gravitating filament: a dispersion relation, A&A, 564, A7

Fridman A. M., Polyachenko V. L., 1985, Book-Review - Physics of Gravitating Systems - Part One - Equilibrium and Stability, S&T, 70, 230

Fumagalli M., Cantalupo S., Dekel A., Morris S. L., O'Meara J. M., Prochaska J. X., Theuns T., 2016, MUSE searches for galaxies near very metal-poor gas clouds at z∼3: new constraints for cold accretion models, MNRAS, 462, 1978

Gaspari M., Ruszkowski M., Sharma P., 2012, Cause and Effect of Feedback: Multiphase Gas in Cluster Cores Heated by AGN Jets, ApJ, 746, 94

Geller M. J., Huchra J. P., 1989, Mapping the universe, Science, 246, 897

Gnat O., Sternberg A., 2007, Time-dependent Ionization in Radiatively Cooling Gas, ApJS, 168, 213

Goerdt T., Ceverino D., 2015a, Inflow velocities of cold flows streaming into massive galaxies at high redshifts, MNRAS, 450, 3359

Goerdt T., Ceverino D., 2015b, Inflow velocities of cold flows streaming into massive galaxies at high redshifts, MNRAS, 450, 3359

Gómez G. C., Vázquez-Semadeni E., 2014, Filaments in Simulations of Molecular Cloud Formation, ApJ, 791, 124

Gray W. J., Scannapieco E., 2013, Thermal and Chemical Evolution of Collapsing Filaments, ApJ, 768, 174

Gressel O., 2009, A Field-length based refinement criterion for adaptive mesh simulations of the interstellar medium, A&A, 498, 661

Guillard P., Boulanger F., Pineau Des Forêts G., Appleton P. N., 2009, H_2 formation and excitation in the Stephan's Quintet galaxy-wide collision, A&A, 502, 515

Guillard P., Boulanger F., Cluver M. E., Appleton P. N., Pineau Des Forêts G., Ogle P., 2010, Observations and modeling of the dust emission from the H_2-bright galaxy-wide shock in Stephan's Quintet, A&A, 518, A59

Hahn O., Abel T., 2011, Multi-scale initial conditions for cosmological simulations, MNRAS, 415, 2101

Hamer S. L., et al., 2016, Optical emission line nebulae in galaxy cluster cores 1: the morphological, kinematic and spectral properties of the sample, MNRAS, 460, 1758

Harford A. G., Hamilton A. J. S., 2011, Intergalactic filaments as isothermal gas cylinders, MNRAS, 416, 2678

Harford A. G., Hamilton A. J. S., Gnedin N. Y., 2008, Intergalactic baryon-rich regions at high redshift, MNRAS, 389, 880

Hayes M., Melinder J., Östlin G., Scarlata C., Lehnert M. D., Mannerström-Jansson G., 2016, O vi Emission Imaging of a Galaxy with the Hubble Space Telescope: a Warm Gas Halo Surrounding the Intense Starburst SDSS J115630.63+500822.1, ApJ, 828, 49

Heckman T. M., Thompson T. A., 2017, A Brief Review of Galactic Winds, preprint, (arXiv:1701.09062)

Heckman T. M., Armus L., Miley G. K., 1990, On the nature and implications of starburst-driven galactic superwinds, ApJS, 74, 833

Heigl S., Burkert A., Gritschneder M., 2017, Accretion driven turbulence in filaments I: Non-gravitational accretion, preprint, (arXiv:1705.03894)

Heitsch F., 2013a, Gravitational Infall onto Molecular Filaments, ApJ, 769, 115

Heitsch F., 2013b, Gravitational Infall onto Molecular Filaments. II. Externally Pressurized Cylinders, ApJ, 776, 62

Hennebelle P., Chabrier G., 2009, Analytical Theory for the Initial Mass Function. II. Properties of the Flow, ApJ, 702, 1428

Hennebelle P., Pérault M., 1999, Dynamical condensation in a thermally bistable flow. Application to interstellar cirrus, A&A, 351, 309

Hidding J., Shandarin S. F., van de Weygaert R., 2014, The Zel'dovich approximation: key to understanding cosmic web complexity, MNRAS, 437, 3442

Hill T., et al., 2011, Filaments and ridges in Vela C revealed by Herschel: from low-mass to high-mass star-forming sites, A&A, 533, A94

Hopkins P. F., Quataert E., Murray N., 2012, Stellar feedback in galaxies and the origin of galaxy-scale winds, MNRAS, 421, 3522

Hopkins P. F., Torrey P., Faucher-Giguère C.-A., Quataert E., Murray N., 2016, Stellar and quasar feedback in concert: effects on AGN accretion, obscuration, and outflows, MNRAS, 458, 816

Horedt G., 1970, Gravitational instability of polytropic gas spheres under external pressure, MNRAS, 151, 81

Horedt G. P., 1983, Level surface approach for uniformly rotating, axisymmetric polytropes, ApJ, 269, 303

Horedt G. P., 1986a, Seven-digit tables of Lane-Emden functions, Ap&SS, 126, 357

Horedt G. P., 1986b, Exact solutions of the Lane-Emden equation in N-dimensional space, A&A, 160, 148

Horedt G. P., 1987a, Physical characteristics of N-dimensional, radially-symmetric polytropes, Ap&SS, 133, 81

Horedt G. P., 1987b, Approximate analytical solutions of the Lane-Emden equation in N-dimensional space, A&A, 172, 359

Horedt G. P., 1987c, Topology of the Lane-Emden equation, A&A, 177, 117

Horedt G. P., ed. 2004, Polytropes - Applications in Astrophysics and Related Fields Astrophysics and Space Science Library Vol. 306, doi:10.1007/978-1-4020-2351-4.

Hoyle F., 1951, in Problems of Cosmical Aerodynamics. p. 195

Hu C.-Y., Naab T., Walch S., Moster B. P., Oser L., 2014, SPHGal: smoothed particle hydrodynamics with improved accuracy for galaxy simulations, MNRAS, 443, 1173

Jaffe W., Bremer M. N., Baker K., 2005, HII and H_2 in the envelopes of cooling flow central galaxies, MNRAS, 360, 748

Juvela M., Malinen J., Lunttila T., 2012, Profiles of interstellar cloud filaments. Observational effects in synthetic sub-millimetre observations, A&A, 544, A141

Kang H., Ryu D., Cen R., Song D., 2005, Shock-heated Gas in the Large-Scale Structure of the Universe, ApJ, 620, 21

Kereš D., Hernquist L., 2009, Seeding the Formation of Cold Gaseous Clouds in Milky Way-Size Halos, ApJ, 700, L1

Kereš D., Katz N., Weinberg D. H., Davé R., 2005, How do galaxies get their gas?, MNRAS, 363, 2

Klypin A. A., Shandarin S. F., 1983, Three-dimensional numerical model of the formation of large-scale structure in the Universe, MNRAS, 204, 891

Kornreich P., Scalo J., 2000, The Galactic Shock Pump: A Source of Supersonic Internal Motions in the Cool Interstellar Medium, ApJ, 531, 366

Koyama H., Inutsuka S.-i., 2004, The Field Condition: A New Constraint on Spatial Resolution in Simulations of the Nonlinear Development of Thermal Instability, ApJ, 602, L25

Kritsuk A. G., Norman M. L., 2002a, Thermal Instability-induced Interstellar Turbulence, ApJ, 569, L127

Kritsuk A. G., Norman M. L., 2002b, Interstellar Phase Transitions Stimulated by Time-dependent Heating, ApJ, 580, L51

Kritsuk A. G., et al., 2011, Comparing Numerical Methods for Isothermal Magnetized Supersonic Turbulence, ApJ, 737, 13

Laigle C., et al., 2015, Swirling around filaments: are large-scale structure vortices spinning up dark haloes?, MNRAS, 446, 2744

Landau L. D., Lifshitz E. M., 1987, Course of Theoretical Physics, 2nd edition edn. Vol. 6. Fluid Mechanics, Butterworth–Heinemann

Lehnert M. D., Heckman T. M., 1995, Ionized gas in the halos of edge-on, starburst galaxies: Data and results, ApJS, 97, 89

Lehnert M. D., Heckman T. M., 1996, Ionized Gas in the Halos of Edge-on Starburst Galaxies: Evidence for Supernova-driven Superwinds, ApJ, 462, 651

Lehnert M. D., Le Tiran L., Nesvadba N. P. H., van Driel W., Boulanger F., Di Matteo P., 2013, On the self-regulation of intense star-formation in galaxies at z = 1-3, A&A, 555, A72

Lehnert M. D., van Driel W., Le Tiran L., Di Matteo P., Haywood M., 2015, On the cosmic evolution of the specific star formation rate, A&A, 577, A112

Libeskind N. I., Hoffman Y., Knebe A., Steinmetz M., Gottlöber S., Metuki O., Yepes G., 2012, The cosmic web and the orientation of angular momenta, MNRAS, 421, L137

Libeskind N. I., Hoffman Y., Forero-Romero J., Gottlöber S., Knebe A., Steinmetz M., Klypin A., 2013a, The velocity shear tensor: tracer of halo alignment, MNRAS, 428, 2489

Libeskind N. I., Hoffman Y., Steinmetz M., Gottlöber S., Knebe A., Hess S., 2013b, Cosmic Vorticity and the Origin Halo Spins, ApJ, 766, L15

Lu Y., Mo H. J., Wechsler R. H., 2015, Formation of disc galaxies in preheated media: a preventative feedback model, MNRAS, 446, 1907

Madau P., Dickinson M., 2014, Cosmic Star-Formation History, ARA&A, 52, 415

Madau P., Ferguson H. C., Dickinson M. E., Giavalisco M., Steidel C. C., Fruchter A., 1996, High-redshift galaxies in the Hubble Deep Field: colour selection and star formation history to z˜4, MNRAS, 283, 1388

Maller A. H., Bullock J. S., 2004, Multiphase galaxy formation: high-velocity clouds and the missing baryon problem, MNRAS, 355, 694

Mandelker N., Padnos D., Dekel A., Birnboim Y., Burkert A., Krumholz M. R., Steinberg E., 2016, Instability of supersonic cold streams feeding galaxies - I. Linear Kelvin-Helmholtz instability with body modes, MNRAS, 463, 3921

Marlowe A. T., Heckman T. M., Wyse R. F. G., Schommer R., 1995, Observations of the impact of starbursts on the interstellar medium in dwarf galaxies, ApJ, 438, 563

Marlowe A. T., Meurer G. R., Heckman T. M., Schommer R., 1997, The Taxonomy of Blue Amorphous Galaxies. I. Hα and UBVI Data, ApJS, 112, 285

Martin C. L., 1998, The Impact of Star Formation on the Interstellar Medium in Dwarf Galaxies. II. The Formation of Galactic Winds, ApJ, 506, 222

Martin C. L., 2005, Mapping Large-Scale Gaseous Outflows in Ultraluminous Galaxies with Keck II ESI Spectra: Variations in Outflow Velocity with Galactic Mass, ApJ, 621, 227

Martin D. C., Matuszewski M., Morrissey P., Neill J. D., Moore A., Cantalupo S., Prochaska J. X., Chang D., 2015, A giant protogalactic disk linked to the cosmic web, Nature, 524, 192

McCourt M., Sharma P., Quataert E., Parrish I. J., 2012, Thermal instability in gravitationally stratified plasmas: implications for multiphase structure in clusters and galaxy haloes, MNRAS, 419, 3319

Ménard B., Scranton R., Fukugita M., Richards G., 2010, Measuring the galaxy-mass and galaxy-dust correlations through magnification and reddening, MNRAS, 405, 1025

Meshkov E. E., 1969, Instability of the interface of two gases accelerated by a shock wave, Sov.Flu.Dyn, 4, 101

Mo H., van den Bosch F. C., White S., 2010, Galaxy Formation and Evolution

Molina F. Z., Glover S. C. O., Federrath C., Klessen R. S., 2012, The density variance-Mach number relation in supersonic turbulence - I. Isothermal, magnetized gas, MNRAS, 423, 2680

Navarro J. F., Frenk C. S., White S. D. M., 1997, A Universal Density Profile from Hierarchical Clustering, ApJ, 490, 493

Nelson D., Vogelsberger M., Genel S., Sijacki D., Kereš D., Springel V., Hernquist L., 2013, Moving mesh cosmology: tracing cosmological gas accretion, MNRAS, 429, 3353

Nelson D., Genel S., Vogelsberger M., Springel V., Sijacki D., Torrey P., Hernquist L., 2015, The impact of feedback on cosmological gas accretion, MNRAS, 448, 59

Nelson D., Genel S., Pillepich A., Vogelsberger M., Springel V., Hernquist L., 2016, Zooming in on accretion - I. The structure of halo gas, MNRAS, 460, 2881

Nutter D., Kirk J. M., Stamatellos D., Ward-Thompson D., 2008, SCUBA and Spitzer observations of the Taurus molecular cloud - pulling the bull's tail, MNRAS, 384, 755

Ocvirk P., Pichon C., Teyssier R., 2008a, Bimodal gas accretion in the Horizon-MareNostrum galaxy formation simulation, MNRAS, 390, 1326

Ocvirk P., Pichon C., Teyssier R., 2008b, Bimodal gas accretion in the Horizon-MareNostrum galaxy formation simulation, MNRAS, 390, 1326

Ogle P., Boulanger F., Guillard P., Evans D. A., Antonucci R., Appleton P. N., Nesvadba N., Leipski C., 2010, Jet-powered Molecular Hydrogen Emission from Radio Galaxies, ApJ, 724, 1193

Oproiu T., Horedt G. P., 2008, Critically Rotating Polytropic Cylinders, ApJ, 688, 1112

Ostriker J., 1964a, The Equilibrium of Polytropic and Isothermal Cylinders., ApJ, 140, 1056

Ostriker J., 1964b, On the Oscillations and the Stability of a Homogeneous Compressible Cylinder., ApJ, 140, 1529

Padoan P., Juvela M., Goodman A. A., Nordlund Å., 2001, The Turbulent Shock Origin of Proto-Stellar Cores, ApJ, 553, 227

Passot T., Vázquez-Semadeni E., 1998, Density probability distribution in one-dimensional polytropic gas dynamics, Phys. Rev. E, 58, 4501

Peebles P. J. E., 1969, Origin of the Angular Momentum of Galaxies, ApJ, 155, 393

Peek J. E. G., Ménard B., Corrales L., 2015, Dust in the Circumgalactic Medium of Low-redshift Galaxies, ApJ, 813, 7

Peterson J. R., Kahn S. M., Paerels F. B. S., Kaastra J. S., Tamura T., Bleeker J. A. M., Ferrigno C., Jernigan J. G., 2003, High-Resolution X-Ray Spectroscopic Constraints on Cooling-Flow Models for Clusters of Galaxies, ApJ, 590, 207

Peterson B. W., et al., 2012, Detection of Powerful Mid-IR H_2 Emission in the Bridge between the Taffy Galaxies, ApJ, 751, 11

Pichon C., Bernardeau F., 1999, Vorticity generation in large-scale structure caustics, A&A, 343, 663

Pichon C., Pogosyan D., Kimm T., Slyz A., Devriendt J., Dubois Y., 2011, Rigging dark haloes: why is hierarchical galaxy formation consistent with the inside-out build-up of thin discs?, MNRAS, 418, 2493

Pinto C., et al., 2014, Discovery of O VII line emitting gas in elliptical galaxies, A&A, 572, L8

Planck Collaboration et al., 2014, Planck 2013 results. XVI. Cosmological parameters, A&A, 571, A16

Planck Collaboration et al., 2016, Planck 2015 results. XIII. Cosmological parameters, A&A, 594, A13

Powell L. C., Bournaud F., Chapon D., Devriendt J., Slyz A., Teyssier R., 2011, in Carignan C., Combes F., Freeman K. C., eds, IAU Symposium Vol. 277, Tracing the Ancestry of Galaxies. pp 234–237 (arXiv:1102.4195), doi:10.1017/S1743921311022848

Press W. H., Schechter P., 1974, Formation of Galaxies and Clusters of Galaxies by Self-Similar Gravitational Condensation, ApJ, 187, 425

Price D. J., 2012, Resolving high Reynolds numbers in smoothed particle hydrodynamics simulations of subsonic turbulence, MNRAS, 420, L33

Price D. J., Federrath C., Brunt C. M., 2011, The Density Variance-Mach Number Relation in Supersonic, Isothermal Turbulence, ApJ, 727, L21

Rafferty D. A., McNamara B. R., Nulsen P. E. J., 2008, The Regulation of Cooling and Star Formation in Luminous Galaxies by Active Galactic Nucleus Feedback and the Cooling-Time/Entropy Threshold for the Onset of Star Formation, ApJ, 687, 899

Raymond J. C., 1979, Shock waves in the interstellar medium, ApJS, 39, 1

Rees M. J., Ostriker J. P., 1977, Cooling, dynamics and fragmentation of massive gas clouds - Clues to the masses and radii of galaxies and clusters, MNRAS, 179, 541

Richtmyer R. D., 1960, Taylor instability in shock acceleration of compressible fluids, Comm. Pure Appl. Math., 13, 297

Roediger E., Kraft R. P., Forman W. R., Nulsen P. E. J., Churazov E., 2013, Kelvin-Helmholtz Instabilities at the Sloshing Cold Fronts in the Virgo Cluster as a Measure for the Effective Intracluster Medium Viscosity, ApJ, 764, 60

Salomé P., Combes F., Revaz Y., Downes D., Edge A. C., Fabian A. C., 2011, A very extended molecular web around NGC 1275, A&A, 531, A85

Schmalzl M., et al., 2010, Star Formation in the Taurus Filament L 1495: From Dense Cores to Stars, ApJ, 725, 1327

Sharma P., Parrish I. J., Quataert E., 2010, Thermal Instability with Anisotropic Thermal Conduction and Adiabatic Cosmic Rays: Implications for Cold Filaments in Galaxy Clusters, ApJ, 720, 652

Sharma P., McCourt M., Quataert E., Parrish I. J., 2012a, Thermal instability and the feedback regulation of hot haloes in clusters, groups and galaxies, MNRAS, 420, 3174

Sharma P., McCourt M., Parrish I. J., Quataert E., 2012b, On the structure of hot gas in haloes: implications for the L_X-T_X relation and missing baryons, MNRAS, 427, 1219

Silk J., Mamon G. A., 2012, The current status of galaxy formation, Research in Astronomy and Astrophysics, 12, 917

Simon R., 1963, Sur les oscillations non radiales et la stabilité d'un cylindre homogène compressible, Annales d'Astrophysique, 26, 224

Singh A., Sharma P., 2015, The cold mode: a phenomenological model for the evolution of density perturbations in the intracluster medium, MNRAS, 446, 1895

Sousbie T., 2011, The persistent cosmic web and its filamentary structure - I. Theory and implementation, MNRAS, 414, 350

Sousbie T., Pichon C., Kawahara H., 2011, The persistent cosmic web and its filamentary structure - II. Illustrations, MNRAS, 414, 384

Spitzer L., 1962, Physics of Fully Ionized Gases, 2nd edition edn. New York: Interscience

Springel V., et al., 2005, Simulations of the formation, evolution and clustering of galaxies and quasars, Nature, 435, 629

Stewart K. R., Kaufmann T., Bullock J. S., Barton E. J., Maller A. H., Diemand J., Wadsley J., 2011, Orbiting Circumgalactic Gas as a Signature of Cosmological Accretion, ApJ, 738, 39

Stewart K. R., Brooks A. M., Bullock J. S., Maller A. H., Diemand J., Wadsley J., Moustakas L. A., 2013, Angular Momentum Acquisition in Galaxy Halos, ApJ, 769, 74

Stodólkiewicz J. S., 1963, On the Gravitational Instability of Some Magneto-Hydrodynamical Systems of Astrophysical Interest. Part III., Acta Astron., 13, 30

Suresh J., Bird S., Vogelsberger M., Genel S., Torrey P., Sijacki D., Springel V., Hernquist L., 2015, The impact of galactic feedback on the circumgalactic medium, MNRAS, 448, 895

Sutherland R. S., Dopita M. A., 1993, Cooling functions for low-density astrophysical plasmas, ApJS, 88, 253

Sutherland R. S., Bicknell G. V., Dopita M. A., 2003, The Numerical Simulation of Radiative Shocks. II. Thermal Instabilities in Two-dimensional Models, ApJ, 591, 238

Teyssier R., 2002, Cosmological hydrodynamics with adaptive mesh refinement. A new high resolution code called RAMSES, A&A, 385, 337

Thompson T. A., Quataert E., Zhang D., Weinberg D. H., 2016, An origin for multiphase gas in galactic winds and haloes, MNRAS, 455, 1830

Tillson H., Devriendt J., Slyz A., Miller L., Pichon C., 2015, Angular momentum transfer to a Milky Way disc at high redshift, MNRAS, 449, 4363

Tremblay G. R., et al., 2012, Multiphase signatures of active galactic nucleus feedback in Abell 2597, MNRAS, 424, 1026

Tumlinson J., et al., 2011, The Large, Oxygen-Rich Halos of Star-Forming Galaxies Are a Major Reservoir of Galactic Metals, Science, 334, 948

Tweed D., Devriendt J., Blaizot J., Colombi S., Slyz A., 2009, Building merger trees from cosmological N-body simulations. Towards improving galaxy formation models using subhaloes, A&A, 506, 647

Vernet J., et al., 2017a, Are we seeing accretion flows in a 250 kpc Lyα halo at z = 3?, A&A, 602, L6

Vernet J., et al., 2017b, Are we seeing accretion flows in a 250 kpc Lyα halo at z = 3?, A&A, 602, L6

Viala Y., Horedt G. P., 1974a, Emden's functions for polytropes with negative index, A&AS, 16, 173

Viala Y. P., Horedt G., 1974b, Polytropic Sheets, Cylinders and Spheres with Negative Index, A&A, 33, 195

Voit G. M., Donahue M., Bryan G. L., McDonald M., 2015a, Regulation of star formation in giant galaxies by precipitation, feedback and conduction, Nature, 519, 203

Voit G. M., Bryan G. L., O'Shea B. W., Donahue M., 2015b, Precipitation-regulated Star Formation in Galaxies, ApJ, 808, L30

Welker C., Devriendt J., Dubois Y., Pichon C., Peirani S., 2014, Mergers drive spin swings along the cosmic web, MNRAS, 445, L46

Werk J. K., et al., 2014, The COS-Halos Survey: Physical Conditions and Baryonic Mass in the Low-redshift Circumgalactic Medium, ApJ, 792, 8

Wetzel A. R., Nagai D., 2015, The Physical Nature of the Cosmic Accretion of Baryons and Dark Matter into Halos and Their Galaxies, ApJ, 808, 40

White S. D. M., 1984, Angular momentum growth in protogalaxies, ApJ, 286, 38

White S. D. M., Rees M. J., 1978a, Core condensation in heavy halos - A two-stage theory for galaxy formation and clustering, MNRAS, 183, 341

White S. D. M., Rees M. J., 1978b, Core condensation in heavy halos - A two-stage theory for galaxy formation and clustering, MNRAS, 183, 341

Zeldovich I. B., Einasto J., Shandarin S. F., 1982, Giant voids in the universe, Nature, 300, 407

Zhuravleva I., et al., 2014, Turbulent heating in galaxy clusters brightest in X-rays, Nature, 515, 85

de Lapparent V., Geller M. J., Huchra J. P., 1986, A slice of the universe, ApJ, 302, L1

van de Voort F., Schaye J., 2012, Properties of gas in and around galaxy haloes, MNRAS, 423, 2991

van de Voort F., Schaye J., Booth C. M., Dalla Vecchia C., 2011, The drop in the cosmic star formation rate below redshift 2 is caused by a change in the mode of gas accretion and by active galactic nucleus feedback, MNRAS, 415, 2782